5-2023

Lung cancer-kidney crosstalk enhances cisplatin-induced nephrotoxicity.

Andrew Joseph Orwick
University of Louisville

LUNG CANCER-KIDNEY CROSSTALK ENHANCES CISPLATIN-INDUCED NEPHROTOXICITY

By

Andrew Joseph Orwick
Pharm.D., Sullivan University College of Pharmacy, 2012
M.S. Pharmacology and Toxicology, University of Louisville, 2021

A Dissertation
Submitted to the Faculty of the
School of Medicine of the University of Louisville
in Fulfillment of the Requirements for the Degree of

Doctor of Philosophy in Pharmacology and Toxicology

Department of Pharmacology and Toxicology
University of Louisville
Louisville, Kentucky

May 2023

LUNG CANCER-KIDNEY CROSSTALK
ENHANCES CISPLATIN-INDUCED NEPHROTOXICITY

By

Andrew Joseph Orwick

Pharm.D., Sullivan University College of Pharmacy, 2012
M.S. Pharmacology and Toxicology, University of Louisville, 2021

A Dissertation Approved on

March 28th, 2023

by the following Dissertation Committee:

_____
Leah Siskind

_____
Levi Beverly

_____
Bradford Hill

_____
Steven Jones

_____
Geoffrey Clark

DEDICATION

I would like to dedicate this dissertation to the people who have been instrumental in shaping my personal and scientific journey. Firstly, to my mother, who inspired my love for science and medicine and instilled in me a passion for inquiry. Secondly, to my father, who has been a true role model of hard work and sacrifice, engraining in me that if you are going to do something, do it right the first time. I also wish to express my heartfelt appreciation to my wife, Jenna Orwick, who has been a constant source of support throughout this journey, unwaveringly affirming my decision to pursue this path. And to my two precious daughters, Ruby and Elizabeth, whose infectious laughter and boundless energy are always able to rejuvenate me even on the toughest days in the laboratory. I am endlessly grateful for your love and support.

ACKNOWLEDGMENTS

I am grateful to Dr. Leah Siskind, my mentor, for taking a chance on me during the interview process despite my lack of basic laboratory research experience. Her belief in my ability and potential was instrumental in shaping my research career. I am also grateful to everyone in the lab for their invaluable help, support, and camaraderie. Specifically, I would like to thank Sophia Sears and Mark Doll for the countless hours spent training me on various techniques and for always being available to provide feedback on my project. My sincere appreciation also goes to Dr. Levi Beverly for his support and guidance in creating the cancer model and increasing the scientific rigor of the project. I would like to express my gratitude to the committee members, Dr. Bradford Hill, Dr. Steven Jones, and Dr. Geoffrey Clark, for their continuous support, insightful comments, and valuable time spent helping me solidify the project. I would like to dedicate a special thanks to my wife, Jenna, for her support and encouragement throughout this process. Finally, I am thankful to my family members and in-laws, whose support has been a constant source of motivation as I made the decision to pursue a career change in my early thirties.

ABSTRACT

LUNG CANCER-KIDNEY CROSSTALK
ENHANCES CISPLATIN-INDUCED NEPHROTOXICITY

Andrew Joseph Orwick

March 28th, 2023

Cancer patients represent a unique patient population with increased susceptibility to kidney disease. Drug-induced acute kidney injury (AKI) in cancer patients is a common problem. Cisplatin is a highly effective treatment used in many solid organ cancers. However, cisplatin causes AKI in 30% of patients, increasing the risk of chronic kidney disease (CKD) development. The kidneys maintain homeostasis of the body's extracellular fluids and removing waste products. The kidneys filter nearly 170 liters of fluid a day and must reabsorb over 99% of the filtrate. The reabsorption occurs in tubule cells throughout the nephron, which are highly enriched in mitochondria to complete this task. One mechanism by which cisplatin induces nephrotoxicity is by reducing mitochondrial content and biogenesis leading to loss of kidney function, kidney injury, inflammation, and development of fibrosis. Reduced kidney mitochondrial mass and respiration also impairs the tissue repair process. Historically, most preclinical cisplatin toxicity studies have been completed in mice without cancer. We believe the physiology of cancer patients is not adequately represented in these non-cancerous murine models. In this study we used multiple mouse models of lung cancer in combination with repeated low dose cisplatin (RLDC) regimen to determine if cancer alters the nephrotoxicity of cisplatin. Additionally, we pharmacologically induced mitochondrial biogenesis to increase

kidney mitochondrial content to determine if this pathway will protect from cisplatin-induced nephrotoxicity. Our results show that lung cancer combined with cisplatin enhances the nephrotoxicity of cisplatin. Additionally, cancer alone without cisplatin reduced renal function, increased fibrosis, reduced mitochondrial content, and reduced PGC-1α of kidney cortices. Stimulating mitochondrial biogenesis increased kidney mitochondrial content and reduced loss of kidney function, kidney injury, inflammation, and development of fibrosis from RLDC in mice without cancer. However, these effects are nullified when the experiment was repeated in mice with subcutaneous lung cancer. Previous clinical trials on nephroprotective agents have failed, and we propose that poorly representative mouse models may be responsible for misleading preclinical research. Our development of clinically relevant models of cisplatin-induced nephrotoxicity provides a foundation for developing nephron-protective agents that can be used as an adjunctive therapy for cancer patients taking cisplatin.

TABLE OF CONTENTS

LIST OF FIGURES

FIGURE PAGE

CHAPTER 1: BACKGROUND & INTRODUCTION

Kidney disease is a significant public health concern, with acute kidney injury (AKI)[1, 2] and chronic kidney disease (CKD) affecting millions of people worldwide [3-5]. It is estimated that AKI occurs in up to 30% of hospitalized patients and up to 50% in the critically ill patient population [6]. Patients hospitalized for AKI events have higher in-hospital mortality rates and reduced survival at 1 year compared to patients hospitalized for non-AKI events [7]. It was previously thought that AKI incidents had no long-term consequences if renal function recovered [8], but recent studies indicate that patients who develop AKI are 10 times or more likely to develop chronic kidney disease (CKD) [6, 9-12]. Even patients that do not develop clinical AKI are at risk for long-term declines in renal function [13, 14].

CKD affects over 20 million Americans, and over 500,000 have end-stage renal disease (ESRD) [15]. Globally, the incidence and prevalence of CKD are also increasing, with an estimated 800 million people affected [3-5]. Additionally, CKD significantly increases the risk of mortality, with higher stages of CKD associated with a greater risk of death. This risk of mortality is further increased when CKD is accompanied by other comorbidities, such as cardiovascular disease or diabetes [16].

Cancer patients are a unique patient population and their increased susceptibility to kidney disease has led to the rapidly growing specialty of Onconephrology [17-23]. Cancer patients often have decreased kidney function [24-26], and drug-induced acute kidney injury (AKI) is common and remains a hurdle [27-32]. Drug-induced AKI is a common cause of renal dysfunction and is associated with significant morbidity and

mortality [33]. Drugs can cause AKI through a variety of mechanisms, including direct tubular toxicity, intravascular volume depletion, hemodynamic alterations, and immune-mediated processes [34]. The incidence of drug-induced AKI is difficult to estimate due to the wide range of medications that can cause kidney injury and the variability in patient populations [33].

Of particular interest is the incidence of anti-cancer drug-induced AKI, as these medications are frequently prescribed to cancer patients and have been shown to cause renal dysfunction [30, 35-37]. Cisplatin is prescribed to 10-20% of cancer patients [38] and is a highly effective chemotherapeutic agent for the treatment of various solid-organ cancers, including head, neck, testicular, breast, ovary, and lung. [39]. Its approval for the treatment of testicular cancer led to an increase in remission rates from 5% to 80% [40]. However, its usage is limited by its nephrotoxicity, with 30% of patients developing AKI [39]. While newly developed cisplatin derivatives have reduced nephrotoxicity, they are less effective in treating many forms of cancer [41]. Limiting cisplatin toxicity would increase the therapeutic potential in cancer patients, however, there are currently no therapies approved to prevent or treat cisplatin-induced AKI. It is therefore crucial to understand the mechanisms underlying cisplatin-induced kidney injury and to develop strategies to prevent and manage this condition.

KIDNEY PHYISOLOGY

The kidneys maintain the body's fluid homeostasis [42-44]. The kidney has three major avenues to keep the extracellular fluid in steady state. Firstly, the kidney controls fluid volume of the body, osmolarity, electrolyte concentration, and acidity by altering the amount of water and other charged particles excreted in the urine. The kidney can independently regulate the excretion of water and various solutes, including sodium, hydrogen, potassium, calcium, magnesium, and phosphate, by modulating the tubular secretion and reabsorption of each at different segments of the nephron. Secondly, the

kidney eliminates waste products of metabolism such as urea, as well as other exogenous chemicals including toxins, drugs, and drug metabolites. Thirdly, the kidney synthesizes and secretes hormones and enzymes into systemic circulation. Renin is produced and secreted from the kidneys. This enzyme plays a critical role in systemic and renal hemodynamics by catalyzing the formation of angiotensin I which is converted to angiotensin II. Angiotensin II is a key regulator of blood pressure both in the kidney and the body. Additionally, the kidney is involved in the production of erythropoietin, which regulates the production of new red blood cells, and vitamin D metabolism converting calcitriol to its biologically active form 1,25-OH dihydroxy vitamin D, which regulates calcium and phosphate balance. [42-44].

The smallest functional unit of the kidney is the nephron. Nephrons are composed of three major sections with distinct roles; (1) the glomerulus that filters the blood, (2) the tubule that primarily reabsorbs vital nutrients and secretes solutes, and (3) the collecting duct that carries urine to the calyx, then renal pelvis, and finally exits the kidneys via the ureters [45]. There are over 26 different cell types in human adult kidneys to carry out the wide range of functions needed for proper renal function [46].

Glomerular filtration is the first step in urine production and is a passive process powered by hydrostatic pressure from the heart via glomerular capillaries. The glomerular filtration rate (GFR) is the volume of fluid that is filtered per minute. Normal GFR ranges from 90-100 mL/min in women and 115 to 125 mL/min in men. The kidneys account for less than 1% of body weight but receive 20-25% of cardiac output [47, 48]. The calculation of GFR is based on the equation: GFR = renal plasma flow x filtration fraction. Renal plasma flow is approximately 55% of renal blood flow, which is 20-25% of cardiac output, and the filtration fraction is normally 20% and is the ratio of the glomerular filtration rate to renal plasma flow [49-51]. The total daily volume of fluid filtered by the kidneys at 120mL/min is ~170L/day. However, the average adult human only has between 3-5 liters

of circulating blood and produces approximately 1.5 liters of urine [45, 52]. Therefore, to prevent volume depletion and dehydration, reabsorption of nearly all filtered water and solutes is necessary. [42-44]

The proximal convoluted tubule and thick ascending limb are responsible for the bulk of reabsorption, while the distal convoluted tubule and collecting ducts fine-tune the filtrate components/composition This reabsorption occurs through active transport, secondary active transport, and passive diffusion [42-44], and the active transport is performed primarily through the Na^+/K^+ ATPase pump. The Na^+/K^+ ATPase pump moves 3 Na^+ ions out of the cell and 2 K^+ ions into the cell against their respective concentration gradients. The action of the Na^+/K^+ ATPase pump creates a low intracellular sodium level and a net negative charge in the cell, allowing for passive diffusion of sodium from the filtrate into the tubule cells. Coupling the now passive diffusion of sodium to other solutes allows secondary active transport through cotransporters (sodium-glucose) or exchangers (sodium-hydrogen) to not require any additional energy. Additionally, the Na^+/K^+ ATPase pump plays a crucial role in both the development and maintenance of a well-differentiated, polarized epithelial phenotype in epithelial cells [53]. When Na^+/K^+ ATPase pump activity is inhibited, the polarization of epithelial cells is impeded, resulting in the disruption of tight junction structure and function [54]. Loss of appropriate cell polarization and tight junctions in kidney tubule epithelial cells will impair their ability to properly reabsorb solutes from the filtrate. Furthermore, decreased Na^+/K^+ ATPase pump is considered a marker of epithelial to mesenchymal transition (EMT), and in this study down was down regulated by the TGF-β1 [55]. Proper renal function is dependent on healthy tubule epithelial cells that have appropriate mitochondrial mass and Na^+/K^+ ATPase pump activity.

The proximal convoluted tubule, thick ascending limb and distal convoluted tubule cells are highly enriched in mitochondria [43, 56, 57] and use ATP to power reabsorption

through the Na^+/K^+ ATPase pump. The proximal convoluted reabsorbs ~50% of the filtered sodium and water and it reabsorbs almost all the filtered glucose, phosphate, and amino acids. The thick ascending limb is responsible for reabsorbing ions, particularly sodium and chloride, and maintaining the medullary concentration gradient that is crucial to produce concentrated urine. The distal convoluted tubule is responsible for fine-tuning the filtrate composition by reabsorbing ions such as sodium, chloride, and calcium and secreting hydrogen and potassium ions. The collecting ducts are responsible for further adjusting the filtrate composition by reabsorbing water, sodium, and bicarbonate ions, as well as secreting hydrogen and potassium ions.

The reabsorptive capacity of the tubules is remarkable, as demonstrated by the fact that a GFR of 170L/day and a plasma sodium concentration of 140mEq/L results in filtration of over 23,000 mEq of sodium per day. This far exceeds the normal dietary intake of sodium, which ranges from 80-250 mEq/day. To maintain normal plasma sodium levels, the tubules must reabsorb over 99% of the filtered sodium. If there is damage or injury to the tubules which inhibits their ability to maintain this high level of reabsorption a compensatory drop in GFR will occur [58]. Failure to maintain proper sodium reabsorption can quickly lead to hyponatremia. Therefore, the tubules play a crucial role in regulating sodium balance in the body, and any disruption to their function can have serious consequences [42-44].

The inability of the proximal tubule cells to produce energy without oxygen makes them highly susceptible to hypoxia, ischemia reperfusion injury, and vasculature damage. Over 90% of the energy production in the kidney occurs through oxidative phosphorylation, and any disruption to oxygen delivery or mitochondrial function can increase the risk of acute kidney injury (AKI) [59]. Elevated levels of glycolysis and increased mitochondrial dysfunction have been identified as hallmarks of various AKI models.

The proximal tubule produce the majority of the required ATP from β-oxidation of fatty acids in the mitochondrial matrix [60] and very little energy through glycolysis [43]. The proximal tubule's reliance on oxidative phosphorylation for ATP production leaves it highly vulnerable to hypoxia, ischemia-reperfusion injury, vascular damage, and mitochondrial toxins [59]. Kidney injury that disrupts oxygen delivery or mitochondrial function are significant risk factors for the development of AKI [60]. Studies have shown that increased glycolysis and mitochondrial dysfunction are hallmarks of various AKI models [61-63].

ACUTE KIDNEY INJURY

Acute kidney injury (AKI) is a complex and heterogeneous disease process that can be caused by a variety of factors, including decreased blood flow to the kidneys, direct damage to the kidneys, or obstruction of urine flow [59, 64, 65]. Hospital admission is a risk factor for developing AKI, with incidences of 15% for adults and 25% for children after admission [1, 65]. In patients receiving intensive care, the incidence of AKI is even higher, with over 50% of patients developing AKI [66]. The development of AKI is associated with an increased risk of progressing to chronic kidney disease (CKD) [6, 9-12, 65]. Additionally, the risk of mortality is increased 5 to 6-fold higher in patients with AKI when compared to patients without AKI [67, 68].

However, diagnosing AKI remains a challenge, as it is a highly heterogeneous group of conditions that share rapid loss of kidney function as an outcome [59, 64, 65]. Serum creatinine level and urinary output, which are used for diagnosis, are neither sensitive nor specific for AKI. Changes in serum creatinine do not correlate closely with the severity of kidney damage nor indicate the cause of AKI. A better understanding of the underlying molecular pathways of AKI is needed to help improve the assessment of its clinical course and enable a diagnosis based on specific molecular pathways.

AKI can be caused by several factors, including sepsis, major surgery, cardiorenal syndrome, kidney hypoperfusion, systemic inflammation, exposure to nephrotoxins, postrenal urinary tract obstruction, and intra-abdominal hypertension. The broad clinical spectrum raises the question of whether different etiologies of kidney injury activate distinct pathophysiological mechanisms or whether they share a common final pathway. Several studies have identified nephron segment-specific gene expression changes in response to diverse stimuli that can lead to AKI, suggesting that substantially different molecular categories of AKI exist. Even etiologies that were traditionally thought to be related activate functionally unrelated signal transduction pathways and trigger responses in different regions of the kidney, which suggests distinct rather than shared pathologies. [59, 64, 65]

Tracking the incidence and prevalence of Acute Kidney Injury (AKI) is a challenging task due to the varying clinical markers used to diagnose and the broad spectrum of disease classifications [69]. In an attempt to provide measurable criteria to universally define the stages of kidney injury, the Acute Dialysis Quality Initiative proposed the Risk/Injury/Failure/Loss/ESRD (RIFLE) classification for AKI in 2004 [70], followed by the Acute Kidney Injury Network (AKIN) classifications in 2007 [71]. Subsequently, the Kidney Disease: Improving Global Outcomes (KDIGO) group published guidelines combining the RIFLE and AKIN definitions in 2012 [72]. These guidelines were developed to provide measurable criteria to universally define the stages of kidney injury using serum creatinine and urine output.

In conclusion, AKI represents a highly heterogeneous group of conditions that share rapid loss of kidney function as an outcome. The current diagnostic approaches using serum creatinine level and urinary output are neither sensitive nor specific for AKI, and changes in serum creatinine do not correlate closely with the severity of kidney damage nor indicate the cause of AKI. The occurrence of different mechanism of AKI

pathology or markers is relevant to the development of novel strategies for renoprotection, and a better understanding of its underlying mechanisms might help to improve the assessment of the clinical course of AKI.

BIOMARKERS OF AKI

Acute kidney injury (AKI) is defined by a rapid deterioration of kidney function [59, 64, 65]. Clinical markers, such as decreased urine output, elevated serum creatinine (SCr), and blood urea nitrogen (BUN), are currently used to diagnose AKI, but these markers are neither sensitive nor specific for AKI.[65]. Additionally, changes in SCr do not correlate with the severity of kidney damage nor point to the cause of the kidney damage, and their levels are affected by a variety of factors, including age, race, sex, body weight, metabolism, and protein intake. BUN has similar limitations to SCr and only elevates after the renal injury has occurred [69, 73-75].

To address the limitations of clinical markers, new biomarkers that are more specific and sensitive for kidney damage have been sought after. Neutrophil gelatinase-associated lipocalin (NGAL) and kidney injury molecule 1 (Kim-1) are two of the newer biomarkers that have shown promise in diagnosing AKI.

Neutrophil gelatinase-associated lipocalin (NGAL), 25-kDa polypeptide of the lipocalin superfamily, was initially identified in human neutrophil gelatinase [76]. NGAL was first discovered as a biomarker after it was elevated in multiple animal models of AKI [77-79]. NGAL is a rapid response protein to tissue injury, and while elevated during AKI events, NGAL is also elevated during acute and chronic inflammatory conditions [80]. NGAL is released by activated neutrophils during bacterial infections and systemic inflammation, making its use as a biomarker of AKI more complex [81]. NGAL can be assayed from blood or urine, but urinary NGAL appears to carry higher specificity for AKI [82]. Urinary NGAL is approved in Canada and Europe for diagnosing AKI [83, 84].

Kim-1 is a transmembrane cell surface receptor on epithelial and lymphoid/myeloid cells. Kim-1 is a scavenger receptor that removes oxidized LDL particles and interacts with phosphatidylserine to allow apoptotic cells to undergo phagocytosis. Under normal conditions, Kim-1 expression in proximal tubule cells is minimal, but after ischemic or nephrotoxic insult, expression of Kim-1 is significantly upregulated in proximal tubule cells [85, 86]. Kim-1 elevation occurs within 1-3 hours of kidney injury, making it a very early signal of damage [82]. Additionally, urinary excretion of Kim-1 has been approved by the FDA and EMA for preclinical assessment of nephrotoxicity [80, 82].

Despite the development of newer biomarkers, the pathophysiology of AKI remains a complex process that is still not completely understood. The heterogeneity of the kidney in cell type, function, tissue oxygenation, and metabolism further complicates our ability to develop protective measures from AKI [59]. While early recognition and management of AKI are critical to patient outcomes, continued research is necessary to better understand the pathophysiology of AKI and improve our ability to diagnose and manage this complex disease process.

ETIOLOGY OF AKI

AKI can be caused by several factors, including sepsis, major surgery, cardiorenal syndrome, kidney hypoperfusion, systemic inflammation, exposure to nephrotoxins, postrenal urinary tract obstruction, and intra-abdominal hypertension. The process of AKI varies according to the primary insult, but all end with reductions in kidney function. Given the complexity of the kidney and multiple causes of AKI, the classification of AKI is challenging. There are multiple ways to categorize AKI based on clinical setting, reversibility or response to therapy, general mechanism of injury, primary affected anatomical compartment, dominant underlying pathophysiology, or the traditional categories. [59].

The traditional categories of AKI are Prerenal, Intrinsic Renal, and Postrenal [75, 87]. Prerenal AKI is the most common cause and is defined as decreased renal perfusion resulting in lower GFR [87]. The most common cause of prerenal AKI is loss of fluid volume, which can result from excessive vomiting or diarrhea or overuse of diuretic drugs. Other causes of prerenal AKI include decreased perfusion from heart failure, systemic vasodilation from sepsis, and changes to intrarenal vasoconstriction via different medications (NSAIDs, ACE-I, ARBs, Antirejection agents) [87].

Intrinsic AKI, on the other hand, is defined by disruption to the internal processes of the kidney and is further divided up into categories based on the primary affected anatomical compartment, including glomerular damage, tubular damage, interstitial damage, and vascular damage. [75]. Acute tubular necrosis (ATN) is the most common cause of intrinsic AKI in hospitalized patients and is usually caused by ischemia or nephrotoxic agents [75, 87].

ATN-induced AKI involves several pathophysiological processes, including endothelial damage, vascular impairment, tubular cell death, and inflammatory/immune response [88]. This process has been divided into four phases, initiation, extension, maintenance, and recovery.

The initiation phase is characterized by functional damage to the tubule cells from ischemia or nephrotoxic agents and subsequent decreases in renal blood flow, further decreasing the oxygen levels and ATP production. These damaged cells epithelial and endothelial cells release cytokines and chemokines, which initiate the inflammatory cascade. The tubule epithelial cells responsible for most of the kidney's reabsorption function begin to undergo morphological changes and lose their brush border membranes. Loss of brush border membranes reduces their surface area and absorptive capacity. Furthermore, during AKI, the function of the tubules is impaired, which can result in increased delivery of sodium to the macula densa. The macula densa then signals the

afferent arterioles to constrict and reduce the blood flow to the glomerulus. This is known as the tubuloglomerular feedback mechanism and is a critical component of renal autoregulation [58]. Lastly, tubule cells start to undergo apoptosis or necrosis, and the dead cells slough off, leading to tubular obstruction. [75].

During the extension phase of AKI, the initial ischemic or nephrotoxic insult causes persistent hypoxia and inflammatory response. The kidney's heterogeneity of tissue oxygenation results in some areas being more vulnerable to damage than others. In the cortex, oxygen levels return to near-normal levels, and tubule cells start to recover and undergo repair. However, the corticomedullary junction and outer medullary region have lower perfusion levels, leading to cell injury and ongoing apoptosis/necrosis. As cell death occurs in the corticomedullary junction and outer medulla, the glomerular filtration rate (GFR) continues to decline. Furthermore, the production and release of cytokines and chemokines continues in these regions during this phase, which stimulate the inflammatory cascade [75].

The maintenance phase of AKI marks the beginning of repair, increased cell migration, apoptosis, and proliferation as cells attempt to maintain tubule integrity. During this phase, the decline in GFR halts as tubule cells begin to dedifferentiate and migrate towards the damaged area and reestablish tissue structure. Additionally, tissue perfusion returns to baseline during this phase, indicating the recovery of kidney function. It is important to note that the extension and maintenance phases of AKI are not always distinct and can overlap, making it challenging to predict the timing and extent of kidney function recovery [75].

During the recovery phase of acute tubular necrosis, the reestablishment of tubule epithelial cell polarity and structure leads to the restoration of normal cellular and organ function. However, for a full recovery to occur, it is crucial for proinflammatory and profibrotic cells to be cleared. The extent of recovery depends on various factors and

repeated insults can hinder the repair process and result in chronic impairment. Therefore, successful management and prevention of future injury are crucial for the restoration of kidney function and overall patient health [75].

In contrast to prerenal injury, acute tubular necrosis does not recover immediately after removing the nephrotoxic agent or reperfusing the kidney. This is due to the time required for the replenishment of lost tubular cells, which may necessitate renal replacement therapy in severe cases [75, 87].

Acute glomerular damage is a common cause of AKI, resulting from acute inflammation of the blood vessels and glomeruli, leading to loss of renal function. Systemic illnesses such as systemic lupus erythematosus, arthritis, viral infections, and pulmonary-renal syndromes are among the most common causes of glomerulonephritis [75, 87].

AKI can also result from damage to the interstitial tissue of the kidney, commonly caused by allergic reactions to medications or infections. Acute interstitial nephritis generally resolves once the causative agent is removed [75].

The kidney accounts for less than 1% of total body weight but receives over 20% of cardiac output [47, 48], making them highly susceptible to vascular damage-induced AKI. Damage to the intrarenal blood vessels results in decreased perfusion and lower GFR. Arterial catheterization, hypercoagulation disorders, and vascular surgery are common causes of intrarenal vascular damage [75, 87].

Postrenal causes of AKI are a result of obstruction to urine flow. In older men, prostate hyperplasia is a common cause of postrenal AKI. Identification and removal of the obstructing object generally result in a return to baseline [75, 87].

Currently, markers of AKI can only diagnose the condition after the injury has occurred, and renal function has already declined. There are currently no FDA-approved agents to prevent or treat AKI. A better understanding of the disease process is needed to develop potential treatments. It was previously believed that if renal function returned

to baseline after an AKI incident, there would be no long-term consequences [8]. However, recent studies have indicated that patients who develop AKI are up to 10 times more likely to develop chronic kidney disease (CKD) [6, 9-12]. Even patients that do not develop clinical AKI are at risk for long-term declines in renal function [13, 14].

In summary, AKI is a complex disease with a wide range of etiologies that can be classified into traditional categories, including Prerenal, Intrinsic Renal, and Postrenal. Acute tubular necrosis is the most common cause of intrinsic AKI, and its pathophysiology involves four phases. A better understanding of the underlying pathophysiological mechanisms of AKI may help to identify novel therapeutic targets to improve patient outcomes.

CHRONIC KIDNEY DISEASE

CKD affects over 20 million Americans, and over 500,000 have end-stage renal disease (ESRD) [15]. Globally there are estimated to be 800 million people with CKD and the incidence and prevalence are increasing [3-5]. CKD is a heterogeneous disorder characterized by a gradual persistent loss of kidney function for greater than 3 months [8, 89] Clinically CKD is defined as the presence of albuminuria, a marker for kidney damage or decrease in GFR for a duration of greater than 3 months [8, 89]. There are many different insults to the kidney that can lead to CKD. Kidney fibrosis is a common pathway in the development of CKD, regardless of the initial cause of the disease [8, 90, 91]. The most common causes of CKD are diabetes and hypertension [15]. AKI, however, is becoming more recognized as a potential cause of CKD, even after recovery from initial nephrotoxic insult [8]. Additionally, more studies have shown that multiple nephrotoxic events leading to AKI also increase the likelihood of developing CKD [9, 14, 92].

The most common cause of AKI is acute tubular necrosis (see above). After an AKI event, the kidney utilizes a wound healing process to recover from the insult. However, the repair process can go astray if subsequent insults occur during this time resulting in

maladaptive repair. Maladaptive repair during an AKI event can lead to renal fibrosis and CKD [8].

MALADAPTIVE REPAIR & KIDNEY FIBROSIS

Fibrosis is a pathological process that leads to tissue scarring, it occurs when there is damage to tissue, resulting in inflammation, activation and migration of myofibroblasts, and matrix deposition and remodeling of normal tissue architecture [8, 90, 91]. Fibrosis is defined as increased expression and deposition of structural extra cellular matrix (ECM) including proteins such as collagens and fibronectin. Although efforts have been made to understand the mechanisms of kidney fibrosis and develop therapeutic strategies, there has been little to no success, and no treatment specifically targets kidney fibrosis. The risk of kidney fibrosis is increased with age and from repeated insults of nephrotoxic agents leading to a maladaptive repair process [8]. Maladaptive repair refers to the incomplete recovery following an AKI event, which can result in abnormal kidney structure and impaired function. Maladaptive repair is characterized by renal fibrosis, vascular rarefaction, tubular necrosis/apoptosis, glomerulosclerosis, and infiltrating inflammatory cells within the kidney [8].

In the maintenance phase of AKI, tubule cells begin to dedifferentiate and repopulate lost epithelium. Under normal healing conditions, these cells enter the cell cycle and proliferate to maintain tissue structure [93]. Tissue repair is a complex process that requires significant metabolic activity. Adequate mitochondrial mass and mitochondrial respiration are necessary for cell replication, cell growth, and synthesis of macromolecules and proper resolution of injured tissue [94]. In the maladaptive repair process, these cells undergo cell cycle arrest and become senescent. These senescent cells can adopt a secretory phenotype which is associated with the release of transforming growth factor-beta (TGF-β1) and connective tissue growth factors (CTGF). TGF-β1 is a cytokine that is considered the master regulator of fibrosis and promotes the development

glomerular and tubulointerstitial fibrosis [95]. CTGF is secreted protein with low levels of expression in normal healthy kidneys. Following injury CTGF is released by tubular epithelial cells and endothelial cells. CTGF then promotes TGF-β1 activity and release from fibroblast and tubule epithelial cells [96]. CTGF and TGF-β1have been associated with chronic inflammation, collagen deposition, and vascular rarefaction [8, 90, 91].

These secretory senescent cells affect other epithelial cells, pericytes, and the immune system. Particularly these cytokines increase the production of activated myofibroblasts [88]. Fibroblast activation, characterized by α-SMA expression and the production of a large amount of ECM components, is the most important event in kidney fibrogenesis rarefaction [8, 90, 91]. These activated myofibroblasts are considered the primary source of collagen deposition and fibrotic matrix. Activated myofibroblasts are essential to the normal healing process where they deposit extra cellular matrix (ECM), which acts as a scaffold to maintain tissue structure integrity in damaged tissue. Under maladaptive conditions, the myofibroblasts are overstimulated, leading to excessive deposition of ECM and renal fibrosis. The accumulation of ECM in renal tissue starts to disrupt normal tissue structure, impair function, and lead to CKD [97, 98]. In the normal healing process, extra ECM is degraded, and profibrogenic myofibroblasts are removed. However, repeated nephrotoxic events or chronic injury can lead to inadequate removal of ECM, resulting in long-term organ fibrosis [98].

Injured tubule cells release multiple soluble factors including sonic hedgehog (SHH), WNTs, and TGF-β1 that results in the activation of fibroblast [90]. Additionally, Kim-1 is a significant biomarker for tubule injury, and its expression increases drastically in response to tubule damage in both humans and rodents [85, 86]. It plays a crucial role in promoting the clearance of apoptotic cells by tubular epithelia, which is vital for endogenous kidney repair following injury [99]. However, prolonged expression of Kim-1 is linked to a profibrotic phenotype and increased leucocyte recruitment to the injured

kidney [100]. This suggests that Kim-1 may provide a link between injury and fibrosis, where chronic expression of Kim-1 can lead to maladaptive repair and development of fibrosis. The injured tubule cell population can undergo partial EMT, cell-cycle arrest, senescence, and apoptosis, leading to tubular atrophy [101]. Chronic exposure to multiple sublethal injuries can lead to premature cell senescence, causing a failure to respond to subsequent injury with correct adaptive repair. Additionally, repeated insults may cause tubular cells to remain in a dedifferentiated state, continuing to produce profibrotic factors that contribute to the development of fibrosis [8, 90, 91].

The injured tubule cells also secrete proinflammatory cytokines and chemokines, leading to the activation of toll-like receptors (TLR). TLRs are a class of cell-surface proteins that are responsible for activating the innate immune response. Tubule epithelial cells express TLR, and during AKI events, these receptors are activated, resulting in the production of tumor necrosis factor-alpha (TNF-α), monocyte chemoattractant protein 1 (MCP-1), and interleukin 6 (IL-6). Increased cytokine production leads to immune cell recruitment to the damaged kidney [88]. These immune cells are part of the normal healing process and help remove necrotic cells and debris. Chronic production of these cytokines can lead to overactivation of the immune cells and maladaptive repair [8].

Repeated nephrotoxic insults impair the normal healing process in the kidney and can result in maladaptive repair. The maladaptive repair process contributes to the loss of kidney function as normal tissue structure is not restored in the kidney following injury. Chronic inflammation and excessive fibrosis are characteristics of the maladaptive repair process.

Kidney fibrosis is not uniform across the tissue but develops in specific areas of injury. The reason why certain sites of injury repair normally and others progress to fibrosis is unknown. Recent work has proposed the idea of a fibrogenic niche or microenvironment that promotes fibroblast activation and the accumulation of extra cellular matrix (ECM)

[90]. Similar to the features of maladaptive repair, the fibrogenic niche that promotes fibrosis in CKD patients is characterized by fibroblast activation, persistent inflammation, tubular atrophy, and vascular rarefaction [8, 90, 91]. The trigger for the formation of the fibrogenic niche after kidney injury is unknown, but it is believed that the release of soluble factors following initial tubular injury triggers interstitial fibroblasts to express Tenascin-C (TNC), which is the primary organizer of the fibrogenic niche [102]. Decellularized kidney tissue scaffolds are a model system to investigate the effect of the fibrogenic niche on kidney cells. The kidney tissue scaffolds have no cellular contents, extracellular vesicles or soluble factors, but do contain structure and composition of the ECM. When kidney cells are seeded onto kidney tissue scaffolds from fibrotic kidneys, fibroblasts proliferate, tubular cells undergo EMT, macrophages are activated, and endothelial cells undergo apoptosis. These results suggest the ECM of the fibrotic niche is able to induce fibrosis and recruit adjacent cells to in a similar phenotype.

Targeting and disrupting the maladaptive repair process and the formation of the fibrogenic niche may represent a promising and innovative therapeutic approach for the treatment of fibrosis and CKD. By interrupting the signaling pathways and molecular interactions, it may be possible to prevent the activation of fibroblasts, the induction of epithelial-to-mesenchymal transition, and the recruitment of inflammatory cells that lead to tissue fibrosis. Such therapies could provide a significant improvement over existing treatments, which often focus on symptomatic relief and do not address the underlying disease mechanisms.

CISPLATIN

Cisplatin is a widely used and highly effective chemotherapeutic agent for the treatment of various solid-organ cancers, including head, neck, testicular, breast, ovary, and lung. [39]. Its approval for the treatment of testicular cancer led to an increase in

remission rates from 5% to 80% [40]. However, its usage is limited by its nephrotoxicity, with 30% of patients developing acute kidney injury (AKI) [39].

The systematic chemical name of cisplatin is *cis*-Diamminedichloroplatinum (II). Cisplatin is an inorganic water-soluble planar molecule consisting of only 11 atoms. Its molecular structure features a single central platinum atom surrounded by two chloride and two ammonium atoms in the cis position. Although it was first synthesized in 1845 [103], its structure remained unknown until Alfred Werner published his transformative paper in 1893 detailing the co-ordination theory of complex compounds and revealed the chemical structure of cisplatin. Alfred would go on to receive a Noble Prize in Chemistry for this work in 1913 [104, 105]. Platinum molecules were thought to have no biological activity until Barnett Rosenberg at Michigan State University accidentally discovered its cytotoxicity in 1965 [38, 103]. Dr. Rosenberg's laboratory was investigating the effects of electricity on bacterial cell growth. To deliver the current to culture media, they used platinum electrodes and observed that the addition of electrical current stopped the cell division of bacterial cells. Two years later, the laboratory discovered that electricity was causing the release of platinum molecules, which were responsible for inhibiting bacterial cell growth and they were using platinum electrodes to deliver the current to culture media [106]. Building on this discovery, the Rosenberg laboratory demonstrated that cisplatin to inhibit tumor growth of sarcoma 180 and leukemia L1210 cells, and reduce tumor size in a rat sarcoma model [107]. By 1972, the National Cancer Institute began clinical trials using cisplatin for advanced testicular cancer, leading to its FDA approval for testicular, ovarian, and bladder cancer in 1978 [38]. Cisplatin was the first inorganic heavy metal used for cancer chemotherapy and changed how inorganic molecules were viewed [108]. Cisplatin’s mechanism of action involves the formation of DNA, RNA, and protein adducts, which in turn inhibits DNA synthesis and replication of rapidly dividing cells [109, 110].

The effectiveness of cisplatin is impaired by its dose-limiting side effect, nephrotoxicity. AKI is a serious concern for patients receiving cisplatin, with up to 30% of patients developing this life-threatening condition [39]. AKI from cisplatin can prevent effective cancer treatment, often requiring a change in therapy or dosage reduction. Although newer derivatives of cisplatin, such as carboplatin and oxaliplatin, have reduced nephrotoxicity, they are often less effective in treating certain types of cancer [41]. Cisplatin would be a much more effective cancer treatment if this toxicity could be prevented; however, there are currently no therapies approved to prevent or treat cisplatin-induced AKI. Understanding how cisplatin induces nephrotoxicity and AKI is crucial to our ability to develop preventative measures.

AKI and CKD are interconnected syndromes [6] and each AKI event increases the likelihood of developing CKD. While the incidence of AKI after a single dose of cisplatin is 30%, most patients receive multiple cycles of the drug over the course of several weeks or months. One study found that repeated cycles of cisplatin almost tripled the risk of developing CKD [14]. Patients who develop stage 3 CKD (GFR < 60 ml/min) after multiple cycles of cisplatin now fall into a patient group that are at increased risk of reduced overall survival and cancer-related mortality [111, 112]. Understanding the mechanisms behind the development of CKD from repeated cycles of cisplatin is critical to improving outcomes for these patients.

CISPLATIN'S MECHANISMS OF NEPHROTOXICITY

Cisplatin's nephrotoxicity correlates with the patient's dose, frequency, and cumulative exposure [113]. Renal cells are exposed to high levels of cisplatin [47], the kidney receives between 20-25% of the cardiac output while only accounting for less than 1% of the body weight. Cisplatin in the blood is uncharged and is cleared from the body by the kidney via glomerular filtration and tubular secretion [114]. Cisplatin, once inside the cell, becomes charged and has been shown to accumulate in kidney tubule epithelial

cells, leading to cisplatin concentrations higher in the kidney than in the blood [39]. Copper transporter (Ctr1) and the organic cation transporter (OCT2), both of which are highly expressed on proximal tubule cells, transport cisplatin intracellularly and increase their susceptibility to cisplatin toxicity [115]. In vitro studies have shown that downregulating Ctr1 in kidney cells protects against cisplatin toxicity by reducing uptake into the cell [116], and coadministration of OCT2 substrate reduces cisplatin uptake and toxicity [117, 118]. In vivo work has shown that the knockout of OCT2 protects mice from cisplatin nephrotoxicity [119, 120]. Cisplatin-induced nephrotoxicity involves multiple mechanism including proximal tubule cell damage, increased oxidative stress, inflammatory response, and vascular injury [39, 115, 121].

The mechanism of cisplatin toxicity is through its interaction with DNA [109, 122, 123]. High concentrations of chloride in the blood limit the replacement of cisplatin's two chloride ligands, but once inside the cell, cisplatin is hydrolyzed, and the chloride ligand is replaced by a water molecule [123, 124]. This hydrolyzed cisplatin is a reactive positively charged electrophile that forms adducts with nucleophilic sites on DNA, RNA, and protein[122, 123], inhibiting the cell's ability to synthesize DNA and resulting in cell cycle arrest of rapidly dividing cells[109, 110]. Cisplatin is able to bind to DNA and form a variety of adducts, including monoadducts, DNA-protein cross-links, interstrand cross-links, and the most common intrastrand cross-link adducts.

The belief that cisplatin's anti-tumor effects occur primarily through binding to nuclear DNA has been challenged by in vitro studies. In vitro work has shown that only a small percentage of cellular platinum is bound to nDNA, and sensitivity to cisplatin cell death poorly correlates with the extent of nDNA platination [125]. Additionally, this study found that cisplatin-DNA adducts bind at a higher level in mtDNA compared to nDNA, and there is a lack of removal of adducts in mtDNA [126]. This concept was further supported by experiments showing that enucleated cells, which lack nDNA, are susceptible to

cisplatin-induced apoptosis, independent of nDNA damage. By comparison, etoposide, known DNA damaging agent, was not able to induce apoptosis in these enucleated cells, indicating that cisplatin had unique cytosolic targets [127].

More recent studies indicate that cisplatin primarily targets mitochondria and mtDNA leading to toxicity. [128]. When cisplatin is converted into a positively charged species, it accumulates in mitochondria, which have a negative charge, and this accumulation is thought to contribute to cisplatin's toxicity [39, 129]. Furthermore, the density of mitochondria and their membrane potential have been found to correlate with the degree of sensitivity to cisplatin[130, 131]. Depletion of mtDNA using ethidium bromide has been shown to result in cells that are highly resistant to cisplatin toxicity [130]. Since mitochondria lack effective DNA repair mechanisms, mtDNA is more susceptible to cisplatin-induced DNA damage than nDNA [132-134]. These findings provide compelling evidence that mitochondria and mtDNA are critical factors in the toxicity of cisplatin.

The tubule cells in the proximal convoluted tubule, thick ascending limb, and distal convoluted tubule have high mitochondrial density [43, 56, 57, 135], and we believe this makes them highly susceptible to cisplatin-induced toxicity. Additionally, proximal tubule cells express both Crt1 and OCT2 making them very sensitive to cisplatin toxicity. Proximal tubule cells produce the majority of their energy from β-oxidation of fatty acids in the mitochondrial matrix [60]; cisplatin has been shown to disrupt mitochondrial energetics and fatty acid oxidation [136-138]. Defective fatty acid oxidation has been associated with a decline in renal function and the development of renal fibrosis [139-141]. Increasing fatty acid oxidation protected from cisplatin nephrotoxicity in vivo [137, 138]. Additionally, damage or loss of mtDNA from cisplatin leads to a loss in mitochondrial protein levels and a disruption of the mito-nuclear protein ratio leads to reduced respiratory capacity and malfunctioning proximal tubule cells [142, 143]. Cisplatin also induces cell death in tubule cells via multiple mechanisms including the extrinsic pathway activated through death

receptors, the intrinsic mitochondrial pathway, and the endoplasmic reticulum stress pathway [39].

Cisplatin-induced inflammation is a significant mechanism of nephrotoxicity that has been extensively studied in the context of cisplatin-induced kidney injury. Injured tubule cells release endogenous intracellular molecules known as damage-associated molecular patterns (DAMPs), which activate Toll-like receptors (TLRs). The activation of TLRs by DAMPs can result in a positive feedback loop where high levels of tissue damage lead to a pro-inflammatory response, resulting in more tissue damage and chronic inflammation [144].

Studies have shown that cisplatin treatment is associated with increased expression of many different proinflammatory cytokines and chemokines, including interleukin 1 beta (IL-1β), IL-6, MCP-1, and TNF-α [115, 121]. Cisplatin-induced inflammation occurs through TLR4, as TLR4 knockout mice are resistant to cisplatin-induced nephrotoxicity as compared to wild type mice [145]. Ramesh and Reeves used TNF-α knockout mice and a pharmacological inhibitor of TNF-α and demonstrated that both models provided protection against cisplatin-induced kidney injury [146]. Inhibition of TNF-α signaling also reduced the production of other key pro-inflammatory mediators, highlighting the role of TNF-α in the development of inflammation in cisplatin-induced kidney injury. Furthermore, Maekawa et. al. demonstrated how cisplatin induces mitochondrial damage and leakage of mtDNA into the cytosol. Cytosolic mtDNA activates the cGAS-STING pathway leading to inflammation which contributes to the development of cisplatin-induced kidney injury [147], again highlighting the importance of mitochondria in cisplatin-induced kidney injury.

Cisplatin's nephrotoxicity is not limited to tubule cell death and inflammation but also involves damage to vascular endothelial cells. This damage causes vasoconstriction,

leading to reduced renal blood flow creating a more hypoxic environment in the kidney, and there a subsequent drop in GFR. The resulting hypoxic conditions further exacerbate tubule cell death and inflammation. The mechanism of cisplatin's nephrotoxicity involves tubule cell death, inflammation, and vascular damage; these pathways are interconnected and show the complexity of cisplatin-induced kidney injury [121].

The nephrotoxicity of cisplatin has been a problem since it was first introduced into the clinic. Multiple strategies have been developed to prevent cisplatin toxicity. The adjunct treatment with hydration regimens and the use of diuretics such as mannitol have been tried with mixed results [148]. Additionally, reduction in dose and extension in the duration of administration time have been adopted. Unfortunately, there are no preventative measures approved for cisplatin-induced AKI. The current clinical guidelines recommend pre-hydration with normal saline and avoiding the use of diuretics for patient receiving cisplatin therapy [149]. However, there is still a need for more effective preventative measures to reduce the incidence and severity of cisplatin-induced nephrotoxicity.

MODELS OF CISPLATIN TOXICITY

Approximately 30% of patients receiving cisplatin treatment develop acute kidney injury (AKI), which is characterized by elevated levels of blood urea nitrogen (BUN) and serum creatinine (SCr), indicating a rapid decline in renal function [39]. In the past, it was believed that if renal function recovered after an AKI incident, there would be no long-term consequences [8]. However, recent studies suggest that patients who experience AKI are at a higher risk of developing chronic kidney disease (CKD) [6, 9-12] and even those who do not develop clinical AKI are at risk for long-term declines in renal function] [13, 14]. For the remaining 70% of patients who have subclinical kidney damage following cisplatin treatment, little is known about their risk of developing CKD.

Traditionally, the standard model of cisplatin-induced kidney injury has been to use a single high dose (10-30 mg/kg) of cisplatin. This model leads to high levels of tubular

necrosis, rapid decline in renal function, and is fatal to mice within 3-4 days of cisplatin administration [150, 151]. While this model has allowed researchers to identify the mechanisms underlying AKI in patients receiving cisplatin, it does not permit long-term studies [40, 151]. In the clinic, patients are usually treated with periodic low doses of cisplatin over weeks to months, rather than a single high dose. The single high dose model of cisplatin toxicity is not a clinically relevant way to study cisplatin induced AKI to CKD.

Given the limitations of the previous approaches, the Siskind Lab and others have recently developed repeated low dose cisplatin (RLDC) models that more closely mimic the dose regimen of cisplatin in the clinic and enables the study of long-term impacts on the kidney and the transition from AKI to CKD [150-158]. In the RLDC model, mice receive 7-9 mg/kg cisplatin once a week for four weeks. The mice treated with the RLDC regimen can survive 6 months following treatment. Published data from various studies suggest that the RLDC model induces a low level of repeated injury, leading to fibrosis and progression to CKD [152-157]. Importantly, the cellular processes induced in the kidney by the RLDC model differ greatly from those induced by a single high dose of cisplatin [152-157]. Notably, the mild injury caused by RLDC, which may not meet the clinical criteria for AKI, can still progress to CKD [152].

The RLDC model can be divided into two distinct phases: the injury and progression phases. During the four-week injury phase, mice are subjected to mild cisplatin-induced kidney damage, resulting in a decline in kidney function, cell-cycle arrest, ER stress, increased levels of kidney damage markers (such as Kim-1 and NGAL), inflammation, and the development of fibrosis [152-157]. The progression phase begins when the nephrotoxic agent is removed, and the markers of AKI return to baseline levels. However, persistent inflammation, increased fibrosis, and the development of CKD still occur [152-157]. Although mice show only mild increases in BUN levels during the injury phase, they experience a progressive and permanent loss of kidney function, leading to

higher BUN levels compared to vehicle-treated mice and the injury phase counterparts after six months of treatment. These results suggest that mice experience kidney function deterioration and progression following the RLDC regimen, even without elevated clinical markers of AKI during the injury phase [152]. The cellular biology of each phase is significantly different, and the mechanisms involved in both phases of the RLDC model are still not fully understood [153]. Identifying these mechanisms is crucial to identifying potential therapeutic targets for cisplatin-induced kidney injury.

Recent work on the RLDC model has helped shed light on the mechanism driving AKI to CKD transition from RLDC. This study used single-nucleus transcriptional profiling to analyze the changes in gene transcriptional profiles at the single-cell level in the kidneys of mice following RLDC [159]. The study identified a unique proximal tubule cell population that co-expressed proliferation markers (Ki-67) and proximal tubule injury marker (Kim-1), indicating their significance in tubular repair and recovery after cisplatin treatment. The study also identified several new proximal tubule injury responsive genes and revealed the induction of key inflammatory chemokine and cytokine genes in proximal tubule cells after cisplatin treatment. Additionally, this study investigated the mechanisms behind repeated cisplatin-induced kidney injury in mice, focusing on DNA damage caused by each injection [160].. The study found that administering higher doses (10mg/kg compared to 6mg/kg) of cisplatin repeatedly in a shorter interval led to severe DNA damage in renal tubular cells. Although normal quiescent renal proximal tubular cells have low rates of cell proliferation, in response to tubular injury and cell death, the surviving tubular epithelial cells enter the cell cycle and rapidly proliferate. Active proliferation of tubular epithelial cells after repeated cisplatin-induced kidney injury did not lead to complete repair and may have promoted kidney injury by exposing the dividing cells to more cumulative DNA damage. The study concluded that the dose, frequency, and interval of cisplatin administration determines the severity of DNA damage, and robust DNA damage was

observed when higher doses of cisplatin were repeatedly administered in a shorter interval. Additionally, single low doses of cisplatin produce mild recoverable injury, however with repeated administration of cisplatin the kidney injury is exacerbated. These studies helped uncover the distinct injury/repair tubule cells population in a proinflammatory failed-repaired state, which provides strong evidence that repeated dosing of cisplatin induces a maladaptive repair state leading to the development of CKD and fibrosis. Understanding these molecular mechanisms underlying kidney repair after injury may contribute to the development of new therapies for chronic kidney disease. Mitochondrial dysfunction has been identified as a key contributor to the development and progression of CKD [161-163]. The effects of RLDC on kidney mitochondria has not been investigated.

MITOCHONDRIAL BIOGENESIS

Mitochondria are vital intracellular organelles with a multitude of functions, including ATP production, co-factor synthesis, amino acid metabolism, calcium homeostasis, regulation of cellular redox state, and innate immune signaling [164, 165]. The dysfunction of mitochondria can lead to an imbalance in these processes, ultimately leading to cell death and tissue damage. In recent years, numerous studies have highlighted the importance of mitochondrial quality control in kidney injury and repair, as well as potential therapeutic approaches targeting mitochondrial dysfunction in kidney injury, inflammation, and disease [161-163]. Additionally, research has shown that mitochondrial dysfunction plays a critical role in the transition from AKI to CKD [166]. Therefore, understanding the pathophysiology of mitochondrial dysfunction in RLDC induced injury is important to our understanding of the disease process and development of CKD.

The kidney cortex contains an abundance of mitochondria and consumes a high amount of oxygen per unit of tissue [56, 167]. The tubule cells located in the cortex play a

crucial role in reabsorption, utilizing active and passive transport mechanisms to maintain homeostasis [42-44]. The proximal convoluted tubule, thick ascending limb and distal convoluted tubule cells are highly enriched in mitochondria [43, 56, 57]. The reabsorption process is powered by the Na^+/K^+ ATPase pump, which relies on functional mitochondria to generate ATP. Loss of mitochondrial function results in reduced ATP levels and decreased Na^+/K^+ ATPase pump activity, leading to increased delivery of Na^+ in the distal tubule and compensatory reduction in GFR via tubuloglomerular feedback [58]. Additionally, decreased expression of Na^+/K^+ ATPase pump is a marker of epithelial to mesenchymal transition [55].

In addition, inherited genetic mitochondrial diseases frequently coincide with renal impairment, with the most common kidney-related manifestations being tubular defects [168-172]. For instance, Fanconi Syndrome is a mitochondrial cytopathy characterized by tubular defects and resulting electrolyte disturbances. The proximal tubule cells are particularly reliant on mitochondrial function, as they cannot synthesize ATP anaerobically from glycolysis [173].

Each mitochondrion has its own circular genome, and there are multiple copies (100-10,000) per cell [133, 134]. Mitochondria are dynamic organelles with inner and outer membranes that undergo continuous fusion and fission events, collectively known as mitochondrial dynamics [161]. The balance between fusion and fission processes is essential for maintaining mitochondrial morphology, and excessive activation of either process can lead to fragmentation or hypertubulation, ultimately resulting in mitochondrial dysfunction[161]. Mitophagy is a selective autophagy process that degrades damaged mitochondria. During AKI events, damaged mitochondria are cleared via mitophagy and need to be replaced with new mitochondria. New mitochondria are created from existing ones by a process called mitochondrial biogenesis. Mitochondrial biogenesis (MB) involves the production of new mitochondrial mass and replication of mtDNA. MB and

replication of mtDNA occurs independent of the cell cycle unlike replication of nDNA [133]. The regulation of MB is complex and involves a set of transcription factors that link environmental cues to the cellular energy status and adaptive stress response. The master regulator of MB is a transcriptional coactivator, peroxisome proliferator-activated receptor-γ coactivator-1α (PGC-1α) [141, 174-176].

PGC-1α was identified in brown adipose tissue as a cold-inducible regulator of adaptive thermogenesis in 1998 by the Spiegelman laboratory [177]. The name is derived from the originally identified interaction between the PGC-1α protein and PPARγ (peroxisome proliferator-activated receptor-γ) protein. The Spiegelman laboratory would go on to show PGC-1α's role in mitochondrial biogenesis. They demonstrated that PGC-1α activated the transcription factor Nrf-1 (Nuclear Respiratory Factor 1), which subsequently leads to the expression of Tfam (Transcription factor A, mitochondrial) and other nuclear-encoded mitochondrial proteins [178]. The PGC-1α protein is interesting, as it does not directly bind to DNA, but it binds to other transcription factors already bound at their respective response elements. The binding of PGC-1α to the already bound transcription factors coactivates them to exert their regulatory effect [141, 163, 174-176]. PGC-1α is highly expressed in metabolically active tissues such as the heart, kidneys, liver, skeletal muscle, brain, and brown adipose tissue.

PGC-1α is a key transcriptional regulator of various pathways, such as mitochondrial biogenesis, fatty acid oxidation, lipogenesis, thermogenesis, and glucose metabolism[141, 174-176]. The expression of PGC-1α can be induced by diverse stimuli, including exercise, fasting/nutrient deprivation, hypoxia, cAMP activation, and oxidant stress. The primary transcription factors that regulate PGC-1α expression are myocyte enhancer factor-2 (MEF2), activating-transcription factor 2 (ATF2), and cAMP response element-binding protein (CREB). The promotor region for PGC-1α contains binding sites for MEF2, ATF2, and CREB that increase the expression of PGC-1α. ATF2 and CREB

bind to the CREB-responsive element (CRE) site, and MEF2 binds to its own specific site on the PGC-1α promotor. Additionally, PGC-1α expression can be suppressed by external stimuli, including pro-inflammatory and pro-fibrotic mediators. The pro-inflammatory factor, TNF-α, activates NF-κB, which leads to epigenetic downregulation of PGC-1α via histone H3 deacetylation [179]. Furthermore, Notch signaling and its downstream target Hes1, a profibrotic transcription factor, directly bind to the PGC-1α promoter region and inhibit its expression [180]. TGF-β1 also leads to decreased PGC-1α levels through epigenetic downregulation by stimulating the activation of Smad3 [140]. Additionally, long noncoding RNA (lncRNA) taurine-upregulated gene 1 (Tug1) interacts with PGC-1α, acting as a scaffold and allowing PGC-1α to bind to its own promoter and increase its expression [181]. Activation of TLRs by various stimuli can also lead to decreased PGC-1α expression through the MEK1/2, ERK1/2 pathway, which interacts with CREB [182].

Post-translational modifications play an important role in regulating the activity and stability of PGC-1α, as well as determining which transcription factor interacts with it. Phosphorylation, acetylation, and methylation are among the modifications that can affect PGC-1α. Multiple serine and threonine sites on PGC-1α can be phosphorylated by several kinases, including p38 MAPK, AKT, AMPK, S6 kinase, and GSK3β. AMPK and p38 MAPK phosphorylation activates PGC-1α, while AKT inhibits activity and GSK3β increases its degradation[141, 174-176]. The half-life of the PGC-1α protein is only 2-3 hours, and the phosphorylation p38 MAPK also helps stabilize the PGC-1α protein, allowing for a longer activity window [183]. Additionally, PGC-1α can be activated by deacetylation of lysine residues by SIRT1 and methylation of arginine residues by PRMT1(protein arginine methyltransferase 1) [141, 174-176]. These findings highlight the fine-tuned and highly responsive nature of PGC-1α expression and activity, which allow the cell to adjust gene expression in response to changes in energy and metabolic demand.

Mitochondria house more than 1,500 proteins, almost all of which are encoded by the nuclear genome. The mitochondrial genome, in contrast, only encodes two ribosomal RNAs, 22 transfer RNAs, and 13 messenger RNAs required for the formation of electron transport chain super-complexes [133, 134, 184]. As proper mitochondrial function necessitates coordination between mitochondrial genes encoded by the nucleus and those by the mtDNA, any inhibition or damage to mtDNA replication or synthesis can decrease steady-state levels of mtDNA-encoded proteins. This decrease leads to a mito-nuclear protein imbalance and reduction in cellular respiration [133, 134, 184]. As mentioned earlier, PGC-1α governs NRF-1 (Nuclear Respiratory Factor 1) expression, a transcription factor that oversees the transcription of nuclear-encoded electron transport chain components, such as β-ATP synthase, cytochrome c, and cytochrome c oxidase subunits. NRF-1 also triggers the expression of Tfam (Transcription factor A, mitochondrial), which translocate from the nucleus to the mitochondria, where it fully coats mtDNA, organizes its structure, and is critical for mtDNA maintenance[185]. Tfam binds to and activates transcription at the two major promoters of mtDNA [186]. Tfam's indispensability is evident from the embryonic lethality of global Tfam knockout mice [187] and the renal inflammation and fibrosis that occur by six weeks of age upon tubule-specific deletion of Tfam [188]. Through regulation of NRF1/2 and Tfam, PGC-1α controls the expression of mitochondrial proteins encoded in both the nuclear and mitochondrial genome.

Increased mitochondrial electron transport chain activity can result in elevated production of reactive oxygen species (ROS), which, in excess, can cause DNA damage and cell death. Therefore, PGC-1α is also involved in upregulating enzymes necessary for ROS detoxification. PGC-1α induces expression of the antioxidant enzymes superoxide dismutase, catalase, and glutathione peroxidase [189, 190].

PGC-1α is highly expressed in the proximal tubule cells [191]. However, studies on human biopsies from patients with AKI/CKD have shown reduced levels of PGC-1α compared to normal kidney tissue [140, 192, 193]. In addition, kidney tissue from patients with diabetic kidney disease has been found to have lower PGC-1α expression and dysregulated mitochondrial function when compared to healthy controls [193]. Reduced mitochondrial bioenergetics can lead to dysfunctional tubule cells and overall loss of renal function [139]. PGC-1α is a regulator of energy metabolism and respiratory capacity and decreased levels of this protein result in reduced mitochondrial bioenergetics and a decline in renal function.

Several studies have examined the role of PGC-1α in both AKI and fibrosis models [179, 192, 194-205]. During AKI, damaged mitochondria are removed from cells via mitophagy and need to be replaced by the generation of new mitochondria via MB. PGC-1α is the master regulator of mitochondrial biogenesis and bioenergetics; increasing PGC-1α expression has provided protection against ischemia-reperfusion injury (IRI) [192, 203-205], sepsis [200, 201], folic acid [179, 196-199], and single high dose cisplatin [194, 195, 206] induced AKI. PGC-1α has also been identified as a key mediator in renal fibrosis and CKD development [140, 141, 163, 176, 180, 193]. Studies by the Susztak lab have shown that restoring mitochondrial energetics through increased fatty acid oxidation protects against folic acid-induced kidney fibrosis [140].

In mouse models of global and renal proximal tubule-specific PGC-1α knockout, both PGC-1α null mice were unable to recover from sepsis-induced AKI when compared to wild-type mice [207]. Additionally, *in vitro* work from the Schnellmann lab showed that the overexpression of PGC-1α in proximal tubular cells produced a significant increase in mitochondria number, respiratory capacity, and intracellular ATP and improved recovery

from oxidative damage. This suggests increasing PGC-1α levels after an AKI may promote repair and recovery [208].

Our hypothesis is that repeated administration of cisplatin damages the mitochondria in tubule cells, leading to reduced ATP levels, impairs the energy intensive repair process, and lowers Na^+/K^+ ATPase pump a marker of EMT, ultimately causing renal function to decline. In the microenvironment created by RLDC, the kidney is exposed to high levels of inflammatory (TNF-α, IL-6, NLRP3) and fibrotic (TGF-β1) mediators [152-157] which suppress PGC-1α [140, 179, 207]. Insufficient PGC-1α levels impair the kidney's ability to recover properly from injury, resulting in a maladaptive phenotype and progression to CKD. We propose that targeting PGC-1α is particularly promising in the RLDC model, as it is involved in both AKI and renal fibrosis/CKD development.

OVERALL GOALS & SPECIFIC AIMS

Cisplatin is a commonly used chemotherapeutic for many solid organ cancers, but up to thirty percent of cancer patients treated with cisplatin develop AKI [39]. AKI is a life-threatening condition defined as a rapid decrease in renal function [209]. AKI and CKD are interconnected syndromes [6] and each AKI event increases the likelihood of developing CKD. Most patients in the clinic will receive multiple cycles of cisplatin over week to months and repeated cycles of cisplatin increase the development of CKD almost three-fold [14]. There is great need to understand the mechanism driving the development of CKD from repeated cycles of cisplatin, and as there a no FDA approved treatments for CKD or kidney fibrosis. Cisplatin-induced nephrotoxicity has been studied extensively [39, 115, 121, 210, 211], and most of this work has been completed in mouse models without cancer. We believe the altered physiology of cancer patients is not adequately represented in these models, and adding the comorbidity of cancer to this model will further our understanding of the pathophysiology.

Preclinical models of cisplatin-induced nephrotoxicity have failed to include the critical variable of cancer and only patients with cancer will receive cisplatin therapy. There is a need to understand how the comorbidity of cancer affects the nephrotoxicity of cisplatin. Additionally, our preliminary results show that RLDC model reduces kidney function, induces kidney injury and the development of fibrosis, along with reducing mitochondrial content and PGC-1α expression. Further work is needed to determine the role of kidney mitochondrial biogenesis in cisplatin-induced CKD.

The goal of this dissertation is to increase the clinical relevancy of the RLDC model by including the comorbidity of lung cancer and determine if the 5HT-$_{1F}$ agonist can protect from cisplatin-induced CKD through increased kidney mitochondrial biogenesis and content. These goals will be met via three aims: **Aim 1**: Determine if 5HT-$_{1F}$ agonist, LY344864 will protect from RLDC induced AKI-CKD development. **Aim 2:** Use multiple mouse models of lung cancer in combination with RLDC regimen to determine if lung cancer enhances the nephrotoxicity of cisplatin. **Aim 3**: Determine if 5HT-1F agonist LY344864 will protect from cisplatin induced nephrotoxicity in mice with subcutaneous lung cancer. Understanding how lung cancer alters kidney biology and sensitizes the kidney to cisplatin toxicity is vital to our ability to develop nephroprotective strategies.

CHAPTER 2: KIDNEY MITOCHONDRIAL CONTENT AND BIOGENESIS ARE REDUCED BY REPEATED LOW DOSE ADMINISTRATION OF CISPLATIN.

INTRODUCTION

Cisplatin is a widely used and highly effective chemotherapeutic agent for the treatment of various solid-organ cancers, including head, neck, testicular, breast, ovary, and lung. [39]. Its approval for the treatment of testicular cancer led to an increase in remission rates from 5% to 80% [40]. However, its usage is limited by its nephrotoxicity, with 30% of patients developing acute kidney injury (AKI) [39]. AKI is a life-threatening condition characterized by a rapid decline in renal function, and its onset from cisplatin treatment often necessitates a change in therapy or dosage reduction, preventing effective treatment [209]. While newly developed cisplatin derivatives have reduced nephrotoxicity, they are less effective in treating many forms of cancer [41]. Limiting cisplatin toxicity would increase the therapeutic potential in cancer patients, however, there are currently no therapies approved to prevent or treat cisplatin-induced AKI.

Despite the high incidence of AKI associated with cisplatin use, it is still prescribed in 10-20% of all cancer patients as part of their treatment regimen [38]. In the past, it was assumed that if renal function recovered after an AKI incident, there would be no long term consequences [8]. However, recent studies indicate that patients who develop AKI are 10 times or more likely to develop chronic kidney disease (CKD) [6, 9-12]. Even patients that do not develop clinical AKI are at risk for long term declines in renal function [13, 14]. We have previously shown that the RLDC is a model of CKD development, via mild decline in renal function, increased kidney injury, inflammation, and development of interstitial fibrosis [152-157].

The kidney has unique anatomy and physiology which allows it to maintain balance of the body's extracellular fluids. The relatively small plasma volume of the average adult male is filtered 30 to 50 times a day through the kidney. The filtered solutes and water must be efficiently reabsorbed for survival. The proximal convoluted tubule and thick ascending limb are responsible for the bulk of reabsorption, while the distal convoluted tubule and collecting ducts fine-tune the filtrate components/composition. The proximal convoluted tubule, thick ascending limb and distal convoluted tubule cells are highly enriched in mitochondria [2, 12, 13] and use ATP to power active transport by the Na^+/K^+ ATPase pump. The action of the Na^+/K^+ ATPase pump creates a low intracellular sodium level and a net negative charge in the cell, which allows passive diffusion of sodium from the filtrate into the tubule cells. The kidneys take advantage of this gradient to efficiently reabsorb other vital solutes via secondary active transport that does not require any additional energy. Mitochondrial function is important to proper kidney function, as shown by inherited genetic mitochondrial diseases that coincide with renal impairment [168-171]. Additionally, tissue repair is energetically demanding, and adequate mitochondrial mass and mitochondrial respiration are required for proper healing [94]. We propose that reduced PGC-1α expression in the tubule cells after each dose of cisplatin prevents these cells from replacing damaged mitochondrial leading to incomplete repair. The injured/failed repair tubule cell population leads to a maladaptive phenotype to develop.

We hypothesize that repeated insults from the administration of cisplatin damages the mitochondria of tubule cells, creating a microenvironment that is pro-inflammatory and pro-fibrotic. The fibrotic niche, high in TNF-α and TGF-β [90] reduces PGC-1α expression that is needed to replace damaged mitochondria leading to an increase in the injured/failed repair tubule cell population. Ultimately resulting in a decline in renal function [139-141]. Our study aims to investigate how kidney mitochondrial content and PGC-1α expression

are affected by RLDC. PGC-1α is a unique target for the RLDC model because of its role in both AKI and the development of renal fibrosis/CKD.

MATERIALS AND METHODS

ANIMALS

B6129SF1/J (B6;129) male mice were purchased from The Jackson Laboratory. B6;129 mice are a first filial generation hybrids that are the offspring of a cross between C57BL/6J females (B6) and 129S1/SvlmJ males (129). Upon arrival, the mice were allowed to acclimate for 1 week prior to the initiation of the experiment. All mice were maintained on a 12-hour light/dark cycle and provided food and water *ad libitum*. All animal procedures were approved by the Institutional Animal Care and Use Committee and followed the guidelines of the American Veterinary Medical Association.

CISPLATIN DOSING REGIMEN

Pharmaceutical grade cisplatin (NDC 16729-288-38, 1mg/ml) was purchased via the University of Louisville Outpatient Hospital Pharmacy. The repeated low dose cisplatin dosing regimen mice were administered cisplatin or vehicle via intraperitoneal (i.p.) injection once a week between 8-9 a.m. for four weeks. In the vehicle group, 400 µL normal saline was administered via i.p. injection. In the cisplatin treatment groups, 7mg/kg or 9mg/kg of cisplatin in normal saline in a total volume of 400 µL was administered via i.p. injection. All mice were administered 500 µL saline by subcutaneous injection 2 days after dose 3 and 1 day before dose 4 to prevent weight loss. All animals were injected with cisplatin at the same time of day as there are circadian influences on the response of the kidney to cisplatin. Animals were euthanized 72 hours following their final cisplatin injection. Upon euthanasia, blood was collected, and plasma prepared and frozen at -80°C; urine was collected and frozen at -80°C; and kidneys were removed, flash-frozen in liquid nitrogen, and stored at -80°C until use. A cross-section of one kidney from each mouse was fixed in 10% neutral buffered formalin for histology.

BLOOD UREA NITROGEN (BUN), SERUM CREATININE (SCR), AND NEUTROPHIL GELATINASE ASSOCIATED LIPOCALIN (NGAL) DETERMINATION

BUN (AMS Diagnostics, 80146) levels were measured from plasma samples using the indicated kits following the manufactures' instructions. ELISAs for NGAL (R&D Systems, DY1857) were performed on the urine as directed by the manufacturer.

PROTEIN QUANTIFICATION AND WESTERN BLOT ANALYSIS

Kidney tissues were homogenized in cell extraction buffer (Thermo Fisher Scientific) containing a Complete Protease Inhibitor Cocktail Tablet and Phosphatase Inhibitor Cocktail Tablets (Roche). Homogenates were centrifuged at 15,000 X g for 10 min at 4° C. Supernatants were removed and stored at -80°C. Protein concentrations were determined using Bradford Reagent (Bio-Rad). 40 µg of kidney homogenate protein were loaded and separated on 4–12% gradient Tris-Glycine-SDS polyacrylamide gels. Protein was then transferred to PVDF membranes that were blocked in 5% (w/v) dried milk in tris buffered saline 0.1% Tween 20 (TBST) for 1 hour. Membranes were incubated with primary antibody overnight at 4°C. The next morning, membranes were washed 3 times for 5 min each with TBST containing 5% (w/v) dried milk. Membranes were then incubated for 2 hours at room temperature with secondary antibodies conjugated with horseradish peroxidase (1:20,000) in TBST containing 1% (w/v) dried milk. Following 2 washes, 1% (w/v) dried milk and 1 wash in TBST membrane proteins were detected by chemiluminescence substrate.

ANTIBODIES

The following antibodies were purchased from Cell Signaling Technology (Beverly, MA): p44/42 MAP Kinase (Erk1/2) #4695, Phospho-p44/42 MAP Kinase (Erk1/2) (Thr202/Tyr204) #4370, Transforming growth factor-beta (TGF-β) #3711, Mothers against

decapentaplegic homolog 2/3 (SMAD 2/3) #8685, Phospho-Smad3 (Ser423/425) #9520. The following antibodies were purchased from Abcam (Cambridge, CB2 0AX, UK): Peroxisome proliferative activated receptor, gamma, coactivator 1 alpha (PGC-1α, abcam, ab54481) and α-Smooth Muscle Actin (α-SMA, abcam, ab5694). The remaining antibodies include fibronectin (F3648, Sigma-Aldrich), and α-tubulin (SC-5286, Santa Cruz Biotechnology).

Rodent Total OXPHOS Antibody Cocktail (abcam, ab110413) contains 5 mouse mAbs, one each against Complex I subunit NDUFB8 (ab110242), Complex II-30kDa (ab14714), Complex III-Core protein 2 (ab14745), Complex IV subunit I (ab14705) and Complex V alpha subunit (ab14748) as an optimized premixed cocktail.

GENE EXPRESSION

RNA was isolated from kidney tissue using E.Z.N.A. Total RNA Kit 1 (OMEGA) per manufacturer's protocol. cDNA was synthesized with High-Capacity cDNA Reverse Transcriptase PCR (Thermo Fisher Scientific) per manufacturer's instructions. Gene-specific cDNA was quantified with real-time qRT-PCR using either predesigned TAQman assays or self-designed SYBR assays. The following TAQman primers were purchased from Thermo FisherScientific: tumor necrosis factor alpha (TNF-α, Mm00443258_m1), chemokine (C-X-C Motif) ligand 1 (CXCL1, Mm04207460_m1), and the housekeeping gene beta-2-microglobulin (B2M, Mm00437762_m1). The following primers were self-designed: kidney injury molecule-1 (Kim-1, Invitrogen, forward: AGATCCACACATGTACCAACATCAA, reverse: CAGTGCCATTCCAGTCTGGTTT), Peroxisome proliferative activated receptor, gamma, coactivator 1 alpha (PGC-1α, Invitrogen, forward: AACAATGAGCCTGCGAACATATT, reverse: TAGCAAGTTTGCCTCATTCTCTTC), Nuclear Respiratory Factor 1 (NRF1, Invitrogen,

forward: GGATTCCAGTCTCTGTGGACAAA, reverse: CCCCCGACCTGTGGAATACT), Transcription factor A, mitochondrial (TFAM, Eurofins, forward: TTTAAAGCTAAACACCCAGATGCA, reverse: TTCTGGTAGCTCCCTCCACAG), TIMP-1, Invitrogen forward: GCAACTCGGACCTGGTCATAA, reverse: TTAGTCATCTTGATCTTATAACGCTGGTA), *NLRP3*, Invitrogen, forward: AAGATGAAGGACCCACAGTGTAACTT, reverse: CAGATTGAAGTAAGGCCGGAATT), and Col1a1, Invitrogen, forward: CGATGGATTCCCGTTCGAGTA, reverse: GTGGACATTAGGCGCAGGAA) qRT-PCR was done with either iTaq Universal Probes Supermix (172-5134, Bio-Rad) or iTaq Universal SYBR Green Supermix (172–5124, Bio-Rad).

MITOCHONDRIAL DNA TO NUCLEAR DNA ASSAY

DNA was isolated from kidney tissue using E.Z.N.A. Tissue DNA Kit 1 (OMEGA) per the manufacturer's protocol. DNA was quantified using Nanodrop, and 5 ng/µl solutions were prepared for each sample. 20ng of DNA was loaded into each well, followed by quantitative PCR using primers designed for specific amplification of particular mtDNA encoded and nuclear-encoded fragments. Primers were designed to evaluate the relative copy number of mtDNA and nDNA. The mitochondrially encoded genes selected were 16S rRNA and ND1, and the nuclear-encoded gene was Hexokinase 2 (HK2) along with the adaptation of the protocol according to previously published work [212]. Forward and reverse primers 16S rRNA, Invitrogen, forward: CCGCAAGGGAAAGATGAAAGAC, reverse: TCGTTTGGTTTCGGGGTTTC, ND1, Invitrogen, forward: CTAGCAGAAACAAACCGGGC, reverse: CCGGCTGCGTATTCTACGTT, HK2, Invitrogen, forward: GCCAGCCTCTCCTGATTTTAGTGT, reverse GGGAACACAAAAGACCTCTTCTGG. qPCR was done with iTaq Universal SYBR Green Supermix (172–5124, Bio-Rad).

CITRATE SYNTHASE ASSAY

Kidney tissues were homogenized in CHAPS solution (1% CHAPS, 150 mM NaCl, 50 mM Tris, 5 mM ETDA) containing a Complete Protease Inhibitor Cocktail Tablet (Roche). Homogenates were centrifuged at 15,000 X g for 10 min at 4° C. Supernatants were removed and stored at -80°C. Protein concentrations were determined using Bradford Reagent (Bio-Rad). Citrate Synthase Assay Kit (Sigma-Aldrich, #:CS0720) was used to determine relative amounts of citrate synthase per kidney cortices. Citrate synthase is the initial enzyme of the tricarboxylic acid (TCA) cycle. The enzyme catalyzes the reaction of acetyl CoA with oxaloacetate to form the citrate. This enzyme is an exclusive marker of the mitochondrial matrix and is used as a proxy for mitochondrial content. The hydrolysis of the thioester of acetyl CoA results in the formation of CoA with a thiol group (CoA-SH). The thiol reacts with the DTNB in the reaction mixture to form 5-thio-2-nitrobenzoic acid (TNB). This yellow product (TNB) is observed spectrophotometrically by measuring absorbance at 412 nm. Eight (8) µg of kidney protein was loaded in triplicate per sample, and a change in absorbance was recorded. The amount of citrate synthase activity was determined using the manufactures' instructions.

HISTOLOGY

Following formalin fixation, kidney tissue was processed and embedded in paraffin. Kidney sections (5 µm) were stained with hematoxylin and eosin (H&E) and periodic acid schiff (PAS). The degree of morphologic changes was determined by light microscopy. The following measures were assessed as an indication of morphologic damage to the kidney after drug treatment: proximal tubule degradation, loss of brush border, tubular casts, proximal tubule dilation, proximal tubule necrosis, presence of inflammatory cells, and interstitial fibrosis.

SIRIUS RED/FAST GREEN STAINING

Kidney sections (5 μm thick) were rehydrated in Histoclear followed by an ethanol gradient. Slides were then dipped in PBS with 0.1% Tween 20 and incubated for 5 minutes. Slides were washed with distilled water twice for 5 minutes each and then incubated in 1.2% (w/v) saturated picric acid (#5860-32, Ricca Chemicals) containing 0.1% sirius red/direct red 80 (#365548, Sigma) and 0.1% fast green FCF (#F7258, Sigma). Slides were then washed with 5% glacial acetic water until the water ran clear. Tissue samples were then dehydrated and fixed using Permount (#17986-01, Electron Microscopy Sciences).

IMMUNOHISTOCHEMISTRY

Kidney sections (5 μm thick) were rehydrated in Histoclear followed by an ethanol gradient. Antigen retrieval was performed in citric acid buffer (pH 6.0) at 95°C in a steamer for 30 min. Endogenous peroxidases were inhibited with 3% hydrogen peroxide and dual endogenous enzyme blocker (Dako) for 10 min, followed by two 5-min PBS washes. Slides were then blocked with avidin for 10 min followed by a PBS wash and then biotin for 10 min followed by a wash in PBS (Dako). Slides were further blocked with 5% normal goat serum in 0.1% TBST for 1 h at room temperature. α-SMA primary rabbit antibody (Abcam) was added to slides at a concentration of 0.5 μg/ml and allowed to incubate at 4°C overnight. Slides were rinsed with PBS for 5 min, three times. Biotinylated goat anti-rabbit IgG antibody (1: 25,000, BA-1000, Vector Laboratories) was added to each section and incubated for 30 min at room temperature. Slides were rinsed twice with PBS (5 min each). Vector ABC reagent (PK-7100, Vector Laboratories) was added to each section and incubated for 30 min at room temperature. Slides were rinsed two times with PBS followed by the addition of 100 μl of DAB substrate for 5-7 min to detect horseradish

peroxidase (SK-4800, Vector Laboratories). Slides were rinsed in distilled water for 5 min, counterstained with modified Mayer's hematoxylin (no. 72804, Thermo Scientific), and then dehydrated in an ethanol gradient to Histoclear followed by mounting with Permount (SP15, Fisher Scientific). Positive staining for α-SMA indicates the presence of myofibroblasts.

STATISTICAL ANALYSIS DATA

Data are expressed as means ± SEM for all experiments. Multiple comparisons of normally distributed continuous data were analyzed by one-way ANOVA, and group means were compared using Tukey post-tests. Nonparametric continuous data were analyzed with a Kruskal-Wallis test followed by a Dunn’s multiple comparison test. The criterion for statistical differences was $p < 0.05$ for all comparisons.

RESULTS

Repeated low-dose cisplatin (RLDC) induces kidney injury in B6;129 mice.

The B6129SF1/J (B6;129) mouse strain was selected as our lab is developing a syngeneic lung tumor model to investigate the nephrotoxicity of cisplatin with the co-morbidity of cancer. Our lab has seen inter-strain variance [158], and the dose of cisplatin required to induce kidney and fibrosis varies. We performed this initial experiment to optimize the dose of cisplatin for the B6;129 mouse strain. B6;129 male mice were injected (i.p.) with pharmaceutical grade cisplatin 7mg/kg, 9 mg/kg, or saline (vehicle) once a week for four weeks (Figure 1B.). All mice were administered 500 µL saline by subcutaneous injection 2 days after dose 3, and 1 day before dose 4 to prevent dehydration. Mice were sacrificed 72 hours following the last dose. Blood urea nitrogen (BUN), neutrophil gelatinase-associated lipocalin (NGAL), and urinary kidney injury molecule-1 (Kim-1) were used to assess kidney damage. Following RLDC, there was an increase in BUN (Figure 2A), NGAL (Figure 2B), and Kim-1 (Figure 2C) levels between vehicle and cisplatin-treated groups. The weights of the mice were monitored throughout the RLDC regimen as a measure of overt toxicity. The was a significant loss of body weight between the vehicle and cisplatin-treated groups and a significant difference between the 7mg/kg and 9mg/kg cisplatin groups (Figure 2D). Renal histological changes were assessed on 5 µm thick H&E and PAS stained sections. The PAS-stained sections show a loss of brush border in the proximal tubule cells from the cisplatin-treated groups (Figure 3). The H&E stained sections show evidence of tubular necrosis, proximal tubule cast formation, inflammatory cells, tubule degeneration, and tubule dilation in the cisplatin groups (Figure 4). These findings suggest that there is an increase in markers of kidney damage and a decline in renal function following the injury phase of the repeated low-dose model of cisplatin-induced kidney injury. Additionally, the kidney function and injury markers together with the histological changes suggest a dose-response to cisplatin-induced kidney injury with

higher levels of loss of function (BUN), weight, kidney injury (Kim-1 and NGAL), loss of proximal tubule brush border, increased cast formation, increased tubule degeneration, and increased tubule dilation following the injury phase of the repeated low-dose model of cisplatin-induced kidney injury in the 9 mg/ Kg dose group than the 7 mg/ Kg dose group.

A

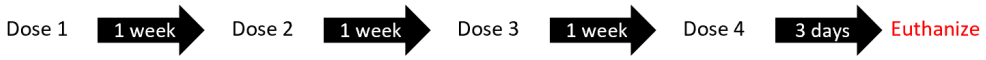

B

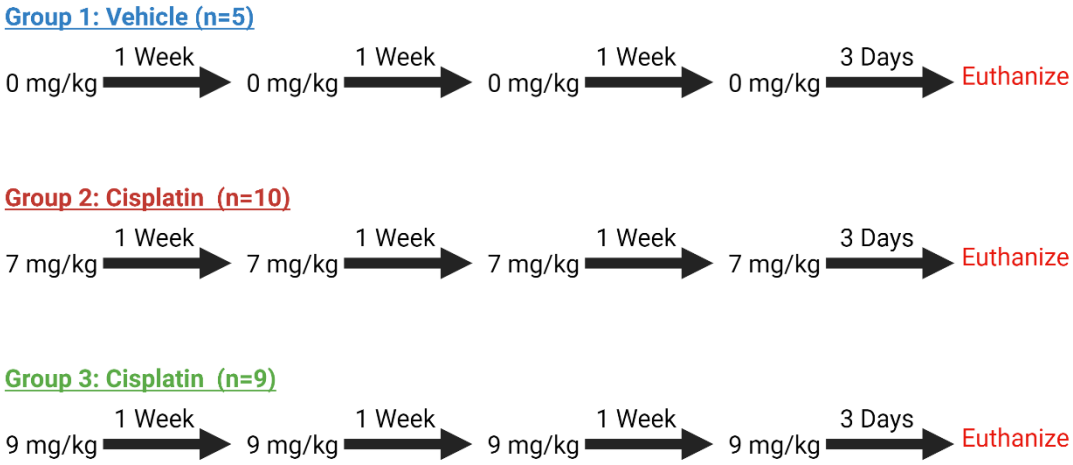

Figure 1. RLDC Experiment Design.

(A) Experiment schematic for RLDC model. (B) Experiment design for the study conducted, B6;129 male mice were injected I.P. with 7-9mg/kg cisplatin or normal saline once a week for four weeks. Mice were euthanized three days following the last dose. Created using BioRender.com.

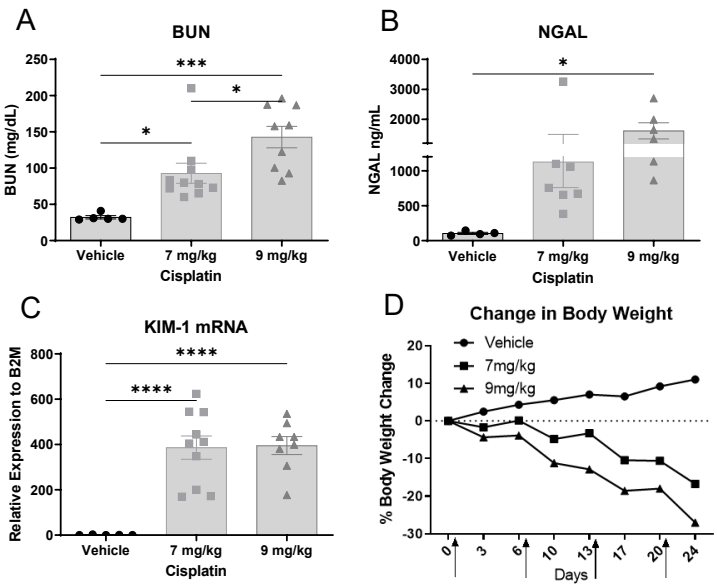

Figure 2. RLDC induced kidney injury.

(A) BUN levels from serum and (B) NGAL levels from urine following 4 doses of cisplatin. (C) Kim-1 mRNA expression from the kidney cortex was measured using qRT-PCR. (D) Percent change in body weight was recorded throughout RLDC regimen as a marker of overt toxicity. Data are expressed as means ± SEM; n=5–10. Statistical significance was determined by 1-way ANOVA followed by Tukey posttest. *p < 0.05, ***p<0.001, ****p < 0.0001

A

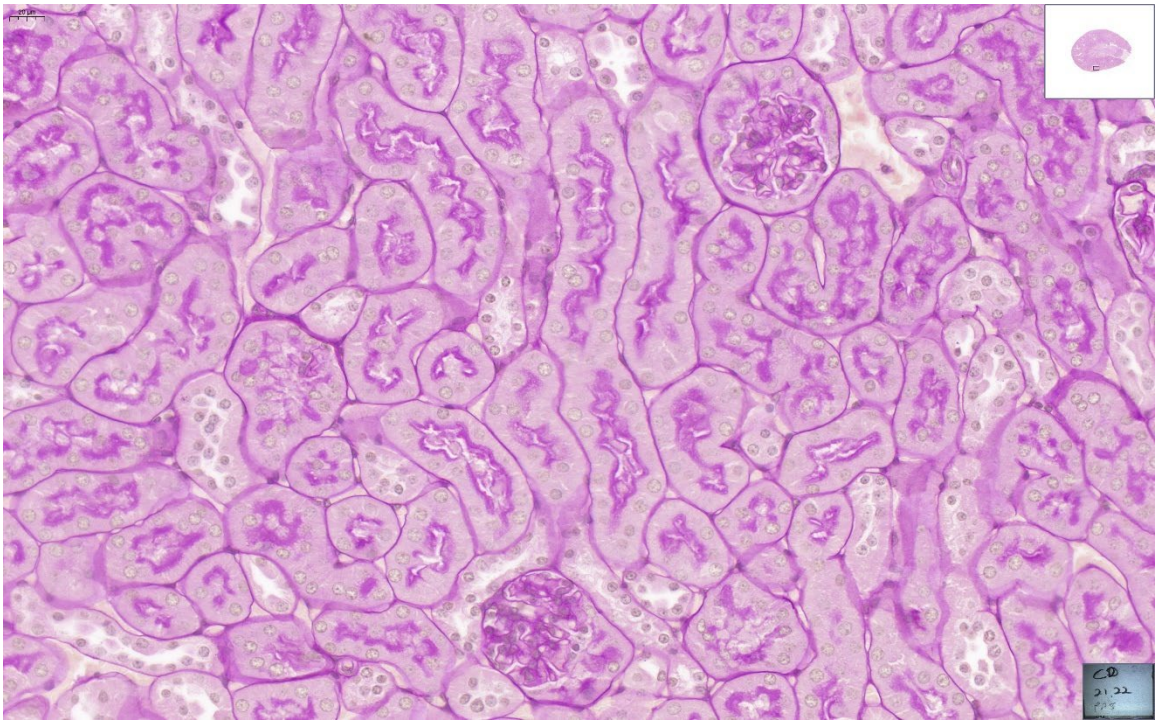

B

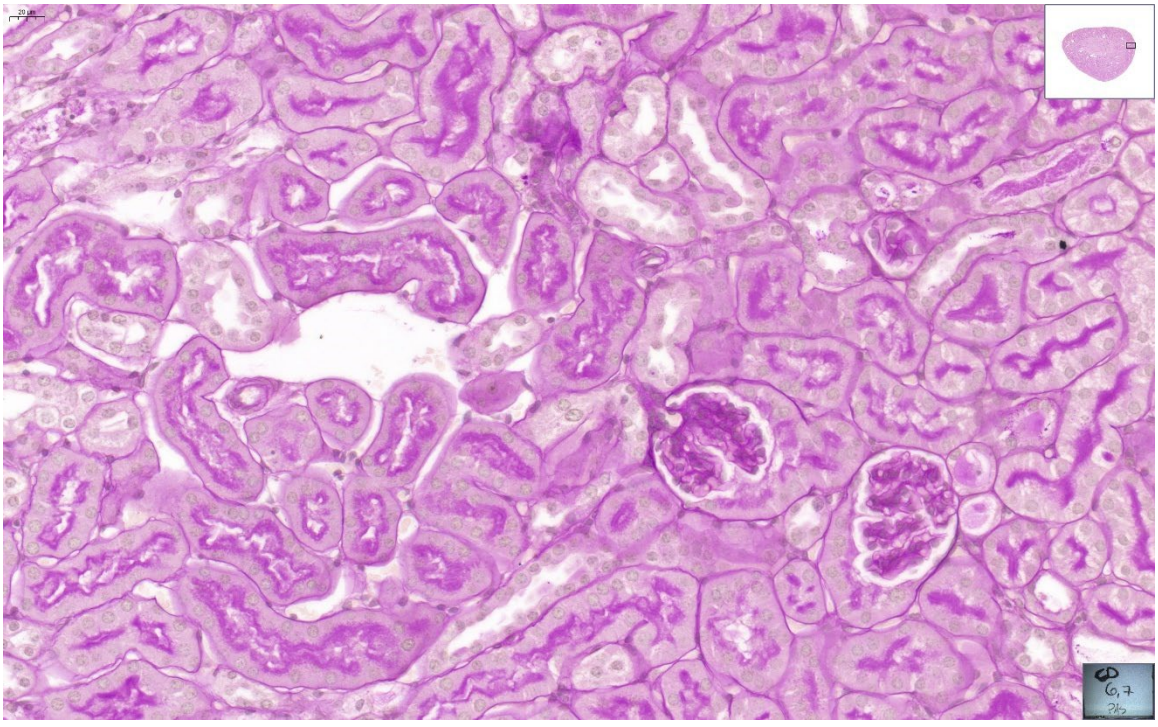

C

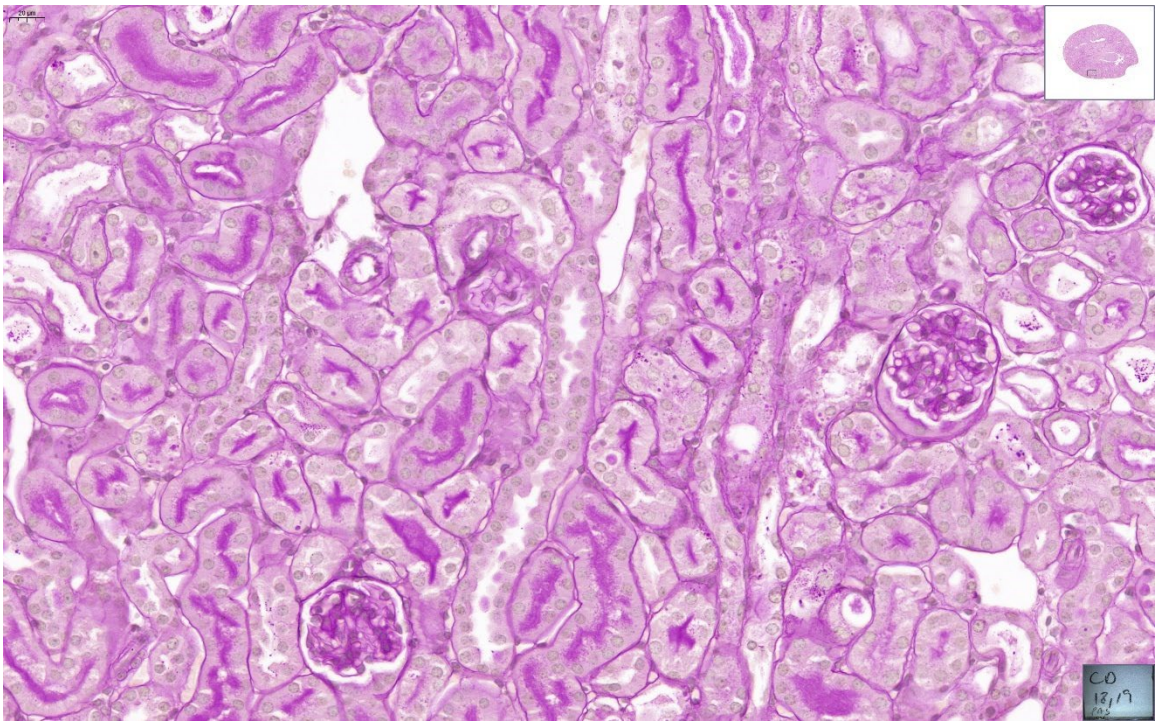

Figure 3. PAS Stain

Renal histological changes were assessed with PAS-stained 5 µm thick sections. PAS is used to identify brush borders of proximal tubule cells. (A) Vehicle Control, (B) 7mg/kg, (C) 9mg/kg. Representative images of renal histology at 40X magnification.

A

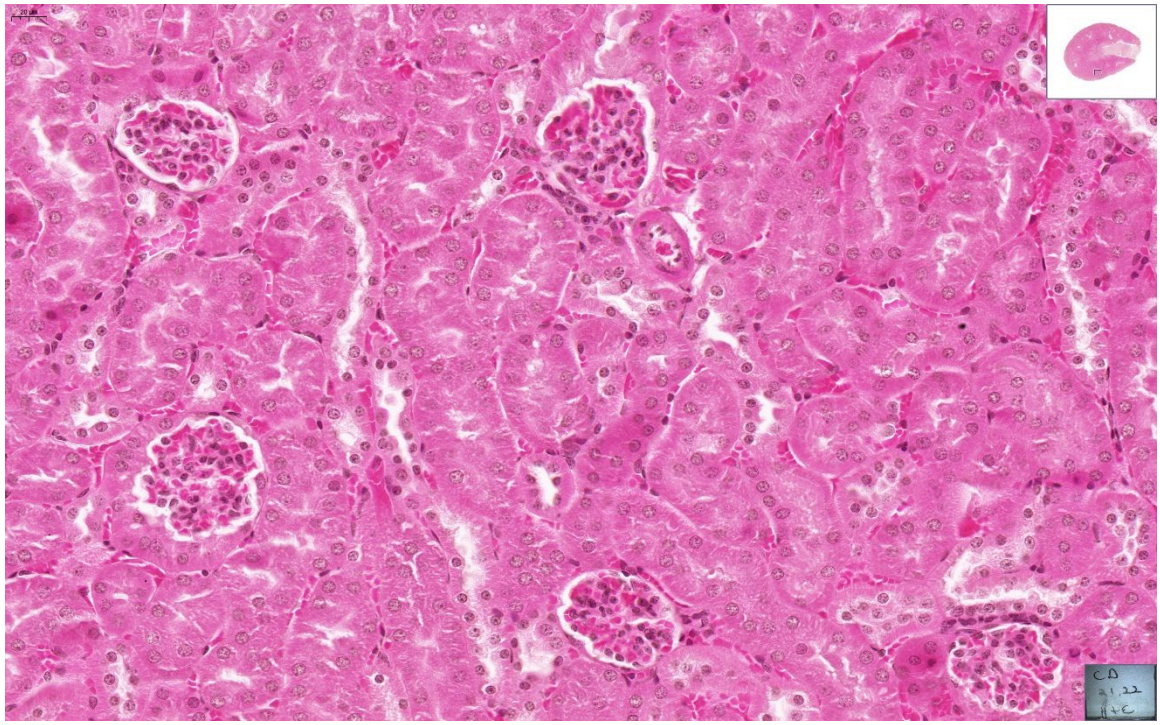

B

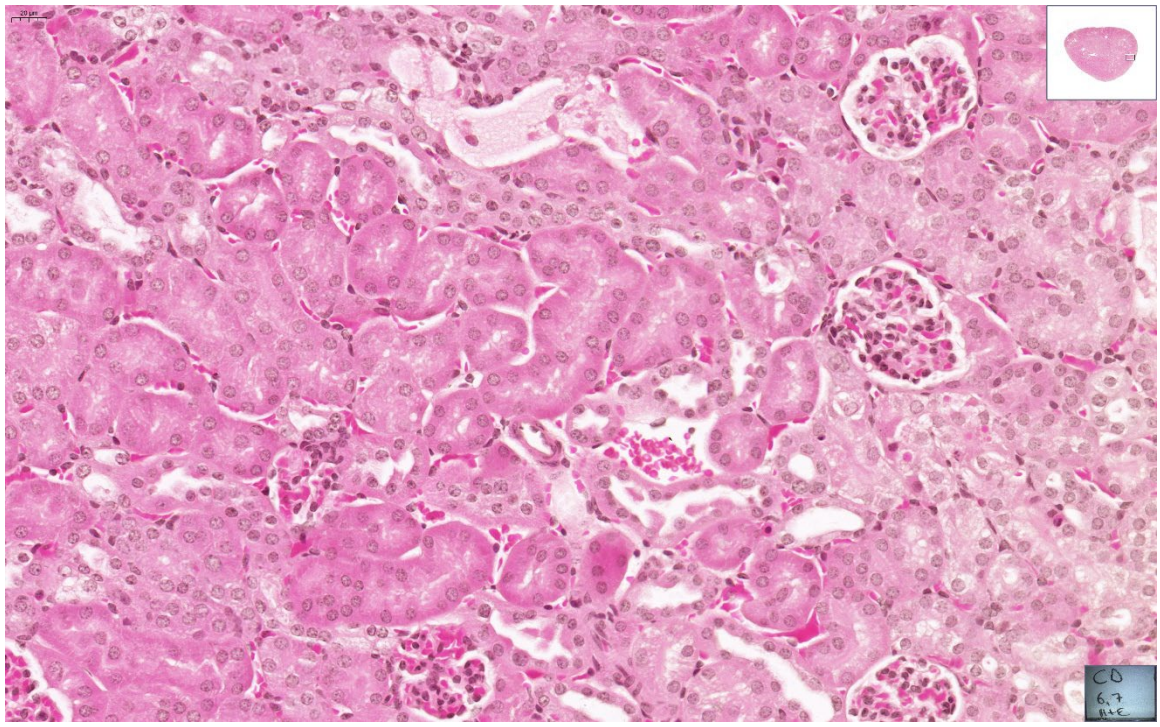

C

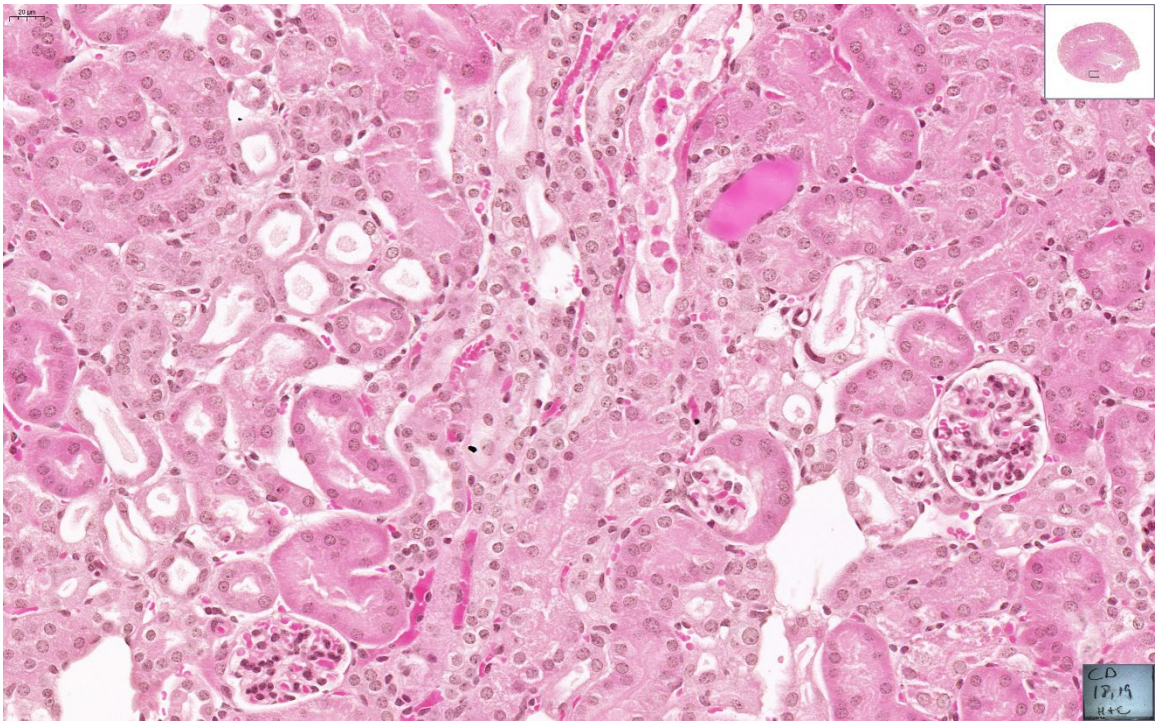

Figure 4. H&E Stain

Renal histological changes were assessed with H&E stain on 5 µm thick sections. H&E stain is used to identify tubular necrosis, proximal tubule cast formation, inflammatory cells, tubule degeneration, and tubule dilation. (A) Vehicle Control, (B) 7mg/kg, (C) 9mg/kg. Representative images of renal histology at 40X magnification.

RLDC induces renal fibrosis. Fibrosis was evaluated via multiple approaches, including histopathology, immunohistochemistry (IHC), western analysis, and real-time qRT-PCR analysis. Sirius red fast green (SRFG) staining indicated collagen accumulation (Figure 5.) and α-smooth muscle actin (α-SMA) IHC (Figure 6.). Positive α-SMA indicates an increased number of myofibroblasts in the kidney following the RLDC regimen and is an indicator of increased fibrosis. Western analysis indicated increased protein levels of fibronectin and α-SMA (Figure 7A) between the vehicle and cisplatin-treated groups. The mRNA expression of markers of fibrosis (TIMP-1, Col1a1) showed a significant increase in the cisplatin-treated groups (Figure 7B, 7C). These findings suggest that there is a significant development of fibrosis following the injury phase of the repeated low-dose model of cisplatin-induced kidney injury.

A

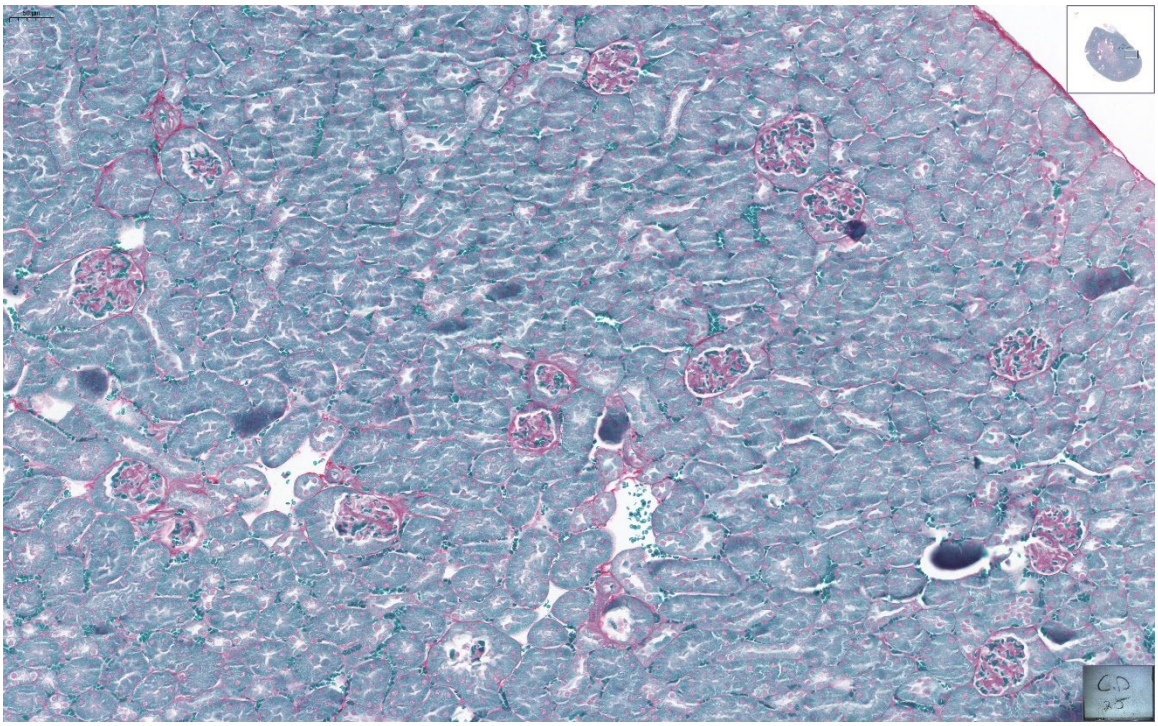

B

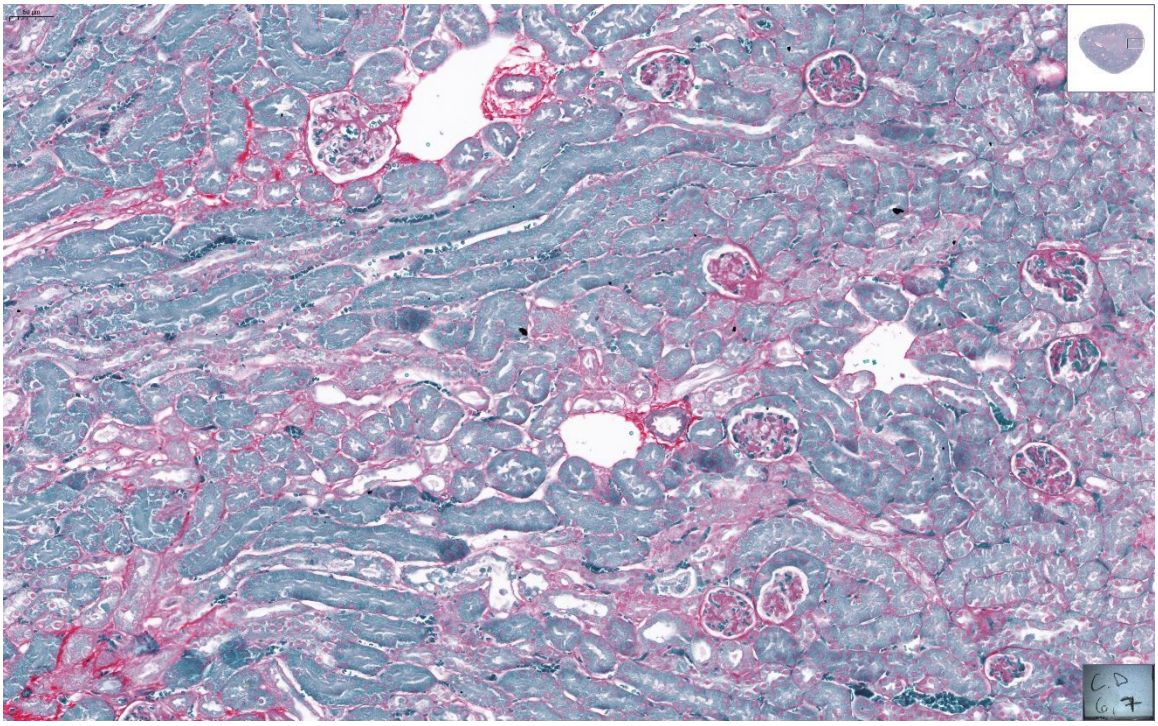

C

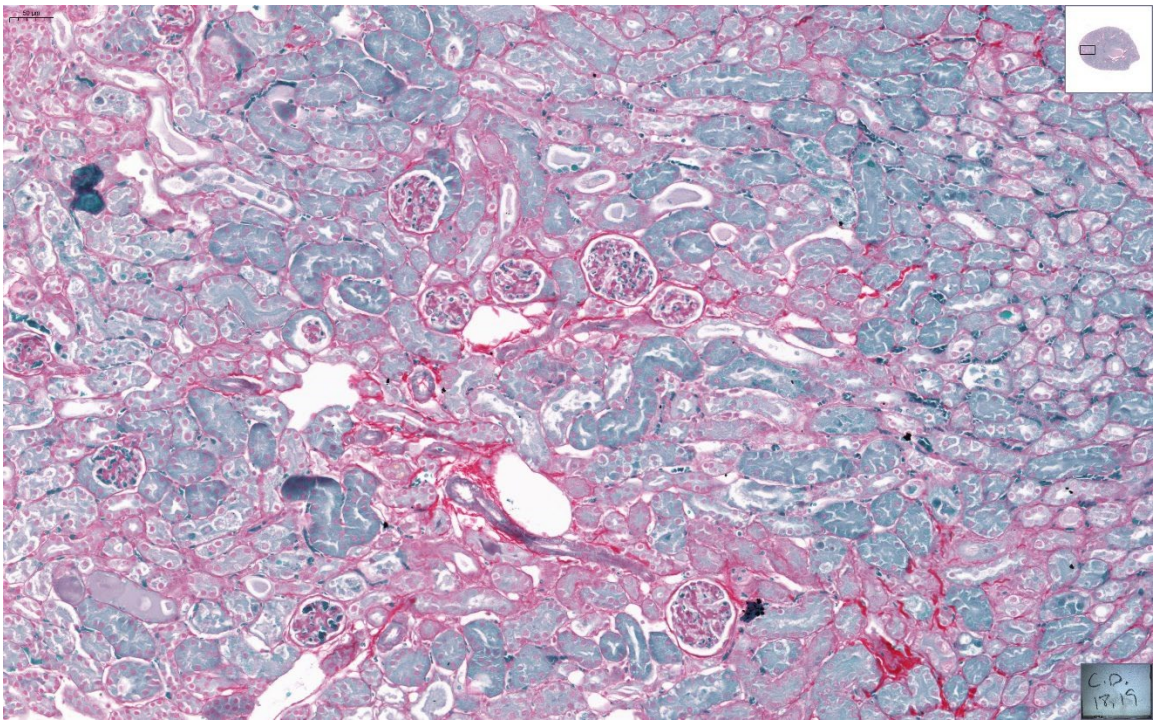

Figure 5. SRFG Stain

Renal histological changes were assessed with SRFG stain on 5 µm thick sections. SRFG stains collagen red and is a marker for interstitial fibrosis. (A) Vehicle Control, (B) 7mg/kg, (C) 9mg/kg. Representative images of renal histology at 20X magnification.

A

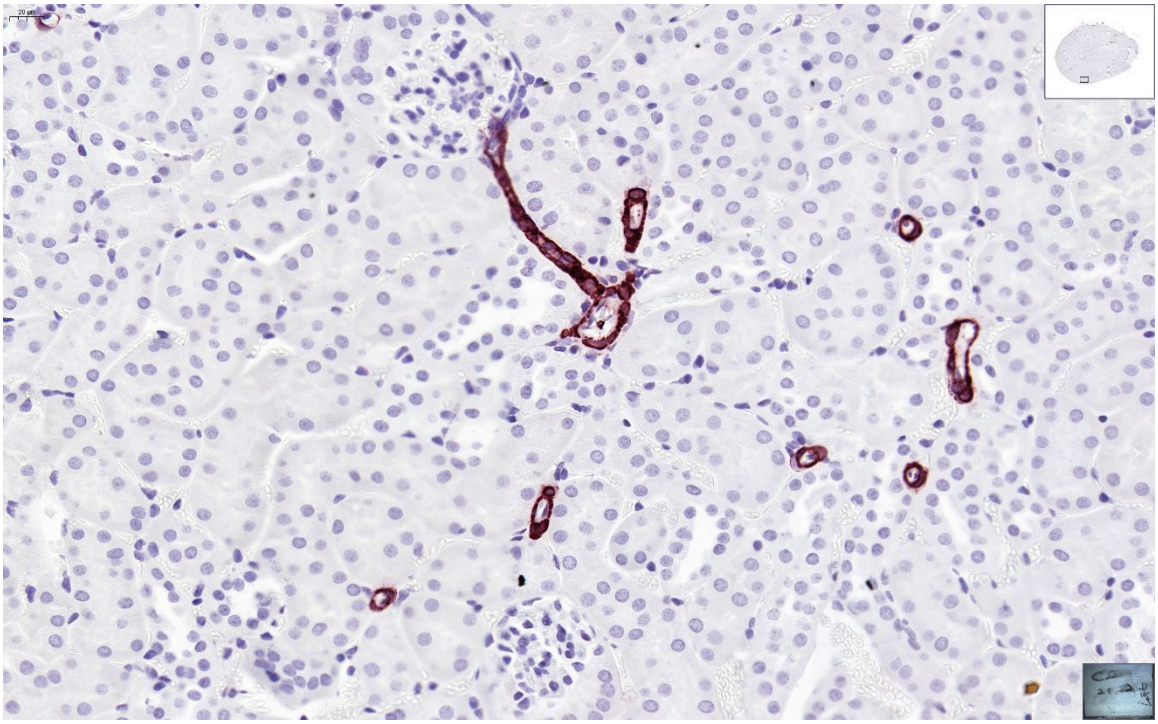

B

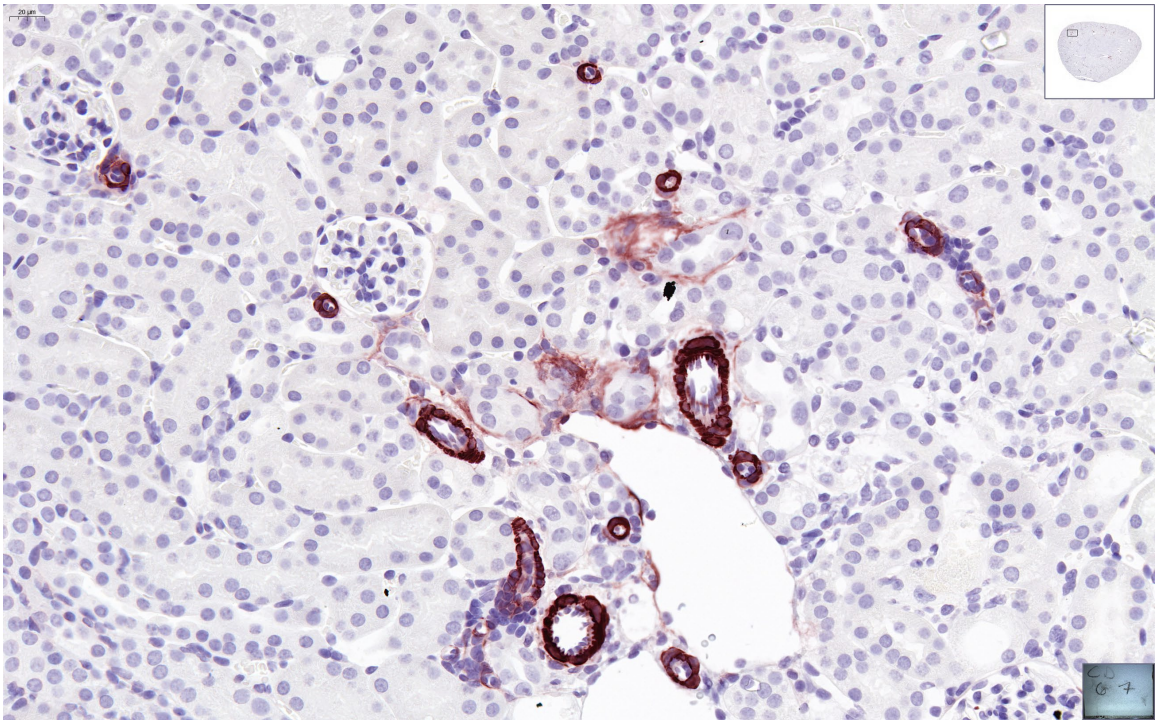

C

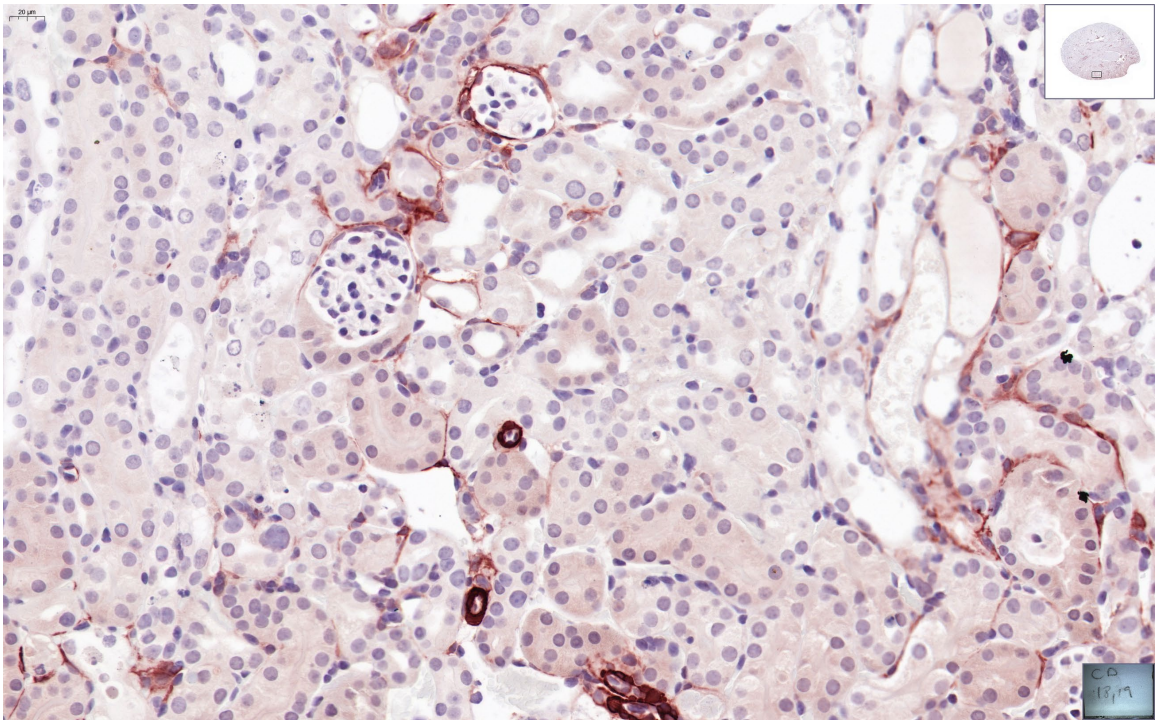

Figure 6. IHC for α-SMA

Renal histological changes were assessed with IHC for α-SMA on 5 µm thick sections. α-SMA IHC indicates an increased number of myofibroblasts in the kidney and is a sign of increased interstitial fibrosis. (A) Vehicle Control, (B) 7mg/kg, (C) 9mg/kg. Representative images of renal histology at 40X magnification.

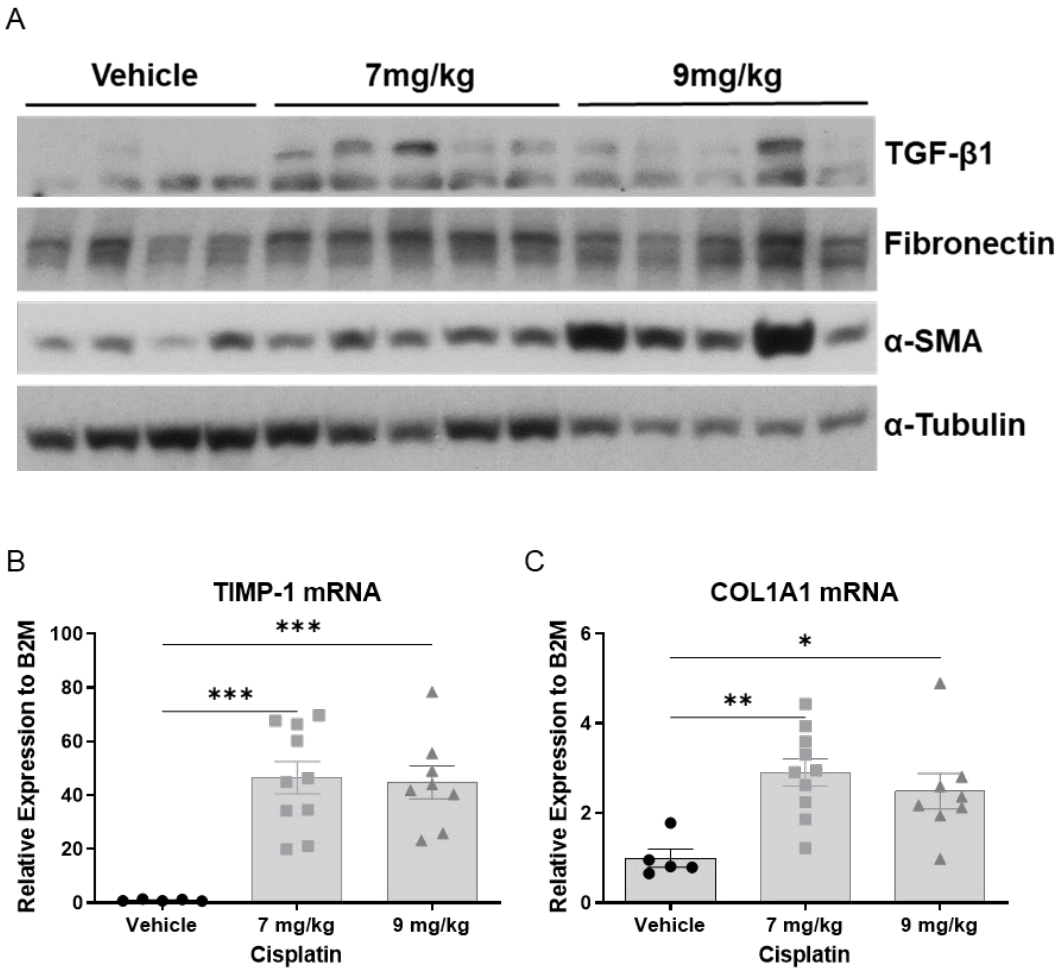

Figure 7. Elevated kidney fibrosis following RLDC

Eight- to ten-week-old B6129 male mice were treated with 0, 7, or 9 mg/kg cisplatin once a week for four weeks. (A) Immunoblotting from kidney cortex homogenates for TGF-β1, Fibronectin, α-SMA, and α-tubulin. (B-C) qRT-PCR of TIMP-1 and COL1A1 in kidney cortex homogenates is normalized to B2M. Data are expressed as means ± SEM; n=5–10. Statistical significance was determined by One-Way ANOVA followed by Tukey post-test. *p < 0.05, **p<0.01, ***p<0.001

RLDC induces renal inflammation. Inflammation was assessed using western analysis, real-time qRT-PCR, and flow cytometry. Western analysis indicated increased protein levels of phosphorylated-nuclear factor kappa-light-chain-enhancer of activated B cells (p-NF-κB) and total NF-κB (Figure 8A) between the vehicle and cisplatin-treated groups. The mRNA expression of inflammatory markers, TNF-α (Figure 8B), CXCL-1 (Figure 8C), and *NLRP3* (Figure 8D) showed a significant increase in the cisplatin-treated groups. These findings suggest that there is a significant increase in kidney inflammation following RLDC.

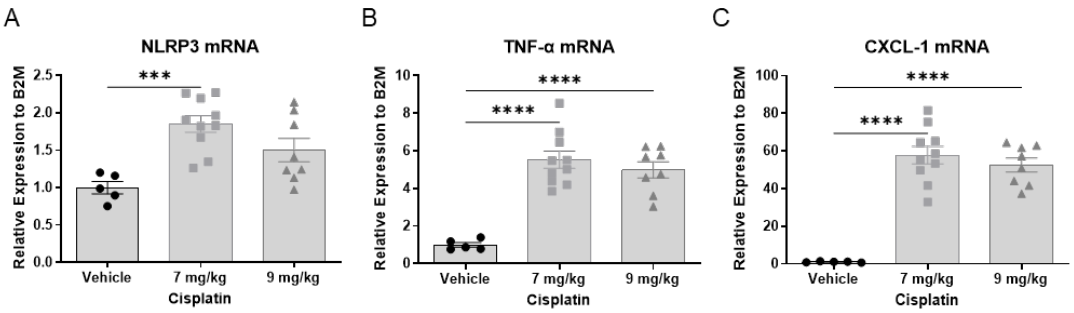

Figure 8. Elevated kidney inflammation following RLDC.

Eight- to ten-week-old B6;129 male mice were treated with 0, 7, or 9 mg/kg cisplatin once a week for four weeks. (A-C) qRT-PCR of *NLRP3*, TNF-α, and CXCL-1 in kidney cortex homogenates is normalized to B2M. Data are expressed as means ± SEM; n=5–10. Statistical significance was determined by One-Way ANOVA followed by Tukey post-test. ***p<0.001, ****p < 0.0001

Kidney mitochondrial content and biogenesis are reduced following RLDC.

As previously mentioned, the high density of mitochondria in the kidney led us to investigate the effects of the RLDC model on kidney mitochondrial content. We performed three different assays to evaluate mitochondrial content in the kidneys following RLDC. First, we quantified the ratio of mtDNA to nDNA as described [212]. RLDC resulted in a significant reduction in the mtDNA/nDNA ratio (Figure 9A), indicating a loss of mtDNA and suggesting a loss of mitochondrial mass. We also evaluated citrate synthase activity on kidney cortex homogenate. Data indicate a significant decrease in citrate synthase activity following RLDC treatment (Figure 9B). Finally, we performed western analysis of the electron transport chain (ETC) proteins. Data indicate a decrease in complexes 1-5 of ETC subunits (Figure 9C). These results suggest that following RLDC, there is a significant reduction in kidney mitochondrial content. These results lead us to investigate how RLDC affected the master regulator of MB. PGC-1α mRNA expression were evaluated by real-time qRT-PCR (Figure 9D). Data indicate decreased levels of PGC-1α at the mRNA. I next evaluated genes whose expression is regulated by PGC-1α. Nuclear respiratory factor 1 (Nrf1) expression is increased by PGC-1α, and it triggers the activation of multiple mitochondrial genes encoded in the nucleus [174]. Nrf1 expression is significantly reduced following RLDC (Figure 9E). One gene whose expression is regulated by Nrf1 is Tfam (transcription factor A, mitochondrial), and its expression is significantly reduced in the RLDC model (Figure 9F). Tfam binds to and activates transcription at the two major promoters of mitochondrial DNA (mtDNA) [186]. Tfam is responsible for organizing and maintaining mtDNA structure [185], and loss of Tfam in a mouse model resulted in the development of renal inflammation and fibrosis by 6 weeks of age [188]. Reduced Tfam results may be related to reduced mtDNA levels as shown in Figure 9A. mtDNA has a less efficient repair process compared to nuclear DNA (nDNA), making mtDNA highly susceptible to cisplatin-induced damage [213, 214]. As previously

stated, PGC-1α expression and activity are finely tuned and highly responsive to changes in the microenvironment. PGC-1α is negatively regulated by pro-inflammatory and profibrotic cytokines. PGC-1α protein is reduced following RLDC (Figure 9G), and the inhibitory pathways that regulate PGC-1α are increased following RLDC (Figure 9G). We looked at profibrotic factor TGF-β1 and phosphorylation of downstream target Smad 3 by western analysis (Figure 9G). As mentioned previously, activation of TLR4 has been seen in cisplatin models of injury. We looked at phosphorylation of ERK1/2, which is a downstream target of TLR4 by western analysis (Figure 9G). Data indicate increased levels of multiple inhibitors of PGC-1α expression and activity following the injury phase of the RLDC model.

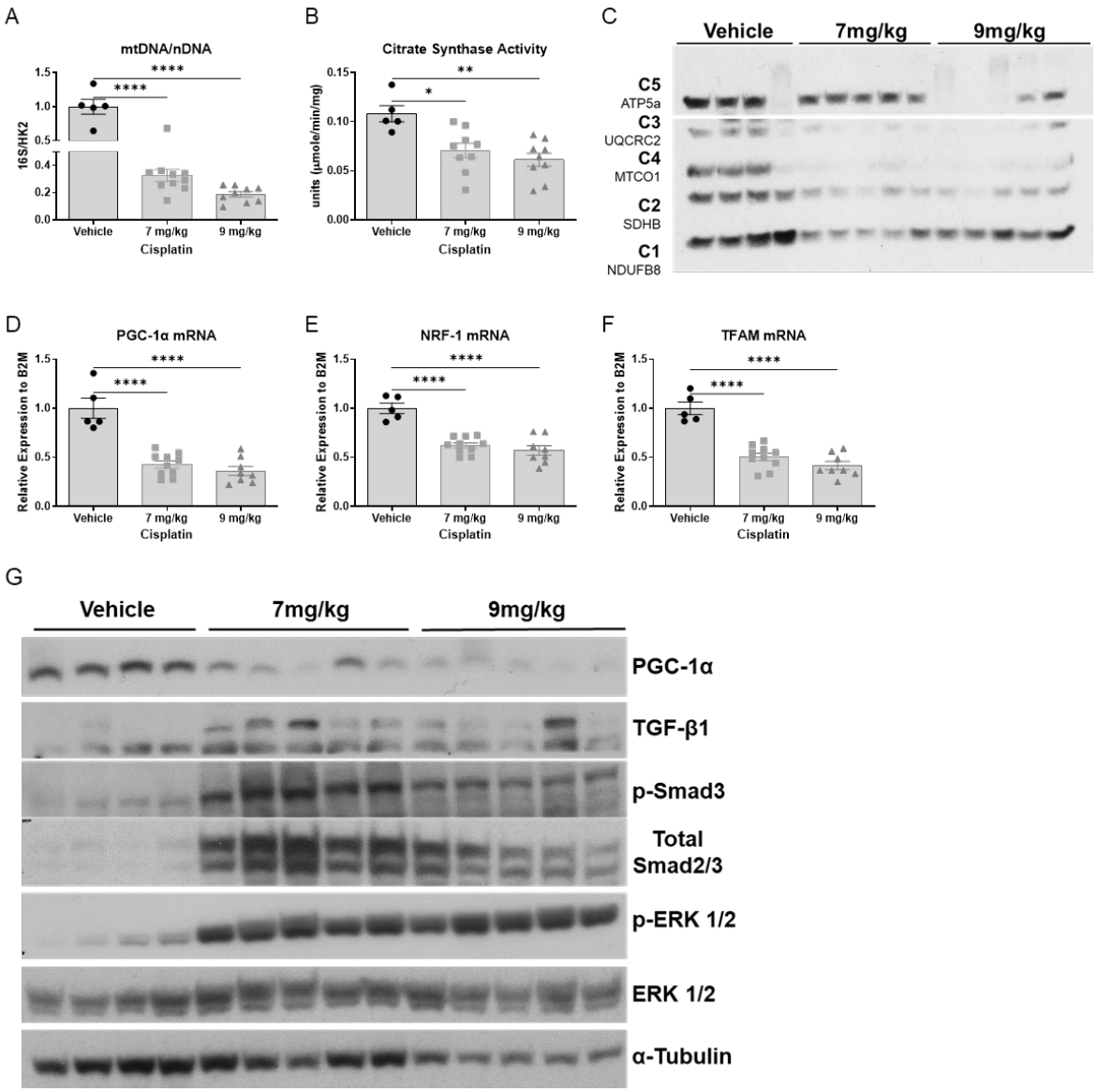

Figure 9. Kidney mitochondrial content and biogenesis are reduced following RLDC.

Eight- to ten-week-old B6;129 male mice were treated with 0, 7, or 9 mg/kg cisplatin once a week for four weeks. (A) qPCR on nuclear-encoded Hexokinase 2 (HK2) and mitochondrial-encoded 16S were used to calculate the ratio between mtDNA to nDNA as a marker for mitochondrial content, normalized to vehicle-treated kidneys. (B) Citrate Synthase Activity measured using Sigma-Aldrich kit (CS0720). (C) Immunoblotting for electron transport chain (ETC) subunit proteins: Complex 1 (NDUFB8), Complex 2 (SDHB), Complex 3 (UQCRC2), Complex 4 (MTCO1), and Complex 5 (ATP5a) of kidney cortex homogenates. (D-F) qRT-PCR of PGC-1α, NRF-1, and TFAM in kidney cortex homogenates is normalized to B2M. (G) Immunoblotting for PGC-1α, TGF-β1, p-Smad3, total Smad 2/3, p-ERK1/2, total ERK1/2, and α-Tubulin. Data are expressed as means ± SEM; n=5–10. Statistical significance was determined by 1-way ANOVA followed by Tukey posttest. *P< 0.05, **P<0.01, and ****P < 0.0001.

DISCUSSION

The kidney tubule cells are highly enriched in mitochondria and are the primary site of cisplatin-induced nephrotoxicity. Our study demonstrates that the RLDC model results in decline kidney function, increase in kidney injury, inflammation, and the development of fibrosis, all evidence that the maladaptive repair process is in effect. Additionally, we observed a significant decrease in kidney mitochondrial content and mitochondrial biogenesis. These findings are particularly exciting as they suggest that the reduced mitochondrial content and biogenesis may contribute to the failed-repair tubule cell population. This discovery provides a novel pathway to explore for preventing RLDC-induced kidney injury, furthering our understanding of the complex pathophysiology of CKD and uncovering potential driving mechanisms. Importantly, there are currently no effective treatments for CKD or options specifically targeted at preventing kidney fibrosis, underscoring the significance of our results.

These findings are consistent with previous research that has shown reduced expression of PGC-1α in human renal biopsies from AKI/CKD patients compared to normal kidney tissue [140, 192, 193]. Lower PGC-1α expression is seen in other models of AKI and increasing PGC-1α expression has provided protection in the IRI [192, 203-205], sepsis [200, 201], folic acid [179, 196-199], and single high dose cisplatin [194, 195, 206] models. Moreover, mitochondrial diseases associated with genetic inheritance have been found to coincide with renal impairment, particularly tubular defects [168-172]. Additionally we believe the tubule cells are highly susceptible to cisplatin toxicity, as shown by in vitro studies where cisplatin was found to preferentially accumulate in mitochondria [39, 129], and sensitivity to cisplatin correlates with mitochondria density and membrane potential [130, 131]. The repeated insult of cisplatin produces a failed-repaired tubule cell population [160], which can lead to a maladaptive repair process, fibrosis, and ultimately, CKD. Tissue repair is energetically demanding, and adequate mitochondrial mass and

mitochondrial respiration are required for proper healing [94]. Augmenting the kidney's mitochondrial content and biogenesis during the RLDC model could allow for more complete repair.

These findings strongly suggest that the repeated insults of cisplatin administration damage the mitochondria of tubule cells, creating a pro-inflammatory and pro-fibrotic microenvironment that inhibits PGC-1α expression, thereby preventing appropriate mitochondrial biogenesis and recovery. The significance of PGC-1α in the RLDC model requires further investigation. Future studies should explore the relationship between kidney PGC-1α expression, mitochondrial content, and the development of fibrosis/CKD to better understand their significance. Our hypothesis is that increasing PGC-1α expression leading to increased kidney mitochondrial content will protect against kidney injury and prevent progression to CKD caused by RLDC. Additional experiments using pharmacological inducers of PGC-1α, as well as transgenic mice overexpressing PGC-1α and mice that have conditional knockout of PGC-1α, are necessary to determine the role of PGC-1α in preventing RLDC-induced nephrotoxicity. This information will be instrumental in developing future therapeutic agents for clinical practice and could ultimately improve the quality of life for those with CKD.

CHAPTER 3: 5-HYDROTRYPTAMINE-1F RECEPTOR AGONIST PROTECTS FROM REPEATED LOW DOSE CISPLATIN INDUCED NEPHROTOXICITY

INTRODUCTION

Cisplatin is a commonly used chemotherapeutic but has the unfortunate drawback that up to thirty percent of cancer patients treated with cisplatin develop AKI [39]. AKI is a life-threatening condition defined as a rapid decrease in renal function [209]. In the clinic cisplatin is given on repeated cycles over weeks or months. Unfortunately, the repeated dosing of cisplatin is associated with increased rates of chronic kidney disease (CKD) [14]. Previous studies have shown that the repeated low dose cisplatin (RLDC) model induces kidney injury and the development of fibrosis, along with reduced kidney mitochondrial content and PGC-1α expression. Mitochondrial dysfunction have been identified as hallmarks of various AKI [61-63] and CKD models [163]. Moreover, tissue repair is energetically demanding, and adequate mitochondrial mass and mitochondrial respiration are required for proper healing [94].

Additionally the tubule cells are highly susceptible to cisplatin toxicity, as cisplatin has been shown to preferentially accumulate in mitochondria [39, 129], and sensitivity to cisplatin correlates with mitochondria density and membrane potential [130, 131]. The tubule cells and their mitochondria are damaged by each cycle of cisplatin and need to be replaced by mitochondrial biogenesis. PGC-1α is the master regulator of mitochondrial biogenesis and bioenergetics and increasing PGC-1α expression has provided protection against ischemia-reperfusion injury (IRI) [192, 203-205], sepsis [200, 201], folic acid [179, 196-199], and single high dose cisplatin [194, 195, 206] induced AKI. More recently, PGC-1α has been shown to be a key mediator in renal fibrosis and CKD development

[140, 141, 163, 176, 180, 193]. Therefore, our laboratory aimed to investigate the potential of pharmacological inducers of PGC-1α to protect against cisplatin-induced kidney injury and the progression to CKD.

The 5HT-$_{1F}$ agonist, LY344864 has been shown to provide protection from AKI [215] and from spinal cord injury [216] by increased PGC-1α and mitochondrial biogenesis. The 5HT-$_{1F}$ receptor is a G-protein coupled receptor (GPCR) whose functions outside of the central nervous system are not completely characterized [217-221]. The 5HT-$_{1F}$ receptor has been found on freshly isolated tubule cells and on cultured renal proximal tubule epithelial cells [215]. Additionally, the knockout of 5HT-$_{1F}$ receptor in mice impairs the injury repair process in the kidney and worsens AKI events [222].

This study was designed to determine if 5HT-$_{1F}$ agonist, LY344864 will protect from RLDC induced AKI-CKD development. Our hypothesis is that by increasing PGC-1α expression through the 5HT-1F receptor, kidney mitochondrial biogenesis and mitochondrial content will be enhanced, leading to a decrease in injured/failed-repair tubule cell population, resulting in improved renal function and reduced fibrosis.

MATERIALS AND METHODS

ANIMALS

B6129SF1/J (B6;129) male mice were purchased from The Jackson Laboratory. B6;129 mice are a first filial generation hybrids that are the offspring of a cross between C57BL/6J females (B6) and 129S1/SvlmJ males (129). Upon arrival, the mice were allowed to acclimate for 1 week prior to the initiation of the experiment. All mice were maintained on a 12-hour light/dark cycle and provided food and water *ad libitum*. All animal procedures were approved by the Institutional Animal Care and Use Committee and followed the guidelines of the American Veterinary Medical Association.

CISPLATIN DOSING REGIMEN

Pharmaceutical grade cisplatin (NDC 16729-288-38, 1mg/ml) was purchased via the University of Louisville Outpatient Hospital Pharmacy. The repeated low dose cisplatin dosing regimen mice were administered cisplatin or vehicle via intraperitoneal (i.p.) injection once a week between 8-9 a.m. for four weeks. In the vehicle group, 400 µL normal saline was administered via i.p. injection. In the cisplatin treatment groups, 7mg/kg cisplatin in normal saline with a total volume of 400 µL was administered via i.p. injection. All animals were injected with cisplatin at the same time of day as there are circadian influences on the response of the kidney to cisplatin. Animals were euthanized 72 hours following their final cisplatin injection. Upon euthanasia, blood was collected, and plasma prepared and frozen at -80°C; urine was collected and frozen at -80°C; and kidneys were removed, flash-frozen in liquid nitrogen, and stored at -80°C until use. A cross-section of one kidney from each mouse was fixed in 10% neutral buffered formalin for histology.

LY344864 DOSING REGIMEN

The serotonin receptor (5HT) subtype 1F agonist (5HT-$_{1F}$), LY344864 (item #, 29496, CAS # 1217756-94-9) was purchased from Cayman Chemical Company (Ann Arbor, Michigan;

United States). LY344864 was dissolved in normal saline, mice were administered vehicle or LY344864 via intraperitoneal (i.p.). Following the first dose of cisplatin mice were administered LY344864 (2mg/kg) or saline 6 days a week via i.p. injection for the duration of the study. All mice were administered 20 doses of saline or LY344864 in a final volume of 200 µL to control for fluid delivery. Mice were randomly assigned into the following four groups: 1. Vehicle/Vehicle, 2. Vehicle/LY344864, 3. Cisplatin/Vehicle, 4. Cisplatin/LY344864 (Cisplatin/LY-20). Additionally, a fifth group was used to assess if LY344864 protection could occur partially through the RLDC regimen. Group 5. Cisplatin/LY344864 only received 10 doses of LY344864 over the course of the experiment, starting 5 days after the second dose of cisplatin on day 12 of the experiment. Group 4 will be referred to as LY-20 and Group 5 will be referred to as LY-10 (Cisplatin/LY-10). The LY344864 and cisplatin dosing regimen is shown in Figure 10A.

A

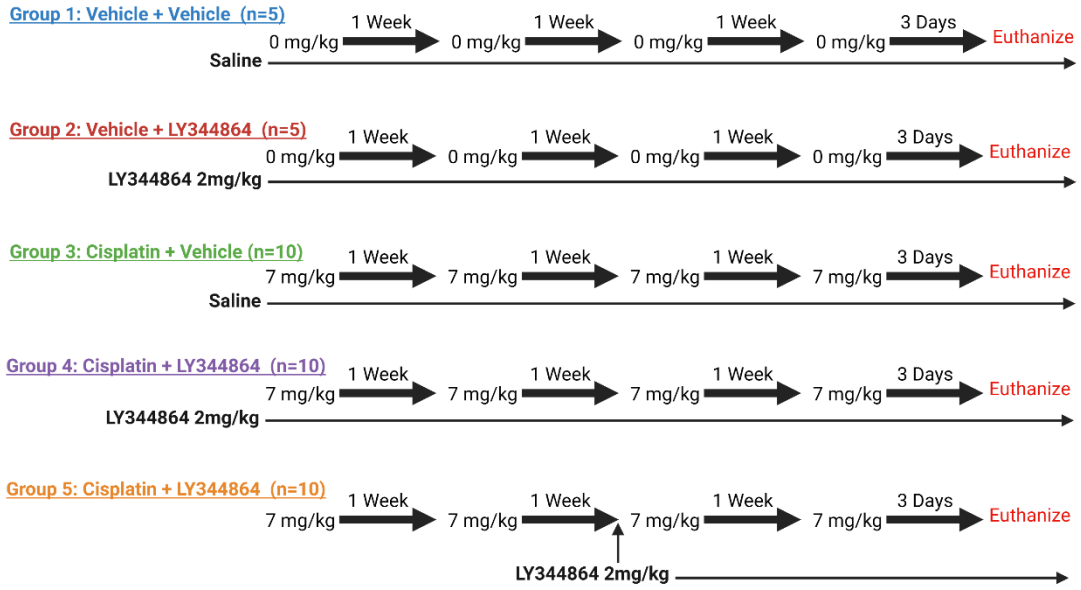

Figure 10. Experimental design for RLDC with LY344864 treatment study.

Eight- to ten-week-old B6;129 male mice were treated with 0 or 7 mg/kg cisplatin once a week for four weeks. Additionally, mice were treated with vehicle (normal saline) or LY344864 via IP injection daily for a total of 20 doses (LY-20). In group 5 (LY-10), the mice did not start LY344864 treatment until 5 days after the second dose of cisplatin for a total of 10 doses. Cisplatin or saline was administered via intraperitoneal injection once a week for four weeks. Animals were euthanized 72 hours following their final cisplatin injection. (A) Schematic of the experimental design.

BLOOD UREA NITROGEN (BUN), SERUM CREATININE (SCR), AND NEUTROPHIL GELATINASE ASSOCIATED LIPOCALIN (NGAL) DETERMINATION

BUN (AMS Diagnostics, 80146) levels were measured from plasma samples using the indicated kits following the manufactures' instructions. ELISAs for NGAL (R&D Systems, DY1857) were performed on the urine as directed by the manufacturer.

PROTEIN QUANTIFICATION AND WESTERN BLOT ANALYSIS

Kidney tissues were homogenized in cell extraction buffer (Thermo Fisher Scientific) containing a Complete Protease Inhibitor Cocktail Tablet and Phosphatase Inhibitor Cocktail Tablets (Roche). Homogenates were centrifuged at 15,000 X g for 10 min at 4° C. Supernatants were removed and stored at -80°C. Protein concentrations were determined using Bradford Reagent (Bio-Rad). 40 µg of kidney homogenate protein were loaded and separated on 4–12% gradient Tris-Glycine-SDS polyacrylamide gels. Protein was then transferred to PVDF membranes that were blocked in 5% (w/v) dried milk in tris buffered saline 0.1% Tween 20 (TBST) for 1 hour. Membranes were incubated with primary antibody overnight at 4°C. The next morning, membranes were washed 3 times for 5 min each with TBST containing 5% (w/v) dried milk. Membranes were then incubated for 2 hours at room temperature with secondary antibodies conjugated with horseradish peroxidase (1:20,000) in TBST containing 1% (w/v) dried milk. Following 2 washes, 1% (w/v) dried milk and 1 wash in TBST membrane proteins were detected by chemiluminescence substrate.

ANTIBODIES

The following antibodies were purchased from Cell Signaling Technology (Beverly, MA): p44/42 MAP Kinase (Erk1/2) #4695, Phospho-p44/42 MAP Kinase (Erk1/2) (Thr202/Tyr204) #4370, Transforming growth factor-beta (TGF-β) #3711, Mothers against decapentaplegic homolog 2/3 (SMAD 2/3) #8685, Phospho-Smad3 (Ser423/425) #9520,

Phospho-Akt (Ser473) Antibody #9271, total Akt Antibody #9272, and GAPDH (D16H11) #5174. The following antibodies were purchased from Abcam (Cambridge, CB2 0AX, UK): Peroxisome proliferative activated receptor, gamma, coactivator 1 alpha (PGC-1α, abcam, ab54481) and α-Smooth Muscle Actin (α-SMA, abcam, ab5694). The remaining antibodies include fibronectin (F3648, Sigma-Aldrich), and α-tubulin (SC-5286, Santa Cruz Biotechnology).

Rodent Total OXPHOS Antibody Cocktail (abcam, ab110413) contains 5 mouse mAbs, one each against Complex I subunit NDUFB8 (ab110242), Complex II-30kDa (ab14714), Complex III-Core protein 2 (ab14745), Complex IV subunit I (ab14705) and Complex V alpha subunit (ab14748) as an optimized premixed cocktail.

GENE EXPRESSION

RNA was isolated from kidney tissue using E.Z.N.A. Total RNA Kit 1 (OMEGA) per manufacturer's protocol. cDNA was synthesized with High-Capacity cDNA Reverse Transcriptase PCR (Thermo Fisher Scientific) per manufacturer's instructions. Gene-specific cDNA was quantified with real-time qRT-PCR using either predesigned TAQman assays or self-designed SYBR assays. The following TAQman primers were purchased from Thermo FisherScientific: tumor necrosis factor alpha (*Tnf-α*, Mm00443258_m1), chemokine (C-X-C Motif) ligand 1 (*Cxcl1*, Mm04207460_m1), and the housekeeping gene beta-2-microglobulin (*B2m*, Mm00437762_m1). The following primers were self-designed: kidney injury molecule-1 (*Kim-1*, Invitrogen, forward: AGATCCACACATGTACCAACATCAA, reverse: CAGTGCCATTCCAGTCTGGTTT), Peroxisome proliferative activated receptor, gamma, coactivator 1 alpha (*Pgc-1α*, Invitrogen, forward: AACAATGAGCCTGCGAACATATT, reverse: TAGCAAGTTTGCCTCATTCTCTTC), Nuclear Respiratory Factor 1 (*Nrf-1*, Invitrogen,

forward: GGATTCCAGTCTCTGTGGACAAA, reverse: CCCCCGACCTGTGGAATACT), Transcription factor A, mitochondrial (*Tfam*, Eurofins, forward: TTTAAAGCTAAACACCCAGATGCA, reverse: TTCTGGTAGCTCCCTCCACAG), *Timp-1*, Invitrogen forward: GCAACTCGGACCTGGTCATAA, reverse: TTAGTCATCTTGATCTTATAACGCTGGTA), *Nlrp3*, Invitrogen, forward: AAGATGAAGGACCCACAGTGTAACTT, reverse: CAGATTGAAGTAAGGCCGGAATT), and *Col1a1*, Invitrogen, forward: CGATGGATTCCCGTTCGAGTA, reverse: GTGGACATTAGGCGCAGGAA) qRT-PCR was done with either iTaq Universal Probes Supermix (172-5134, Bio-Rad) or iTaq Universal SYBR Green Supermix (172–5124, Bio-Rad).

MITOCHONDRIAL DNA TO NUCLEAR DNA ASSAY

DNA was isolated from kidney tissue using E.Z.N.A. Tissue DNA Kit 1 (OMEGA) per the manufacturer's protocol. DNA was quantified using Nanodrop, and 5 ng/µl solutions were prepared for each sample. 20ng of DNA was loaded into each well, followed by quantitative PCR using primers designed for specific amplification of particular mtDNA encoded and nuclear-encoded fragments. Primers were designed to evaluate the relative copy number of mtDNA and nDNA. The mitochondrially encoded genes selected were *16s rRNA* and *Nd1*, and the nuclear-encoded gene was Hexokinase 2 (*Hk2*) along with the adaptation of the protocol according to previously published work [212]. Forward and reverse primers *16s rRNA*, Invitrogen, forward: CCGCAAGGGAAAGATGAAAGAC, reverse: TCGTTTGGTTTCGGGGTTTC, *Nd1*, Invitrogen, forward: CTAGCAGAAACAAACCGGGC, reverse: CCGGCTGCGTATTCTACGTT, *Hk2*, Invitrogen, forward: GCCAGCCTCTCCTGATTTTAGTGT, reverse GGGAACACAAAAGACCTCTTCTGG. qPCR was done with iTaq Universal SYBR Green Supermix (172–5124, Bio-Rad).

TISSUE HISTOLOGY

Sirius Red/Fast Green (SR/FG) staining was performed on formalin-fixed paraffin-embedded (FFPE) kidney sections (5 μm thick) for total collagen deposition as previously published [152, 223].

SIRIUS RED/FAST GREEN STAINING

Kidney sections (5 μm thick) were rehydrated in Histoclear followed by an ethanol gradient. Slides were then dipped in PBS with 0.1% Tween 20 and incubated for 5 minutes. Slides were washed with distilled water twice for 5 minutes each and then incubated in 1.2% (w/v) saturated picric acid (#5860-32, Ricca Chemicals) containing 0.1% sirius red/direct red 80 (#365548, Sigma) and 0.1% fast green FCF (#F7258, Sigma). Slides were then washed with 5% glacial acetic water until the water ran clear. Tissue samples were then dehydrated and fixed using Permount (#17986-01, Electron Microscopy Sciences).

QUANTIFICATION OF TISSUE HISTOLOGY

Orbit Image Analysis software [224] (version 3.64) was used to quantify positive staining of kidney histology. The Tissue Quantification feature was used to quantify collagen staining. The software developers' protocol was followed for training the software to correctly identify collagen over normal tissue [224, 225]. In the training step the images were labeled by manually drawing several annotations per tissue class (e.g., collagen, normal tissue,). After training the software images were tested to verify correct determination of positive staining. Digital scans of kidney sections were divided into 5-8 sections and the classification (e.g., collagen, normal tissue) of the tissue sections were

assigned by the software. The percentage of collagen per image was used to quantify positive staining.

STATISTICAL ANALYSIS DATA

Quantitative data are expressed as the mean ± SEM for all experiments. Statistical significance was determined using GraphPad Prism software 9.4.1. Statistically significant differences were determined by Two-Way ANOVA followed by Tukey post-test. The criterion for the statistical difference was $P < 0.05$.

RESULTS

Improved kidney function and reduced kidney injury following RLDC in mice treated with LY344864. The administration of LY344864 concurrently in the RLDC model provided protection against cisplatin induced decline in kidney function and kidney injury. The cisplatin/vehicle group had significantly elevated plasma BUN, urinary NGAL, and kidney KIM-1 expression compared to the vehicle/vehicle group (Figure 11A-C). The use of LY344864 in the cisplatin/LY344864 groups partially protected from elevated BUN and NGAL when compared to the cisplatin/vehicle (Figure 11A-C). The use of LY344864 in the cisplatin/LY-20 group reduced Kim-1 expression and this reduction was statistically significant in the cisplatin/LY-10 group compared to cisplatin/vehicle (Figure 11C). There were a number of mice in each of the cisplatin/LY344864 groups that had markers of kidney function and injury that were nearly at baseline compared the vehicle/vehicle mice (Figure 11A-C). There were no significantly elevated markers of kidney function and injury in the cisplatin/LY344864 groups compared to the vehicle/vehicle group. This suggests that the use of LY344864 provides protection from RLDC induced injury. The loss of body weight is used as a general marker of toxicity. The use of LY344864 in the cisplatin/LY344864 groups reduced percentage of body weight loss compared to the cisplatin/vehicle group (Figure 11D). The use of LY344864 in the vehicle/LY344864 group had no toxicity as measured by BUN, NGAL, Kim-1, and loss of body weight (Figure 11A-D). These data suggest the 5HT-$_{1F}$ agonist, LY344864 protects from cisplatin induced injury and this is a novel pathway to prevent cisplatin induced nephrotoxicity.

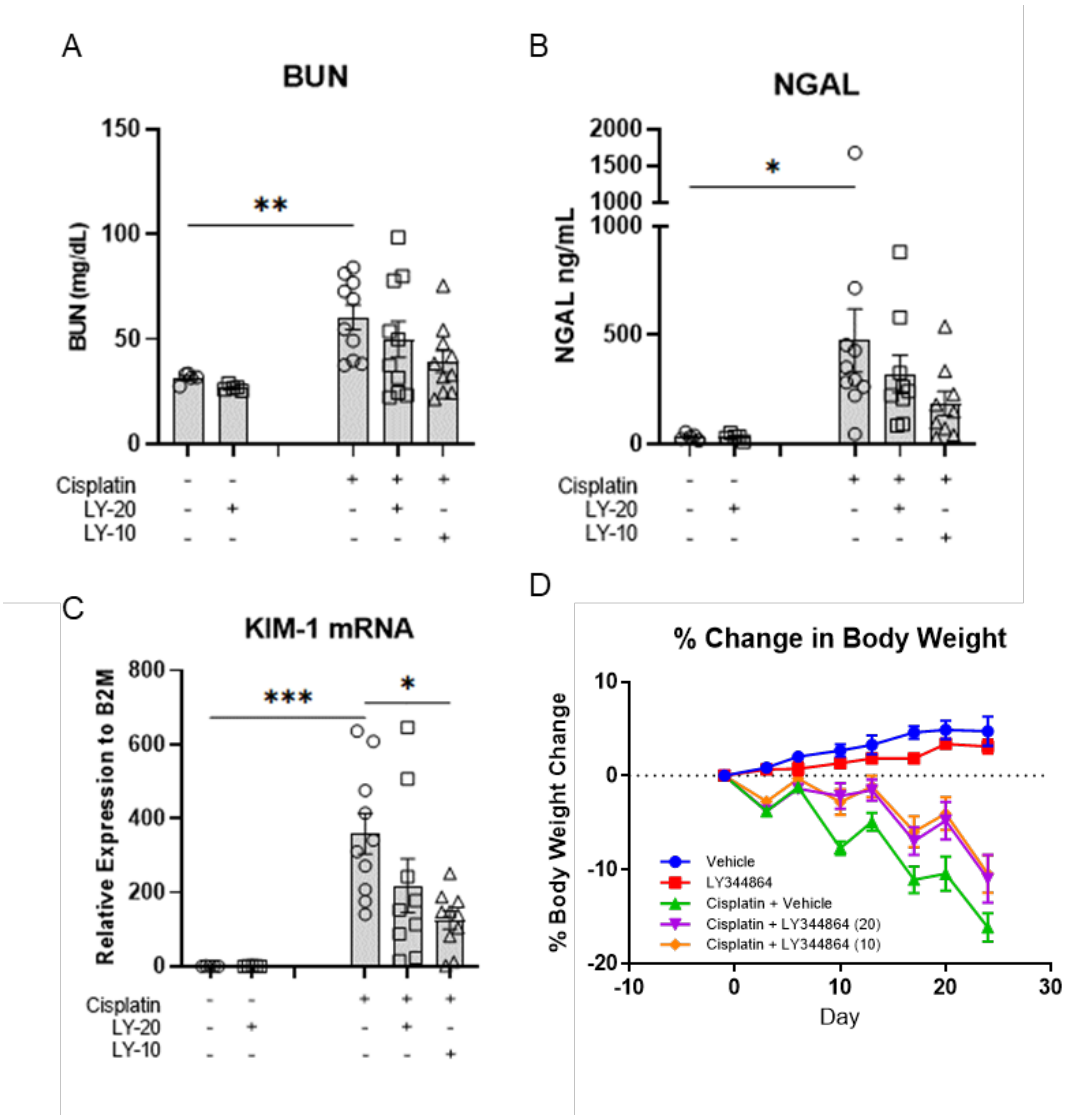

Figure 11. Improved kidney function and reduced kidney injury following RLDC in mice treated with LY344864.

Eight- to ten-week-old B6;129 male mice were treated with 0 or 7 mg/kg cisplatin once a week for four weeks and vehicle or LY344864 daily. (A) BUN levels from plasma and (B) Urine NGAL levels were measured following four doses of cisplatin on Day 24. (C) qRT-PCR of KIM-1 in kidney cortex homogenates is normalized to B2M. (D) Percentage change in body weight. Data are expressed as means ± SEM; n=5–10. Statistical significance was determined by TWO-Way ANOVA followed by a Tukey post-test. *p < 0.05, **p < 0.01 ***p<0.001.

Reduced kidney fibrosis following RLDC in mice treated with LY344864. Fibrosis was evaluated via multiple approaches, including histopathology, western analysis, and real-time qRT-PCR analysis of fibrotic markers. The immunoblots from kidney cortex homogenates show increased levels of fibronectin, α-SMA, and TGF-β1 in the kidneys of the cisplatin/vehicle group compared to the vehicle/vehicle group similar to previous results from our lab and others (Figure 12A; [152-157]) The use of LY344864 in the cisplatin/LY344864 groups reduced protein levels for fibronectin, α-SMA, and TGF-β1 assessed by immunoblotting compared to the cisplatin/vehicle group (Figure 12A). We determined the development of interstitial fibrosis on FFPE kidney sections using SR/FG. SR/FG stains collagen red and indicates collagen accumulation. There was a significant increase in SR/FG positive staining in the cisplatin/vehicle kidneys compared to the vehicle/vehicle kidneys (Figure 12B). The use of LY344864 in the cisplatin/LY344864 groups did not significantly reduce SR/FG staining compared to cisplatin/vehicle (Figure 12B). The mRNA expression of Timp-1 and Col1a1 are significantly increased in the cisplatin/vehicle group compared to the vehicle/vehicle group (Figure 12C-D). The use of LY344864 in the cisplatin/LY344864 groups reduced the mRNA expression of Timp-1 and Col1a1 compared to cisplatin/vehicle group (Figure 12C-D). The use of LY344864 in the vehicle/LY344864 group did not increase the development of interstitial kidney fibrosis as assessed by protein levels, SR/GF staining, and mRNA expression (Figure 12A-D). These data suggest the 5HT-$_{1F}$ agonist, LY344864 may provide some protection from cisplatin induced development of interstitial fibrosis and this is a novel pathway to prevent RLDC induced development of kidney fibrosis.

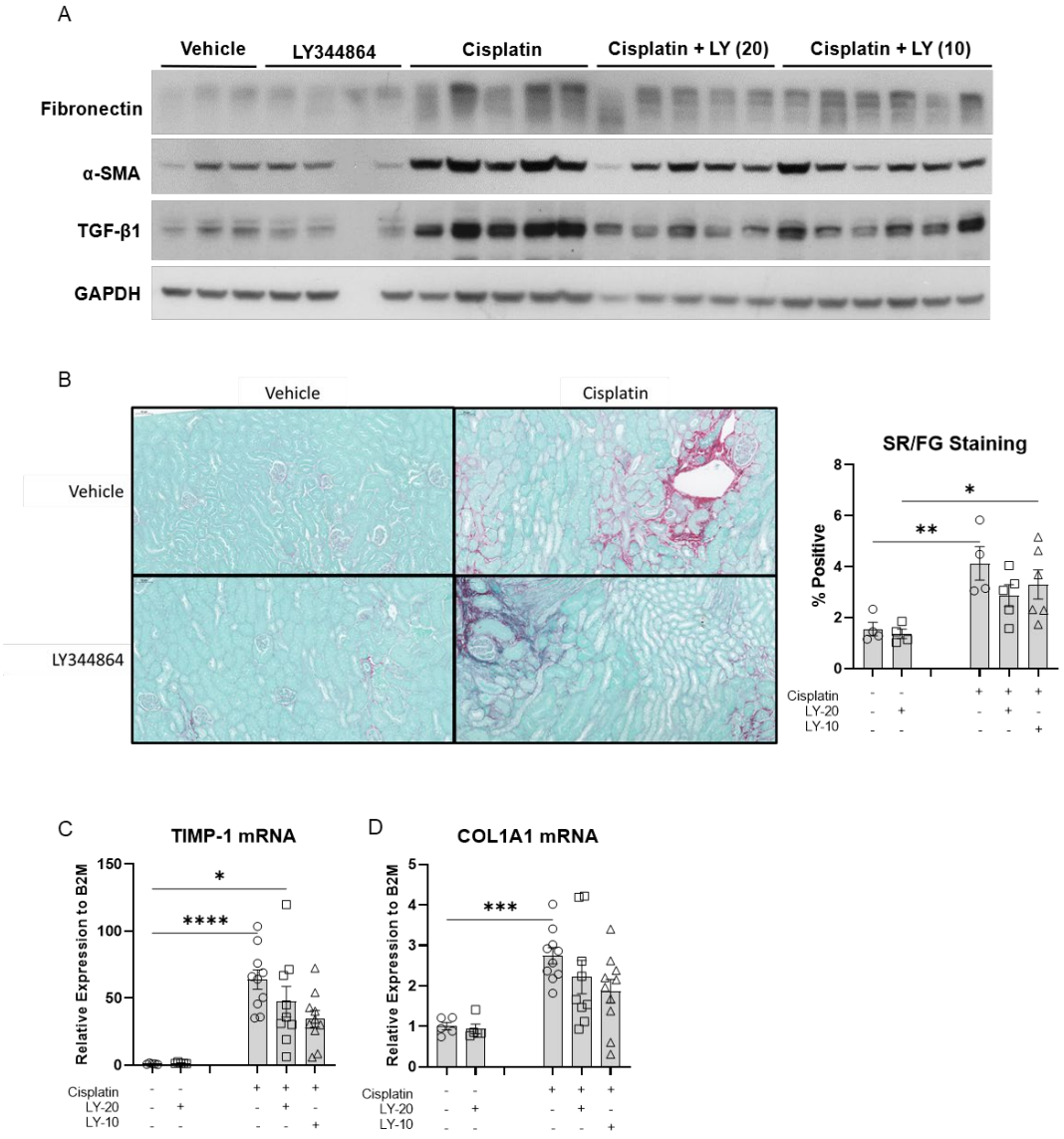

Figure 12 Reduced kidney fibrosis following RLDC in mice treated with LY344864.

Eight- to ten-week-old B6;129 male mice were treated with 0 or 7 mg/kg cisplatin once a week for four weeks and vehicle or LY344864 daily. (A) Immunoblotting from kidney cortex homogenates for Fibronectin, α-SMA, TGF-β1, and GAPDH. (B) SR/FG stain for total collagen levels on 5-µm-thick paraffin-embedded kidney sections and the quantifications. qRT-PCR of TIMP-1 (C) and COL1A1 (D) in kidney cortex homogenates is normalized to B2M Data are expressed as means ± SEM; n=5–10. Statistical significance was determined by TWO-Way ANOVA followed by a Tukey post-test. *p < 0.05, **p < 0.01 ***p<0.001.

Reduced kidney inflammation following RLDC in mice treated with LY344864. The administration of LY344864 concurrently with RLDC provided protection against cisplatin induced kidney inflammation. Kidney inflammation is significantly increased in the cisplatin/vehicle group compared to the vehicle/vehicle group as measured by mRNA expression of *Tnf-α*, *Cxcl1*, and *Nlrp3* (Figure 13A-C). The use of LY344864 in the cisplatin/LY344864 groups did not reduce *Tnf-α* mRNA expression compared to cisplatin/vehicle group (Figure 13A). The use of LY344864 in the cisplatin/LY344864 group reduced mRNA expression of *Cxcl1*, and *Nlrp3* compared to the cisplatin/vehicle group (Figure 13B). *Nlrp3* mRNA expression was significantly reduced in the cisplatin/LY-10 and cisplatin/LY-20 group compared to cisplatin/vehicle. The use of LY344864 in the vehicle/LY344864 group had no increase in kidney inflammation as measured by mRNA expression of *Tnf-α*, *Cxcl1*, and *Nlrp3* mRNA (Figure 13A-C). These data suggest the 5HT-$_{1F}$ agonist, LY344864 protects from some aspects of cisplatin induced kidney inflammation.

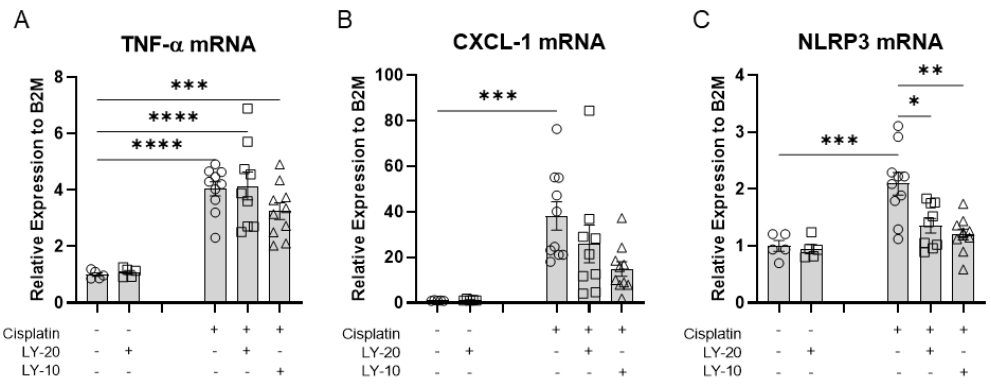

Figure 13. Reduced kidney inflammation following RLDC in mice treated with LY344864.

Eight- to ten-week-old B6;129 male mice were treated with 0 or 7 mg/kg cisplatin once a week for four weeks and vehicle or LY344864 daily. (A-C) qRT-PCR of TNF-α, CXCL-1, and *NLRP3* in kidney cortex homogenates is normalized to B2M. Data are expressed as means ± SEM; n=5–10. Statistical significance was determined by TWO-Way ANOVA followed by a Tukey post-test. *p < 0.05, **p<0.01, ***p<0.001, ****p < 0.0001

Increased kidney mitochondrial content and biogenesis following RLDC in mice treated with LY344864. Mitochondrial content was assessed by the ratio of mitochondrial DNA to nuclear DNA and western analysis of the electron transport chain (ETC) subunit proteins. were measured. The vehicle/cisplatin group had significantly lower mtDNA to nDNA ratios (Figure 14A) and ETC subunit protein levels (Figure 14B) as compared to the vehicle/vehicle group. The mice in the cisplatin/LY344864 groups had partially restored kidney mtDNA to nDNA ratios in both LY-20 and LY-10 groups when compared to the cisplatin/vehicle groups (Figure 14A). The proteins for CI, CII, and CV of ETC subunit proteins were increased in the cisplatin/LY344864 groups when compared to the cisplatin/vehicle group (Figure 14B). Mitochondrial biogenesis (MB) was measured through PGC-1α mRNA expression and protein levels. The mice in the cisplatin/vehicle group had significantly lower PGC-1α mRNA expression compared to vehicle/vehicle mice (Figure 14C). The downstream targets of PGC-1α, Nrf-1 and Tfam which are involved in MB were also significantly lowered in the cisplatin/vehicle group compared to the vehicle/vehicle group (Figure 14D-E). The use of LY344864 in the cisplatin/LY344864 group did not significantly increases PGC-1α mRNA expression when compared to the cisplatin/vehicle (Figure 14 C). LY344864 in the cisplatin/LY344864 group had little to no effect on Nrf-1 or Tfam expression compared to cisplatin/vehicle group (Figure 14. D-E). The lack of an increase in the mRNA expression of PGC-1α, Nrf-1, and Tfam may be explained by the timing of the last dose of LY344864. The mice had not received a dose of LY344864 in over 24 hours in this experiment at the time of euthanasia. Effects of the LY344864 on PGC-1α mRNA expression are likely to have subsided by the time the samples were collected. The suppression of PGC-1α in the cisplatin/vehicle group is also supported by the increase in inhibitory regulators TGF-β1 and p-ERK1/2 when compared to vehicle/vehicle mice (Figure 14 F). The use of LY344864 in the cisplatin/LY344864 group reduced PGC-1α expression inhibitors TGF-β1 and p-ERK1/2 when compared to

cisplatin/vehicle group (Figure 14F). The protein levels of PGC-1α were also reduced by cisplatin in the cisplatin/vehicle group compared to vehicle/vehicle (Figure. 14F). LY344864 in the cisplatin/LY344864 increased kidney PGC-1α protein levels when compared to cisplatin/vehicle group. Additionally, AKT can phosphorylate PGC-1α and reduce its activity. The use of cisplatin increased p-AKT levels in the cisplatin/vehicle group compared to the vehicle/vehicle groups. The use of LY344864 in the cisplatin/LY344864 group reduced p-AKT levels compared to cisplatin/vehicle group. The use of LY344864 in the vehicle/LY344864 group had no effect on kidney mitochondrial content or biogenesis (Figure 14A-F). Mitochondrial biogenesis is a highly regulated process [141, 174-176] and under normal physiological conditions the stimulation of the 5HT-$_{1F}$ receptor is not able to further increase mitochondrial biogenesis or content. These data suggest that the 5HT-$_{1F}$ agonist LY344864 provides protection from cisplatin induced nephrotoxicity by increasing kidney mitochondrial content through increased PGC-1α.

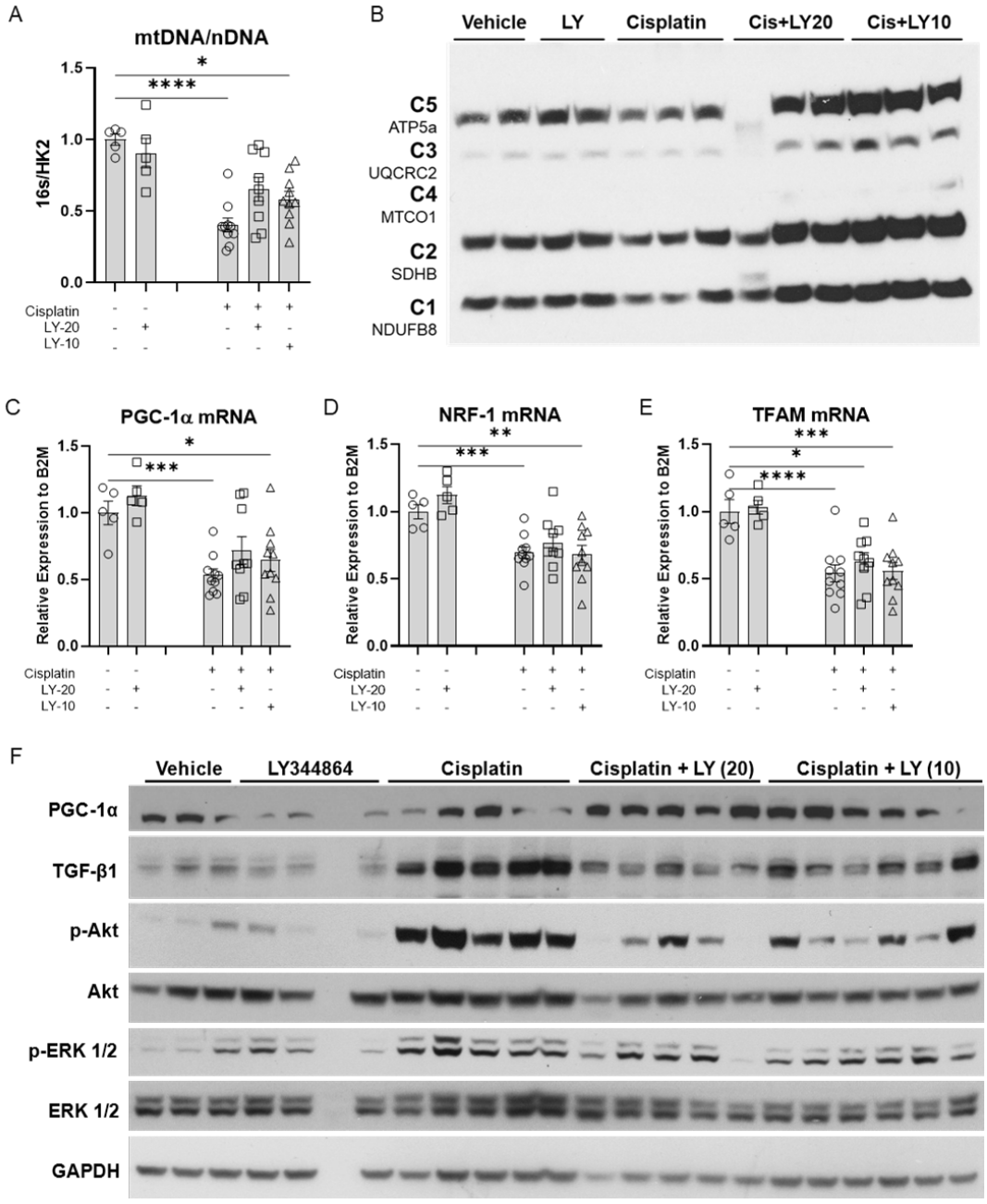

Figure 14. Increased kidney mitochondrial content and biogenesis following RLDC in mice treated with LY344864.

(A) qPCR on nuclear-encoded HK2 and mitochondrial-encoded 16S were used to calculate the ratio between mtDNA to nDNA, normalized to vehicle-treated kidneys. (B) Immunoblotting for ETC subunit proteins: C1 (NDUFB8), C2 (SDHB), C3 (UQCRC2), C4 (MTCO1), and C5 (ATP5a) of kidney cortex homogenates. (C-E) qRT-PCR of PGC-1α, NRF-1, and TFAM in kidney cortex homogenates is normalized to B2M. (C) Immunoblotting for PGC-1α, TGF-β1, p-AKT, AKT, p-ERK1/2, total ERK1/2, and GAPDH. Data are expressed as means ± SEM; n=5–10. Statistical significance was determined by TWO-way ANOVA followed by Tukey posttest. *P< 0.05, **p < 0.01, and ****P < 0.0001.

DISCUSSION

In this study, we investigated the potential of the 5HT-$_{1F}$ agonist, LY344864, to protect against cisplatin-induced kidney injury and fibrosis. Cisplatin is a widely used chemotherapeutic agent for solid-organ cancers, but its dose-limiting side effect is nephrotoxicity, which can lead to a reduction in treatment efficacy or a switch to less effective and less nephrotoxic drugs [39]. Therefore, identifying strategies to protect against cisplatin-induced kidney injury could increase its therapeutic potential and reduce the risk of CKD development in cancer survivors.

Our results demonstrate that LY344864 provides protection against cisplatin-induced kidney injury, interstitial fibrosis, and inflammation. Moreover, we found that LY344864 increases mitochondrial content and biogenesis, which is typically reduced by cisplatin treatment. The RLDC model produces an injury/repair tubule cell population that after repeated doses enters a failed-repair state [159, 160]. We believe these cells contribute to the development of the hallmarks of CKD, fibroblast activation, persistent inflammation, tubular atrophy, and vascular rarefaction. This study suggests that reduced mitochondrial content and biogenesis are drivers of the failed-repair tubule cell population and increasing kidney mitochondrial content and biogenesis allows for a more complete repair following RLDC. These results are helpful in our understanding of the complex pathobiology of kidney fibrosis and help uncover potential driving mechanisms. These findings are important as there are no effective treatments for CKD and no options specifically targeted at preventing kidney fibrosis.

These findings are consistent with previous research that the 5HT-$_{1F}$ agonist, LY344864 improves recovery from IRI-AKI [215] and spinal cord injury [216]. Additionally, our study supports the published data indicating that increasing PGC-1α expression protects in other rodent models of AKI, including IRI [192, 203-205], sepsis [200, 201], folic acid [179, 196-199], and single high dose cisplatin [194, 195, 206]. These results

indicate that diverse etiologies of kidney pathology models share some common pathways.

However, we acknowledge that LY344864 may be working through pathways other than PGC-1α and may be affecting multiple cell types other than just the proximal tubules. Therefore, further experiments are required to determine the mechanism of action of LY344864 and the role of PGC-1α. First, transgenic mice that have tubule specific knockout and overexpression of PGC-1α need to be administered RLDC and nephrotoxicity assessed. Second, in the transgenic mice with tubule specific knockout of PGC-1α on RLDC model will be administered LY344864. These mice should have no nephroprotection from LY344864, if the mechanism is through increased PGC-1α in the tubule cells. Third, a second drug that works through the same 5HT-$_{1F}$ receptor needs to be tested. There is an FDA approved 5HT-$_{1F}$ agonist and subsequent studies should be conducted with Lasmiditan to strengthen the clinical relevance of this work. The ideal study would be a clinical trial using Lasmiditan in cancer patients treated with cisplatin to prevent cisplatin toxicity. Furthermore, we believe that increasing PGC-1α leads to increased mitochondrial biogenesis and content. If all of these experiments fail to provide protection against RLDC, it only shows the limited role of PGC-1α. More experiments altering kidney mitochondrial content alone need to be completed to determine if increasing mitochondrial content through alternative pathways will provide protection.

The repeated insult of cisplatin produces a failed-repaired tubule cell population [160], which can lead to a maladaptive repair process, fibrosis, and ultimately, CKD. Correct adaptive tissue repair is energy intensive, requiring sufficient mitochondrial mass and mitochondrial respiration to produce the necessary building blocks for cell replication and cell growth [94]. Our findings suggest that increasing mitochondrial content in the kidneys can protect against cisplatin-induced nephrotoxicity, allowing for a more complete recovery. However, it is important to note that cisplatin is only used in cancer patients, and

current mouse models used to study cisplatin-induced nephrotoxicity do not fully represent this comorbidity. Therefore, there is a need to include cancer in the RLDC model to understand the role of solid organ tumors in cisplatin-induced nephrotoxicity. The presence of cancer will likely alter the nephrotoxicity of cisplatin and interfere with nephroprotective strategies. Understanding the role of solid organ tumors in cisplatin-induced nephrotoxicity may provide mechanistic insights and novel therapeutic targets for the prevention and effective treatment of cisplatin-induced nephrotoxicity and the development of CKD. In conclusion, our study suggests that LY344864 provides protection against cisplatin-induced kidney injury, interstitial fibrosis, and inflammation by increasing mitochondrial content in mice without cancer.

CHAPTER 4: LUNG CANCER-KIDNEY CROSSTALK INDUCES KIDNEY INJURY, INTERSTITIAL FIBROSIS, AND ENHANCES CISPLATIN-INDUCED NEPHROTOXICITY. (PUBLISHED)

INTRODUCTION

This chapter has been reformatted for the dissertation from the following publication [226].

The altered physiology of cancer patients and their unique susceptibility to kidney disease has led to the rapidly growing specialty of Onconephrology [17-23]. Cancer patients often have decreased kidney function [24-26], and drug-induced acute kidney injury (AKI) is common and remains a hurdle [27-32]. Drug-induced AKI can interrupt therapy and reduce overall survival [111, 112]. Cisplatin is a commonly used chemotherapeutic with cure rates as high as 80% in testicular cancer [227, 228] and prolongs survival in multiple other solid organ cancers [14]. Cisplatin causes AKI in 30% of patients [30, 31, 39], and repeated cycles of cisplatin increase rates of chronic kidney disease (CKD) [14]. AKI and CKD are interconnected syndromes [6] involving maladaptive repair processes [8]. Recent advances have increased our understanding of the pathophysiology of the injury that occurs from repeated low-dose cisplatin (RLDC). Single-nucleus transcriptional profiling analysis following RLDC uncovered a unique proximal tubule cell population in an injury/repair phase [159]. Additionally, injury from cisplatin produces a proinflammatory failed-repaired tubule cell population, and the repeated administration of cisplatin exacerbates kidney injury through the accumulation of DNA damage to tubule cells attempting to repair from the previous round of cisplatin injury [160]. These studies have helped shed light on the mechanism driving AKI to CKD

transition from RLDC. Cisplatin-induced nephrotoxicity has been studied extensively [39, 115, 121, 210, 211], and most of this work has been completed in mouse models without cancer. We believe the altered physiology of cancer patients is not adequately represented in these models, and adding the comorbidity of cancer to this model will further our understanding of the pathophysiology.

Preclinical models of cisplatin-induced nephrotoxicity have failed to include the critical variable of cancer. In this study, we used multiple mouse models of lung cancer in combination with repeated low-dose cisplatin (RLDC) regimen to begin to understand the interplay between lung cancer and cisplatin-induced nephrotoxicity. Data indicate that lung cancer-bearing mice treated with RLDC have increased renal toxicity, injury, and fibrosis as compared to non-lung cancer-bearing mice. Additionally, lung cancer alone induced kidney injury and fibrosis prior to cisplatin treatment. Lung-kidney crosstalk is a known phenomenon [229, 230], and recent work has shown that during AKI events, the kidneys release cytokines that induce lung injury [231]. Further work is required to understand the mechanism driving this process. We believe the presence of lung cancer induces the first hit of injury in the kidney, which potentiates the nephrotoxicity of cisplatin.

The results of this work support the hypothesis that the comorbidity of cancer alters the complexity of cisplatin-induced nephrotoxicity that current models are not capturing. Data presented here suggest that cancer primes kidneys for chemotherapy-induced injury. Understanding mechanisms by which distant tumors affect kidney physiology to cause injury and fibrosis is essential in our ability to develop nephroprotective strategies for cancer patients. We believe these results highlight the necessity of using preclinical models that more accurately capture the complexity of cancer patients treated with cisplatin.

MATERIALS AND METHODS

ANIMALS

All mice were maintained on a 12-hour/12-hour light/dark cycle and provided with food and water *ad libitum*. Animals were maintained under standard laboratory conditions. All animal procedures were approved by the Institutional Animal Care and Use Committee of the University of Louisville (Protocol ID 19568) and followed the guidelines of the American Veterinary Medical Association.

GENETICALLY ENGINEERED MOUSE MODEL OF LUNG CANCER

In the genetically engineered mouse model (GEMM) of lung cancer, at weaning all mice were fed doxycycline chow for 9-10 months, and the mice with both transgenes developed lung adenoma (Figure 15A). Mice expressing clara cell-specific promoter-reverse tetracycline transactivator (CCSP-rtTA) were crossed with mice expressing the tet-Operon of Kras4bG12D (KrasG12D). The rtTA is constitutively expressed in type II lung epithelial cells via a Clara cell-specific promoter (CCSP). In the presence of doxycycline, the rtTA binds to the tet-Operon of Kras4bG12D (KrasG12D), thereby inducing the expression of mutant Kras. Only double transgenic mice (positive for both CCSP-rtTA/tet-O-Kras4bG12D) on a doxycycline diet will develop lung adenoma. Single transgenic mice (positive for CCSP-rtTA or tet-O-Kras4bG12D) were used as littermate controls in this experiment and do not develop lung adenoma in the presence of doxycycline chow. All mice were in doxycycline-containing chow for an identical length of time. The experimental design for this study is shown in Figure 15B, Single (+/-) and double (+/+) transgenic 40-week-old male and female mice on doxycycline chow were administered either saline vehicle (0.9% normal saline) or cisplatin (7 mg/kg; pharmaceutical grade cisplatin, NDC 16729-288-38) once a week for four weeks via intraperitoneal (i.p.) injection at 8-9AM. Animals were euthanized 72 hours following their final cisplatin injection. Mice

were monitored daily and euthanized if they had signs of obvious discomfort/stress and had ≥20% weight loss.

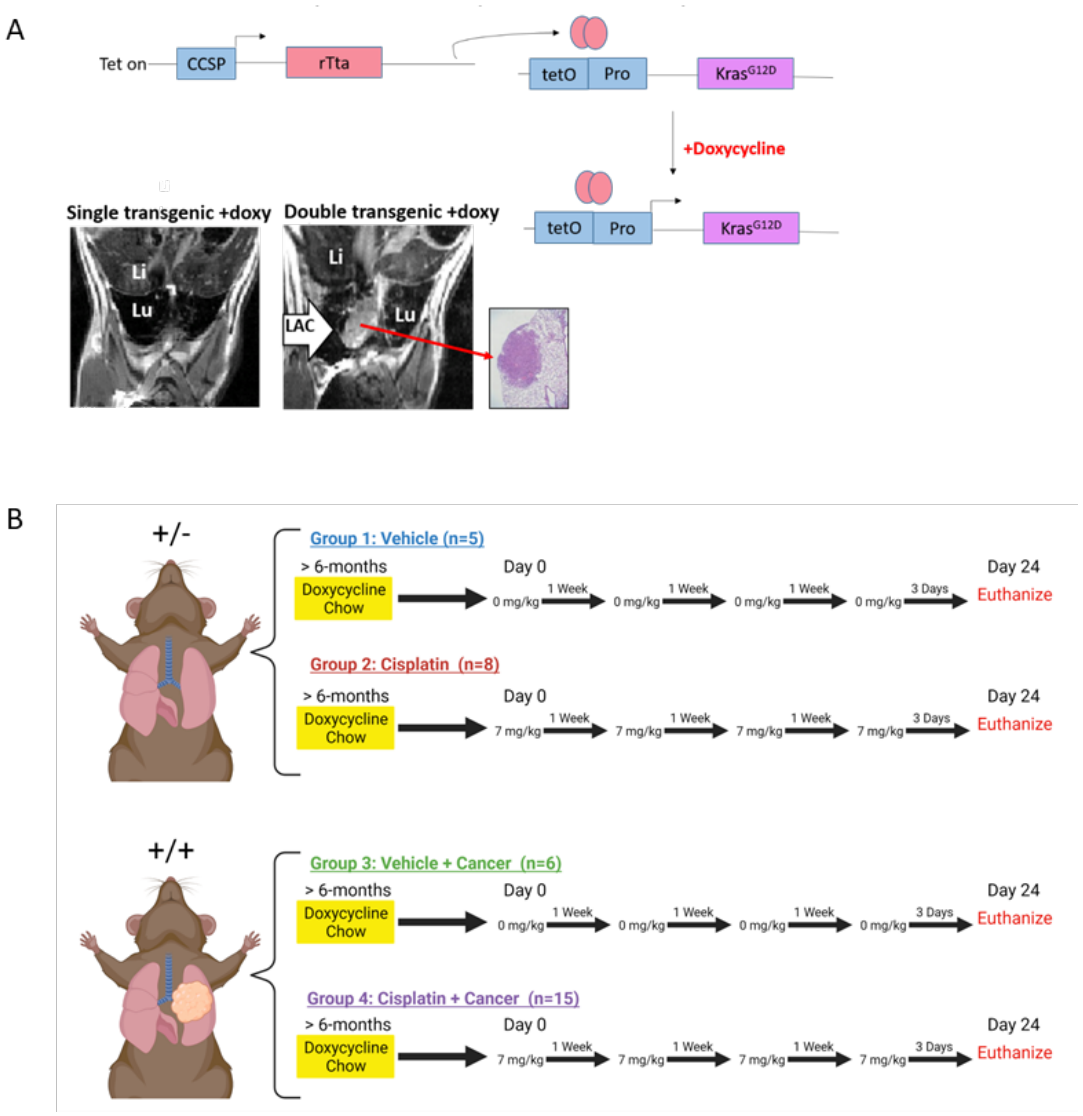

Figure 15. Inducible lung adenocarcinoma model using transgenic mutant Kras mice.

(A) In this double transgenic model, the reverse tetracycline transactivator (rtTA) is constitutively expressed in type II lung epithelial cells via a Clara cell-specific promoter (CCSP). The rtTA, in the presence of doxycycline, binds to the tet-Operon of Kras4bG12D (KrasG12D), thereby activating the expression of mutant Kras. Only mice that have both transgenes for CCSP-rtTA/tet-O-Kras4bG12D and that are on a doxycycline diet will develop lung adenocarcinoma. (B) Single transgenic mice (+/-) were used as littermate controls and do not develop cancer following doxycycline chow. Double transgenic mice (+/+) develop cancer following exposure to doxycycline. Cisplatin or saline was administered via intraperitoneal injection once a week for four weeks. Animals were euthanized 72 hours following their final cisplatin injection. Figure (B) was created using BioRender.com.

SYNGENEIC XENOGRAFT MODEL OF LUNG CANCER

In the syngeneic xenograft model (SXM) of lung cancer, the mouse lung adenocarcinoma cell line (238N1) previously developed [232] was injected subcutaneously into B6129SF1/J male mice. Eight- to ten-week-old male B6129SF1/J (B6129) mice were purchased from The Jackson Laboratory. Mice were randomly assigned into four treatment groups: 1. non-cancer/vehicle, 2. non-cancer/cisplatin, 3. cancer/vehicle, and 4. cancer/cisplatin. In the cancer groups, 10,000 lung adenocarcinoma cells (238N1) were injected subcutaneously in the right rear flank seven days before the start of cisplatin treatment. Experimental Design is shown in Figure 16A. Pharmaceutical grade cisplatin (NDC 16729-288-38, 1 mg/ml) or saline vehicle (0.9% normal saline) was administered via intraperitoneal (i.p.) injection once a week between 8-9AM for four weeks. In the vehicle group, 400 µL normal saline was administered via i.p. injection. In the cisplatin treatment group, 7mg/kg of cisplatin in normal saline in a total volume of 400 µL was administered via i.p. injection. Animals were euthanized 72 hours following their final cisplatin injection.

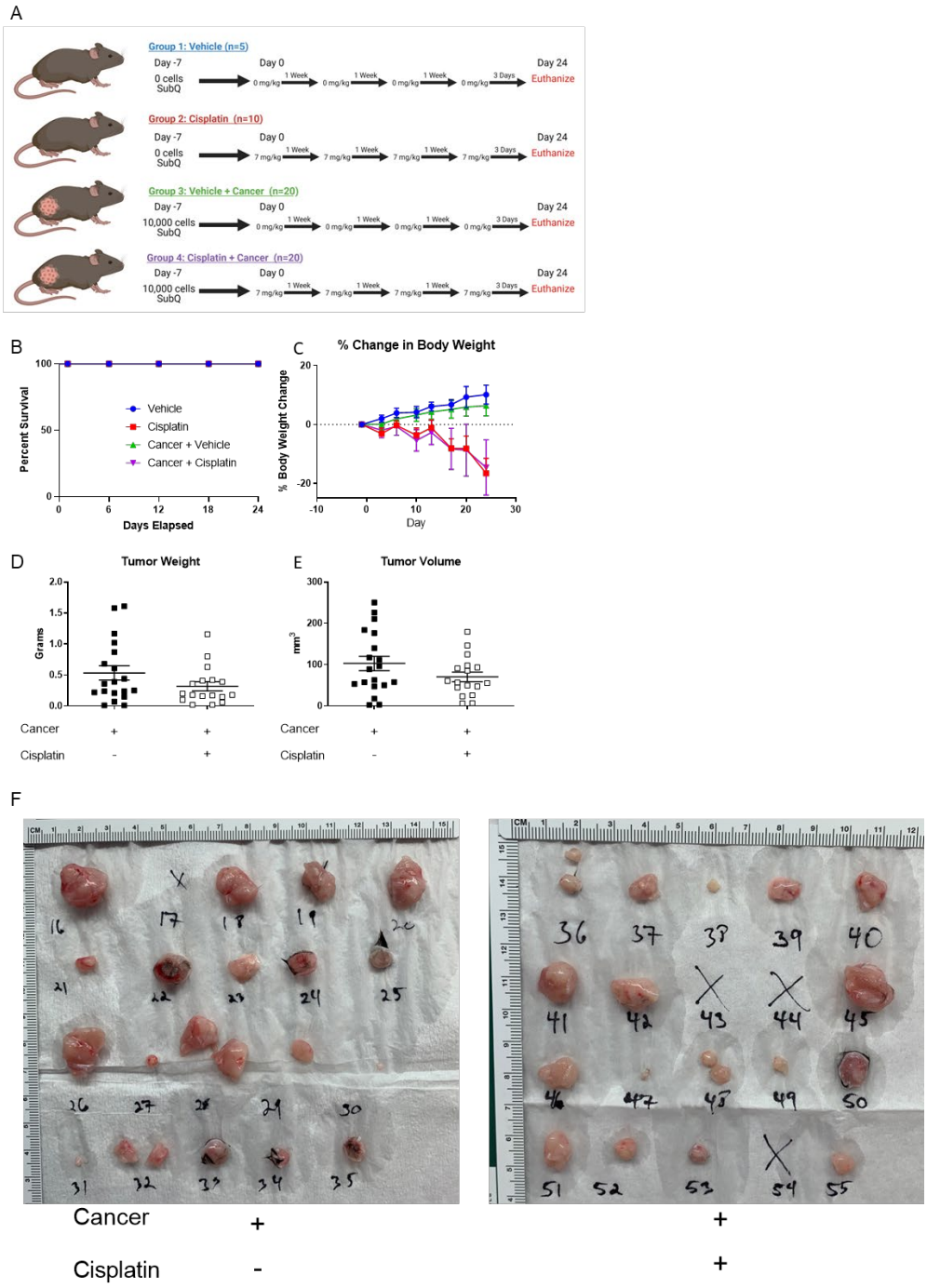

Figure 16. Repeated administration of low-dose cisplatin does not alter overall survival in mice with subcutaneous lung cancer.

Eight- to ten-week-old B6;129 male mice were randomly assigned into four treatment groups: 1. non-cancer + vehicle, 2. non-cancer + cisplatin, 3. cancer + vehicle, 4. cancer + cisplatin. In the cancer groups, 10,000 lung adenocarcinoma cells were injected subcutaneously seven days prior to the start of cisplatin treatment. Cisplatin or saline was administered via intraperitoneal injection once a week for four weeks. Animals were euthanized 72 hours following their final cisplatin injection. (A) Experimental Design, (B)

Survival Plot. (C) Percentage change in body weight for each group. (D) Tumor Weight and (F) Volume for groups 3 and 4. (F) Photos of tumors after euthanasia. Animals were euthanized 72 hours following their final cisplatin injection. Figure (A) was created using BioRender.com.

IMMUNOCOMPROMISED XENOGRAFT MODEL OF LUNG CANCER

In the immunocompromised xenograft model (IXM) of lung cancer, NRGS mice were injected with mouse lung adenocarcinoma cell line (238N1) as detailed in the SXM model. NRGS mice were derived from NOD.*Rag1*$^{-/-}$;*γc*^{null} (NRG) that express human IL-3, GM-CSF, and SF from the SGM3 (3GS) triple co-injected transgenes [233-235]. Eight- to twelve-week-old male NRGS mice were randomly assigned into two groups: 1. non-cancer and 2. cancer. In the cancer group, 10,000 lung adenocarcinoma cells (238N1) were injected subcutaneously (100 µL in Hank's buffered saline) into the right rear flank. The mice were aged out for 31 days to match the same number of days as in previous experiments. Experimental design is shown in Figure 17A.

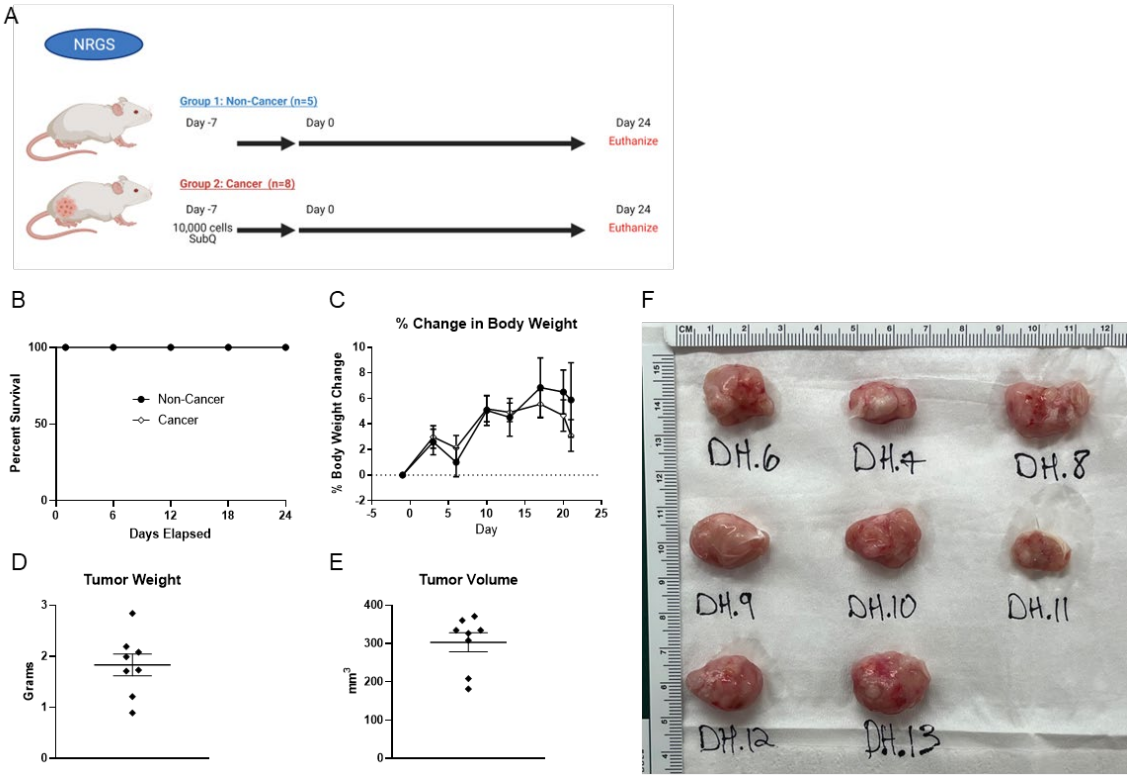

Figure 17. Experimental design for subcutaneous lung cancer model in immunocompromised mice.

(A) Eight- to twelve-week-old NRGS male mice were randomly assigned into two groups: 1. non-cancer, 2. cancer. In the cancer group, 10,000 lung adenocarcinoma cells were injected, and the mice were aged out to match the same number of days as in previous experiments. (B) Survival Plot. (C) Percentage change in body weight for each group. (D) Tumor Weight and (E) Volume. (F) Photos of tumor after euthanasia. Animals were euthanized on day 24 to match previous experiments. Figure (A) was created using BioRender.com.

BLOOD UREA NITROGEN (BUN) AND NEUTROPHIL GELATINASE ASSOCIATED LIPOCALIN (NGAL) DETERMINATION

BUN (AMS Diagnostics, 80146) levels were measured from plasma samples using the indicated kits following the manufacturer's instructions. ELISAs for NGAL (R&D Systems, DY1857) were performed on the urine as directed by the manufacturer, as previously published [152].

PROTEIN QUANTIFICATION AND WESTERN BLOT ANALYSIS

Kidney tissues were homogenized in cell extraction buffer (Thermo Fisher Scientific) containing a Complete Protease Inhibitor Cocktail Tablet and Phosphatase Inhibitor Cocktail Tablet (Roche). Homogenates were centrifuged at 15,000 X g for 10 min at 4° C. Supernatants were removed and stored at -80°C. Protein concentrations were determined using BCA reagent (Thermo Fisher Scientific). 40 µg of kidney homogenate protein were loaded and separated on 4–12% gradient Tris-Glycine-SDS polyacrylamide gels. Protein was then transferred to PVDF membranes that were blocked in 5% (w/v) dried milk in tris buffered saline 0.1% Tween 20 (TBST) for 1 hour. Membranes were incubated with primary antibody overnight at 4°C. The following day, membranes were washed three times for 5 min each with TBST containing 5% (w/v) dried milk. Membranes were then incubated for 2 hours at room temperature with secondary antibodies conjugated with horseradish peroxidase (1:20,000) in TBST containing 1% (w/v) dried milk. Following two washes with 1% (w/v) dried milk and one wash in TBST membrane proteins were detected by chemiluminescence substrate.

ANTIBODIES

The following antibody was purchased from Cell Signaling Technology: Transforming growth factor-beta (TGF-β) #3711. The following antibody was purchased from Abcam: α-Smooth Muscle Actin (α-SMA, Abcam, ab5694). The remaining antibodies include fibronectin (F3648, Sigma-Aldrich) and α-tubulin (SC-5286, Santa Cruz Biotechnology).

GENE EXPRESSION

RNA was isolated from kidney tissue using E.Z.N.A. Total RNA Kit 1 (OMEGA) per manufacturer's protocol. cDNA was synthesized with High-Capacity cDNA Reverse Transcriptase PCR (Thermo Fisher Scientific) per the manufacturer's instructions. Gene-specific cDNA was quantified with real-time qRT-PCR using predesigned TaqMan assays or self-designed SYBR assays. The following TaqMan primers were purchased from Thermo Fisher Scientific: tumor necrosis factor-alpha (*Tnf*-α, Mm00443258_m1), chemokine (C-X-C Motif) ligand 1 (*Cxcl1*, Mm04207460_m1), interleukin-6 [*Il-6* (Mm00446190_m1)], *Mcp-1* (Mm00441242_m1), and the housekeeping gene beta-2-microglobulin (*B2m*, Mm00437762_m1). The following primers were self-designed: kidney injury molecule-1 (*Kim-1*) (For: AGATCCACACATGTACCAACATCAA, Rev: CAGTGCCATTCCAGTCTGGTTT), *Timp-1* (For: GCAACTCGGACCTGGTCATAA, Rev: TTAGTCATCTTGATCTTATAACGCTGGTA), *Nlpr3* (For: AAGATGAAGGACCCACAGTGTAACTT, Rev: CAGATTGAAGTAAGGCCGGAATT) , and *Col1a1* (For: CGATGGATTCCCGTTCGAGTA, Rev: GTGGACATTAGGCGCAGGAA). qRT-PCR was done with either iTaq Universal Probes Supermix (172-5134, Bio-Rad) or iTaq Universal SYBR Green Supermix (172–5124, Bio-Rad).

TISSUE HISTOLOGY

Sirius Red/Fast Green and Masson's Trichrome staining was performed on formalin-fixed paraffin-embedded (FFPE) kidney sections (5 μm thick) for total collagen deposition as previously published [152, 223].

QUANTIFICATION OF TISSUE HISTOLOGY

Orbit Image Analysis software [224] (version 3.64) was used to quantify positive staining of kidney histology. The Tissue Quantification feature was used to quantify collagen staining. The software developers' protocol was followed for training the software to correctly identify collagen over normal tissue [224, 225]. In the training step the images were labeled by manually drawing several annotations per tissue class (e.g., collagen, normal tissue,). After training the software images were tested to verify correct determination of positive staining. Digital scans of kidney sections were divided into 5-8 sections and the classification (e.g. collagen, normal tissue) of the tissue sections were assigned by the software. The percentage of collagen per image was used to quantify positive staining.

FLOW CYTOMETRY

Whole kidneys were homogenized into single-cell suspensions via mechanical disruption and enzymatic digestion with Liberase DL Research Grade (05466202001, Millipore/Sigma). After passing through a 40-μm filter, cells were treated with ACK Lysing Buffer (A1042-01,Thermo Fisher Scientific) for 2 min to remove red blood cells. Cells were then suspended in PBS with 0.5% BSA, 0.01% sodium azide, and 2 mM EDTA. Cells were blocked with CD16/32 (101321; BioLegend) and extracellularly stained with CD45-PerCP (103130; BioLegend), CD3e-PE-Cy7 (552774; BD Biosciences), CD19-PE-CF594 (562329; BD Biosciences), CD4-FITC (100406; BioLegend), CD8a-BUV737 (612759; BD

Biosciences), Ly-6G-Alexa Fluor 700 (561236; BD Biosciences), Ly-6C-APC-Cy7 (560596; BD Biosciences), F4/80-BV421 (565411; BD Biosciences), and CD11b-BV650 (563402; BD Biosciences). After staining, cells were fixed and permeabilized with FoxP3/Transcription Factor Staining Buffer Set (00-5523-00;Thermo Fisher Scientific). Intracellular staining was done with CD206-PE (141705; BioLegend). Hierarchical gating was performed as previously [223]. Data are represented as the percentage of positively stained cells for the indicated population from the total number of single cells observed in that sample. Resident macrophages are identified as CD45+CD3–CD19–CD11b+F4/80 Hi. Infiltrating macrophages are identified as CD45+CD3–CD19–CD11b+F4/80 Lo.

STATISTICAL ANALYSES

Quantitative data are expressed as the mean ± SEM for all experiments. Statistical significance was determined using GraphPad Prism software 9.4.1. Statistically significant differences were determined by Two-Way ANOVA followed by Tukey post-test in the GEMM and SXM. In the IXM, the statistical significance was determined by an unpaired T-test. The criterion for the statistical difference was $P < 0.05$.

RESULTS

Lung cancer reduces overall survival, worsens kidney injury and fibrosis in mice administered RLDC. Cisplatin nephrotoxicity has almost exclusively been studied in mice without cancer. However, only patients with cancer receive cisplatin and the risk of cancer increases with age [236-238]. To model this aging cancer patient population, we used forty-week-old transgenic CCSP-rtTA/Tet-O-Kras mice that develop lung adenoma. Forty-week-old non-cancer mice treated with either 4 doses of vehicle or 4 doses 7 mg/kg cisplatin had 100% survival at Day 24 (Figure 18A). Cancer mice treated with vehicle had 83% survival, and cancer mice treated with 7 mg/kg (4 doses) cisplatin had 47% overall survival (Figure 18A). This is in contrast with multiple studies by our lab and others [152-157, 159, 160, 223, 239] where mice treated with 7 mg/kg of cisplatin once a week for 4 weeks had 100% survival rate at Day 24. BUN and NGAL were used to assess kidney function and injury, respectively. In the cisplatin treated mice with and without lung cancer, there was no difference in BUN (Figure 18B). After 4 doses of cisplatin, NGAL levels increased nearly 80-fold (43 to 3,438 ng/ml) in non-cancer/cisplatin mice, but only 4-fold (325 to 1,258 ng/ml) in cancer/cisplatin mice that survived to Day 24 (Figure 18C). There is however a survivorship bias in these results, as we only have data on the mice that survived the entire treatment regimen. Because of the dramatic drop in survival, we decided to repeat the experiment and collect urine at earlier times (3-6 days after doses 1 and 2 of cisplatin) to assess NGAL levels. Previously we have shown only mild elevation of NGAL after the 2nd dose of cisplatin [152]. After a single dose of cisplatin, cancer mice had a 19-fold (188 to 3,599 ng/ml) increase in urinary NGAL and after 2 doses, over 100-fold (100 to 10,675 ng/ml) compared to non-cancer/cisplatin mice (Figure 18D). These data suggest that mice with cancer have worsened kidney injury that occurs earlier in the dosing regimen compared to mice without cancer.

Multiple studies have shown that the RLDC model induces renal fibrosis [152, 158, 223]. There is no published data on how cancer alters the development of renal fibrosis following cisplatin treatment. TGF-β1is considered a master regulator of fibrosis [95], and TGF-β1protein levels are increased in the non-cancer/cisplatin mice (Figure 18E). These levels are further elevated in the cancer/cisplatin mice (Figure 18E). Fibronectin is a protein found in the extracellular matrix, and its levels were elevated in a similar pattern with cancer increasing the accumulation following cisplatin treatment (Figure 18E). These results were confirmed by SR/FG (Sirius Red/Fast Green) staining for total collagen deposition showing an increase in cisplatin-treated mice that is additionally elevated in cancer mice treated with cisplatin (Figure 18E). Results indicate that the presence of cancer with moderate aging potentiates the nephrotoxicity of cisplatin. Previous work from our lab has shown that moderate aging alone does not alter cisplatin nephrotoxicity [154], however it cannot be ruled out that the combination of cancer and moderate aging is responsible for the increased kidney injury and fibrosis in this model.

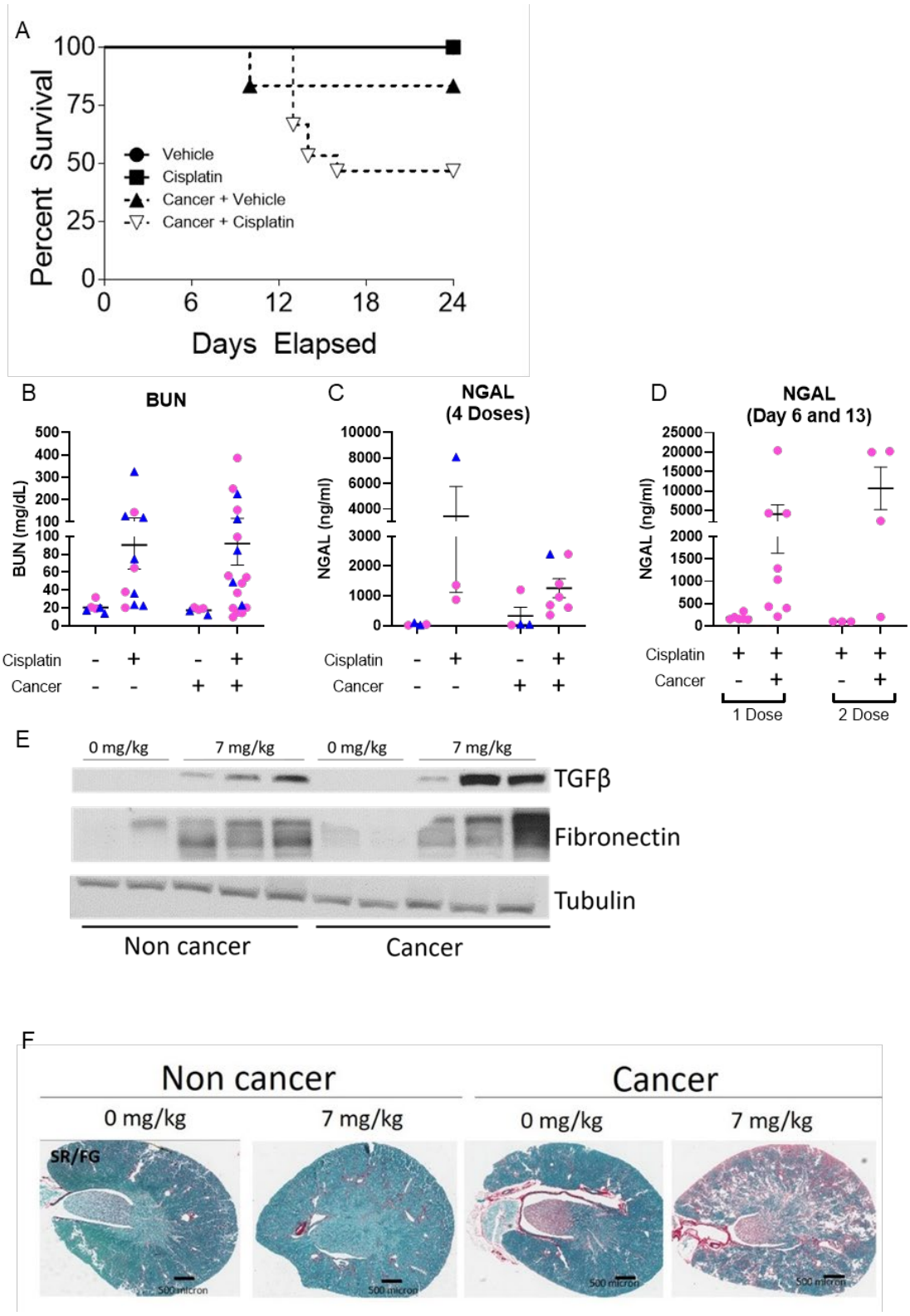
A
Percent Survival
100
75
50
25
0
0
6
12
18
24
Days Elapsed
Vehicle
Cisplatin
Cancer + Vehicle
Cancer + Cisplatin
B
BUN
BUN (mg/dL)
Cisplatin
Cancer
C
NGAL
(4 Doses)
NGAL (ng/ml)
Cisplatin
Cancer
D
NGAL
(Day 6 and 13)
NGAL (ng/ml)
Cisplatin
Cancer
1 Dose
2 Dose
E
0 mg/kg
7 mg/kg
0 mg/kg
7 mg/kg
TGFβ
Fibronectin
Tubulin
Non cancer
Cancer
F
Non cancer
Cancer
0 mg/kg
7 mg/kg
0 mg/kg
7 mg/kg
SR/FG
500 micron

Figure 18. Repeated administration of low-dose cisplatin decreases overall survival in mice with transgenic lung cancer.

Forty-week-old male and female mice with and without cancer were treated with either 0 or 7 mg/kg cisplatin once a week for four weeks. Mice that showed obvious signs of discomfort/stress and that had ≥20% weight loss were euthanized before the end of the study. (A) Survival Plot, (B) BUN levels from plasma, and (C) Urine NGAL levels were measured following four doses of cisplatin on Day 24. (D) Urine NGAL levels were measured on days 6 and 13 in mice treated with 1 or 2 doses of cisplatin, respectively. (E) Protein levels of TGFβ and Fibronectin in kidney cortex homogenates were determined by Western blot. (F) SR/FG stain for total collagen levels. Statistical significance was determined by Two-Way ANOVA followed by Tukey post-test. ▲ = Males, ● = Females

Subcutaneous lung cancer induces kidney injury and exacerbates cisplatin toxicity. The previous GEMM included both lung cancer and moderate aging as variables. We chose a SXM of lung cancer to determine if cancer in young mice will increase the nephrotoxicity of cisplatin. Eight- to ten-week-old B6;129 male mice with and without subcutaneous syngeneic lung adenocarcinoma tumors (Figure 16A), were injected with either cisplatin (7mg/kg) or normal saline (vehicle) once a week for 4 weeks. The mice in this study had a 100% survival rate (Figure 16B). The non-cancer/cisplatin group had decreased kidney function as measured by increased BUN levels, and increased kidney injury shown by increased urinary NGAL and kidney KIM-1 expression (Figure 19A-C), similar to previous results [152, 153, 158]. The cancer/cisplatin group had significantly elevated BUN, NGAL, and KIM-1 expression compared to non-cancer/vehicle group (Figure 19A-C). Comparing non-cancer/cisplatin and cancer/cisplatin we observed no effect on BUN, non-significantly increased urinary NGAL levels, and significantly lowered KIM-1 expression levels (Figure 19A-C). Mice in the cancer/vehicle group had increased BUN, NGAL, and KIM-expression (Figure 19A-C; Figure 20A-C), as compared to the non-cancer/vehicle group. There was a large amount of variability in the tumor sizes between mice (Figure 16D-F). The lack of consistent tumor size obscured the effect of cisplatin to significantly reduce tumor size, subsequent studies with similar tumor burden have resolved this issue (data not shown). Mice in the cancer/vehicle group were grouped by their tumor weight. Data indicate as tumor size increases there is an increasing degree of kidney injury as detected by urinary NGAL (Figure 19E) and KIM-1 mRNA expression (Figure 19F). In some mice in the cancer/vehicle group, kidney injury markers were higher than those in the non-cancer/cisplatin group. The BUN levels (Figure 19D) also trended with increasing tumor size in the cancer/vehicle group. These data suggest that increased tumor burden negatively impacts kidney function and injury.

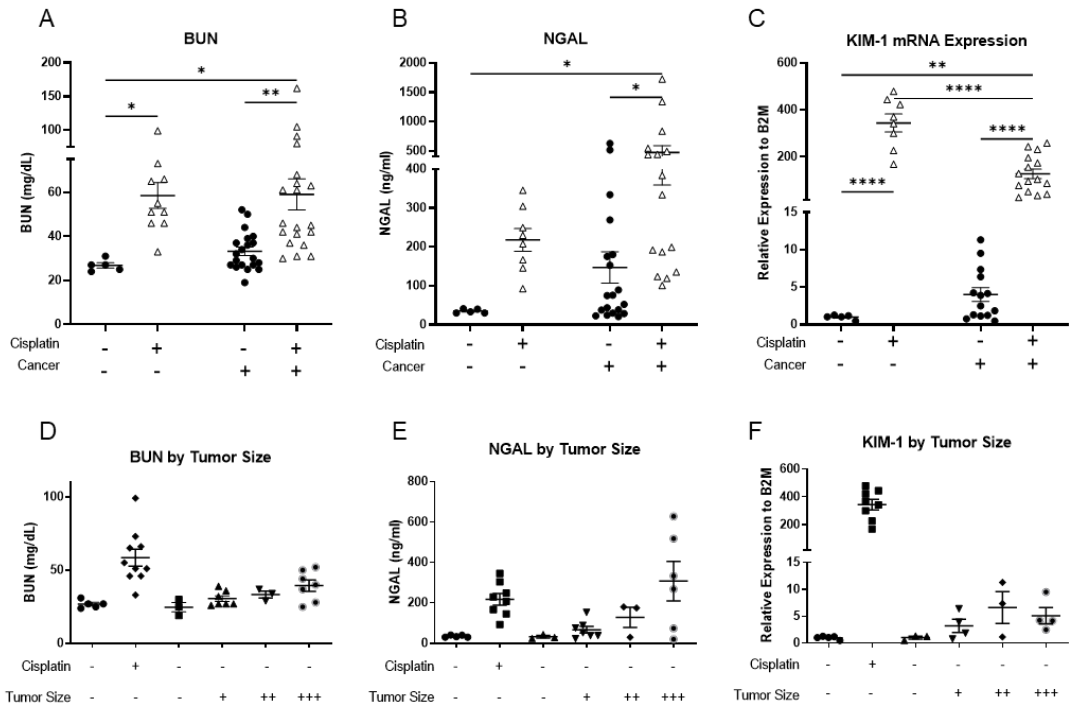

Figure 19. Kidney function and injury following RLDC in mice with and without subcutaneous lung cancer.

Eight- to ten-week-old B6;129 male mice with and without subcutaneous cancer were treated with either 0 or 7 mg/kg cisplatin once a week for four weeks. (A) BUN levels from plasma and (B) Urine NGAL levels were measured following four doses of cisplatin on Day 24. (C) qRT-PCR of KIM-1 in kidney cortex homogenates is normalized to B2M. Figures D-F show data from the Cancer + Vehicle group separated by tumor size from BUN, NGAL, and KIM-1, respectively. Data are expressed as means ± SEM; n=5–10. Statistical significance was determined by Two-Way ANOVA followed by Tukey post-test. *p < 0.05 **p<0.01, ****p < 0.0001

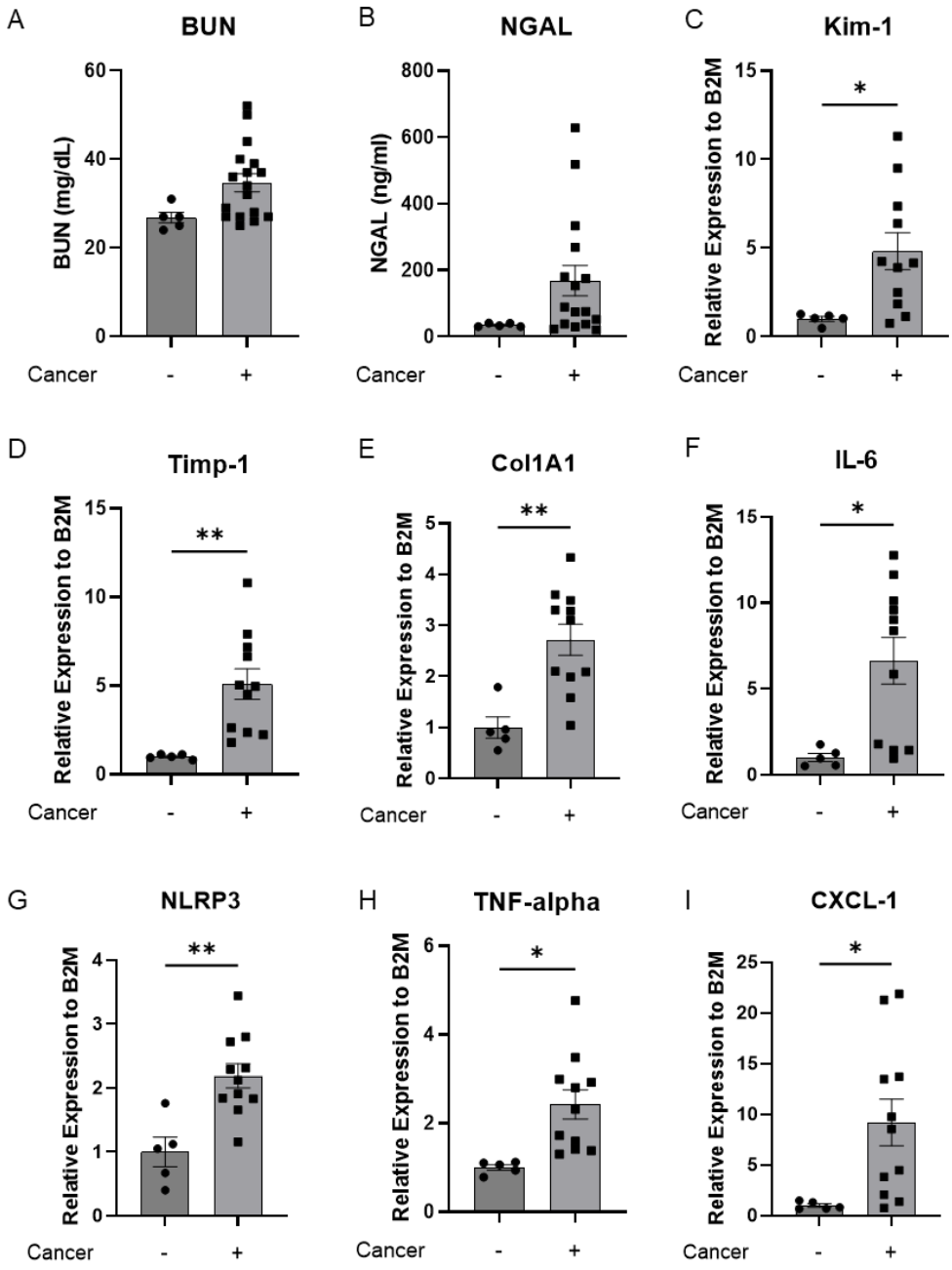

Figure 20. Kidney function, injury, fibrosis, and inflammation in mice with and without subcutaneous lung cancer.

Eight- to ten-week-old B6;129 male mice with and without subcutaneous cancer. (A) BUN levels from plasma and (B) Urine NGAL levels were measured following four doses of cisplatin on Day 24. qRT-PCR of (C) KIM-1, (D) TIMP-1, (E) COL1A1, (F) IL-6, (G) *NLRP3*, (H) TNF-α, and (I) CXCL-1 in kidney cortex homogenates is normalized to B2M. Data are expressed as means ± SEM; n=5–10. Statistical significance was determined by an unpaired t-test. *p < 0.05 **p<0.01

Subcutaneous lung cancer induces kidney fibrosis and increases cisplatin induced kidney fibrosis. We determined the development of interstitial fibrosis on FFPE kidney sections using SR/FG and Masson's trichrome. There was increased SR staining in the no-cancer/cisplatin group as compared to the no-cancer/vehicle group as expected and previously reported (Figure 21A-B; [152, 153, 158]). SR staining was also increased in the cancer/vehicle group as compared to the no-cancer/vehicle group (Figure 21A-B). Comparing non-cancer/cisplatin and cancer/cisplatin we observed additive SR staining in the cancer/cisplatin kidneys (Figure 21A-B). We determined kidney cortex protein levels of fibronectin, α-SMA, and TGF-β1via western analysis. All three markers were increased in the non-cancer/cisplatin group as compared to the non-cancer/vehicle group (Figure 21C). The cancer/vehicle group had increased protein levels of fibronectin, α-SMA, and TGF-β1(Figure 21C) as compared to the non-cancer/vehicle group, which even were further elevated in cancer/cisplatin group (Figure 21C). There was increased expression of Timp-1 and Col1a1 in the cancer/vehicle group as compared to the no-cancer/vehicle group and these levels increased with increasing tumor size (Figure 20D-E, Figure 22A-B). Data indicate as tumor size increases there is an increase in kidney fibrosis.

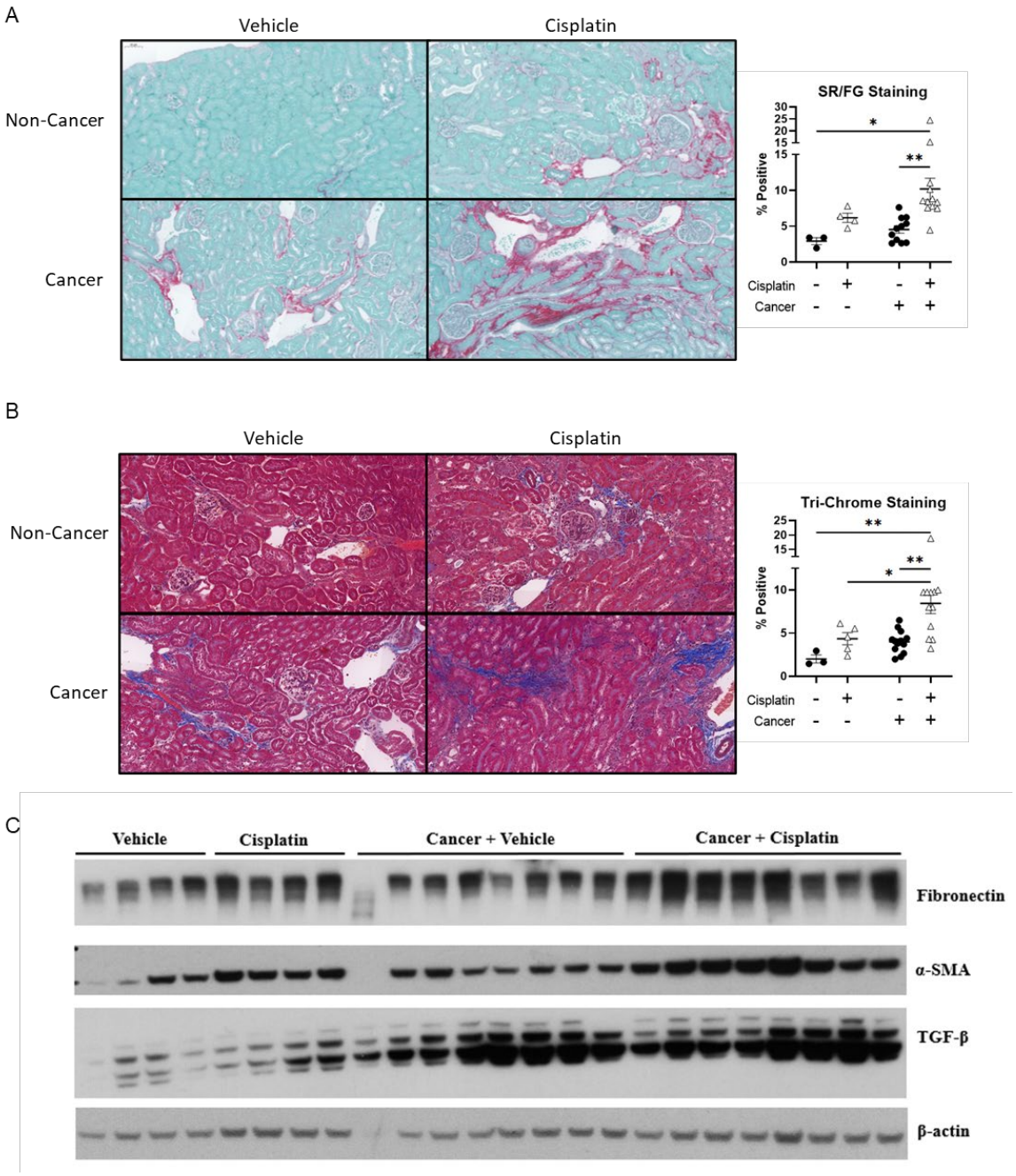

Figure 21. Kidney fibrosis following RLDC in mice with and without subcutaneous lung cancer.

(A) SR/FG stain & (B) Masson's trichrome for total collagen levels on 5-μm-thick paraffin-embedded kidney sections and the quantifications. (C) Protein levels of Fibronectin, α-SMA, TGF-β, and β-Actin in kidney cortex homogenates were determined by Western blot.

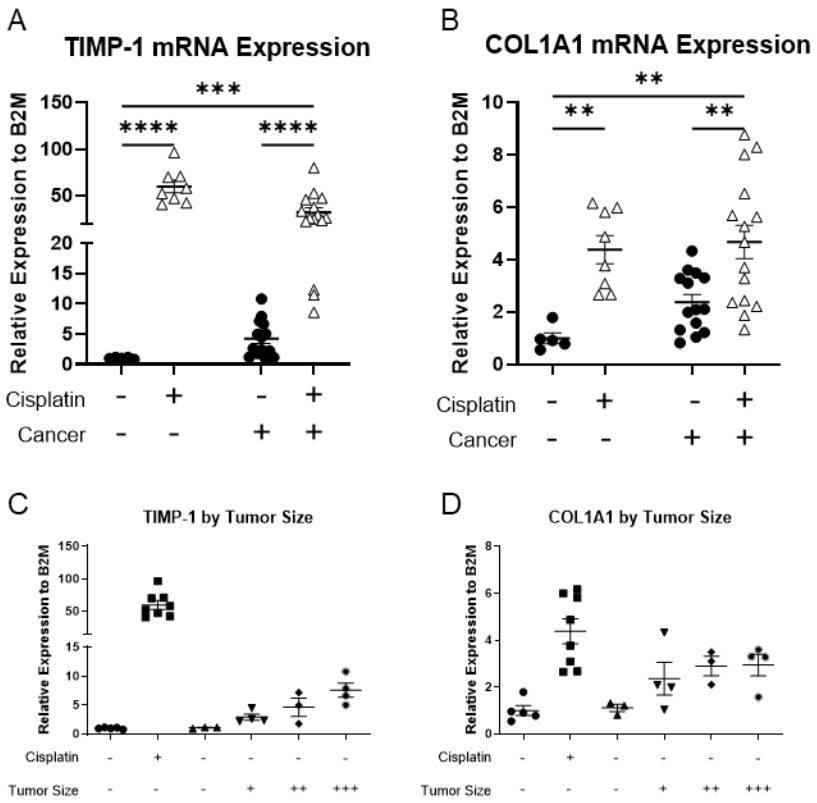

Figure 22. Fibrotic markers in the kidney increase as tumor size increases.

Eight- to ten-week-old B6;129 male mice with and without subcutaneous cancer were treated with either 0 or 7 mg/kg cisplatin once a week for four weeks. mRNA expression via qRT-PCR of (A) TIMP-1, and (B) COL1A1 normalized to B2M. Panels (C) and (D) show data in panels (A) and (B) with the group Cancer + Vehicle group separated by tumor size. Data are expressed as means ± SEM; n=3–15. Statistical significance was determined by Two-Way ANOVA followed by Tukey post-test. **p<0.01, ***p<0.001, ****p < 0.0001

Subcutaneous lung tumors increase kidney inflammation independent of cisplatin treatment. Inflammation plays a role in kidney fibrosis in the RLDC model [223]. We assessed inflammation via expression of kidney inflammatory factors as well as quantification of immune cell infiltrates by flow cytometry. We found increased expression of the inflammation markers *NLRP3*, TNF-α, CXCL1, and IL-6 in the non-cancer/cisplatin group compared to non-cancer/vehicle controls (Figure 23A-D) as expected based off previous work [153, 158, 223]. Inflammatory cytokine and chemokine expression was increased in the cancer/vehicle as compared to the non-cancer/vehicle group (Figure 23A-D; Figure 20F-I). Data indicate as tumor size increases, there is a trend upward in inflammation markers (Figure 24A-D). There is no additive effect to kidney inflammation in the cancer/cisplatin group, when compared to the non-cancer/cisplatin group (Figure 23A-D).

We assessed immune cell infiltration in the kidneys of mice with and without subcutaneous lung cancer following RLDC treated with vehicle or cisplatin. Non-cancer/cisplatin mice had increased infiltration of multiple immune cells types including $CD45^+$, $CD4^+$, and $CD8^+$ cells (Figure 25A-D) in the kidneys compared to vehicle controls, as seen in previous studies [223]. Non-cancer/cisplatin mice had increased $F4/80^{Hi}$ resident macrophages, $F4/80^{Lo}$ infiltrating macrophages, $F4/80^+CD206^+$ macrophages, and $Ly6C^{Hi+}$ cell populations compared to non-cancer/vehicle (Figure 25E-H). In the cancer/vehicle group, we observed variable increases in immune cell infiltration of $CD45^+$, $CD3^+$, $CD4^+$, and $CD8^+$ cells (Figure 25A-D; Figure 26A-D). The $F4/80^{Hi}$, $F4/80^{Lo}$, $F4/80^+CD206^+$, and $Ly6C^{Hi+}$ cell populations were elevated in the cancer/vehicle group as compared to the non-cancer/vehicle controls (Figure 25E-H; Figure 26A-H). We next separated cancer/vehicle group by tumor size and observed that larger tumors had higher levels of immune cell infiltration (Figure 27A-H). In the cancer/cisplatin group, we saw no additive effect on the immune cell population of the kidneys. The combination trended

towards lower immune cell populations compared to non-cancer/cisplatin for $CD45^{+}$, $CD4^{+}$, $CD8^{+}$, $F4/80^{Hi}$, $CD206^{+}$, and $Ly6C^{Hi}$ (Figure 25A-H). These data suggest that lung cancer is altering the immune cell populations of the kidney and hindering immune cell infiltration into the kidney following cisplatin. Tumors have been shown to create microenvironments that benefit that tumor and are immunosuppressive [240-243], a similar process may be occurring in this model.

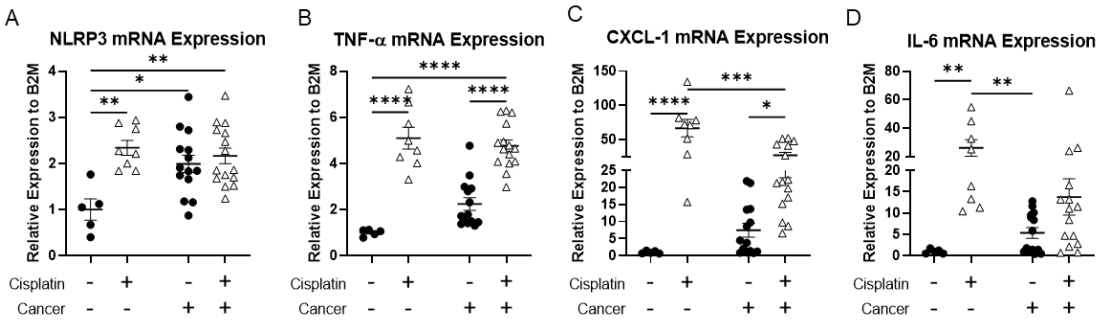

Figure 23. Elevated kidney inflammation following RLDC in mice with and without subcutaneous lung cancer.

Eight- to ten-week-old B6;129 male mice with and without subcutaneous cancer were treated with either 0 or 7 mg/kg cisplatin once a week for four weeks. mRNA expression via qRT-PCR of (A) *NLRP3*, (B) TNF-α , (C) CXCL-1, and (D) IL-6 were measured in the kidney cortex. Data are expressed as means ± SEM; n=5–15. Statistical significance was determined by Two-Way ANOVA followed by Tukey post-test. * p< 0.05, **p<0.01, ***p<0.001, and ****p<0.0001.

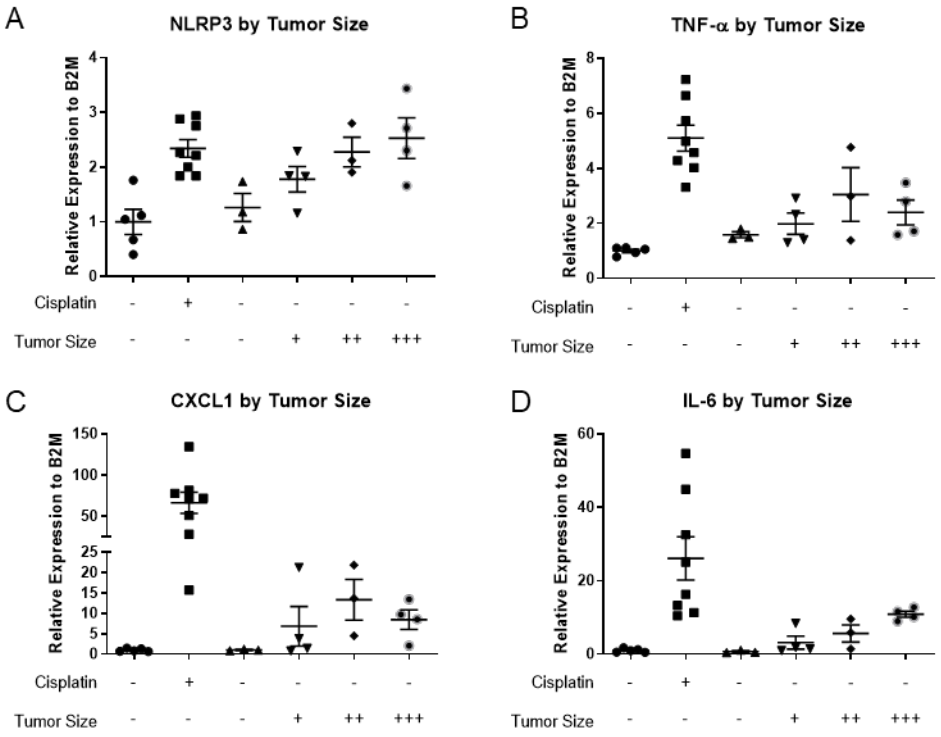

Figure 24. Inflammatory markers in the kidney increase as tumor size increases.

Eight- to ten-week-old B6;129 male mice with and without subcutaneous cancer were treated with either 0 or 7 mg/kg cisplatin once a week for four weeks**.** mRNA expression via qRT-PCR of (A) *NLRP3*, (B) TNF-α, (C) CXCL1, and (D) IL-6 were measured in the kidney cortex and grouped by tumor size from the Cancer + Vehicle group. Data are expressed as means ± SEM; n=3–8

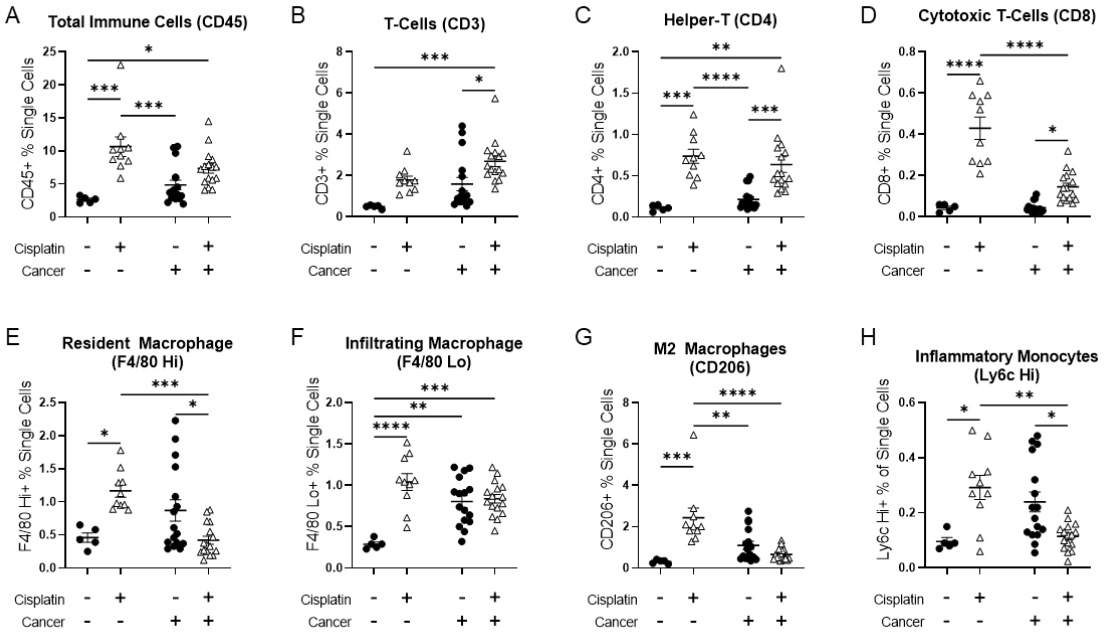

Figure 25. Elevated immune cell infiltration in the kidney following RLDC in mice with and without subcutaneous lung cancer.

Eight- to ten-week-old B6;129 male mice with and without subcutaneous cancer were treated with either 0 or 7 mg/kg cisplatin once a week for four weeks. Flow cytometric analysis of renal immune cells. Whole kidneys were homogenized, made into a single-cell suspension, and then stained with fluorescent antibodies. One million events were collected from each sample. The analysis identified (A) CD45+ immune cells, (B) CD45+ CD3+ T-cells, (C) CD3+CD4+ Helper-T cells, (D) CD3+ CD8+ Cytotoxic T-cells, (E) CD11b+ F4/80 Hi resident macrophages, (F) CD11b+ F4/80 Lo infiltrating macrophages, and (G) F4/80+ CD206+ M2 macrophages, (H) CD11b+ Ly6c Hi inflammatory monocytes. Data are expressed as means ± SEM; n=5–16. Statistical significance was determined by Two-Way ANOVA followed by Tukey post-test. * p< 0.05, **p<0.01, ***p<0.001, and ****p<0.0001.

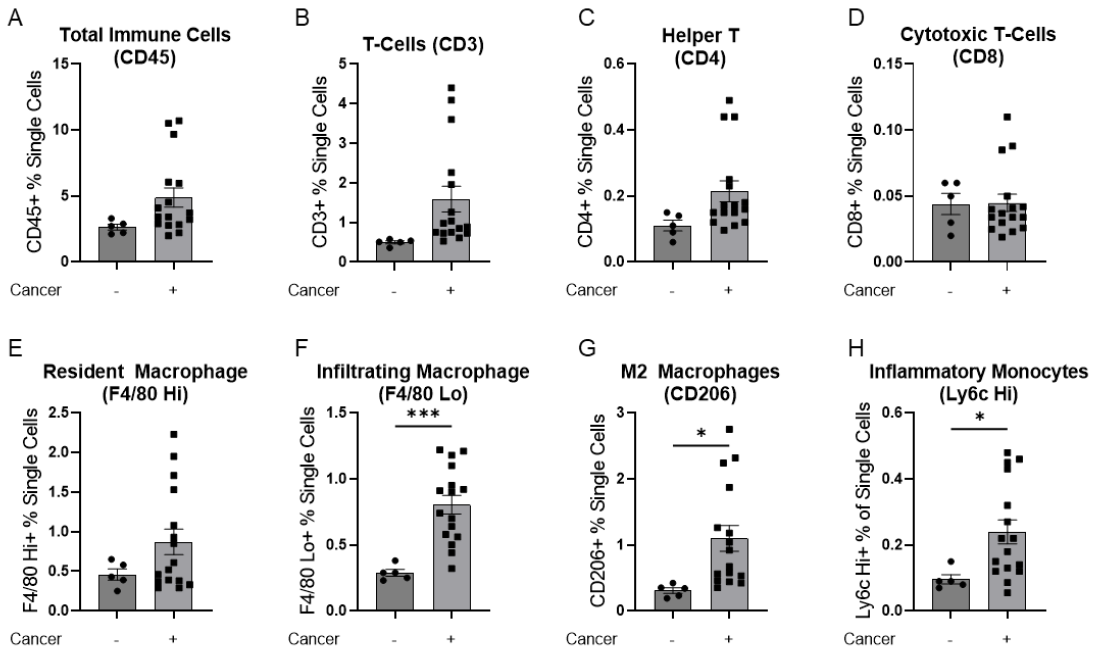

Figure 26. Elevated kidney immune cell infiltration with subcutaneous lung cancer.

Eight- to ten-week-old B6;129 male mice with and without subcutaneous cancer. Flow cytometric analysis of renal immune cells. Whole kidneys were homogenized, made into a single-cell suspension, and then stained with fluorescent antibodies. One million events were collected from each sample. Analysis identified (A) CD45+ immune cells, (B) CD45+ CD3+ T-cells, (C) CD3+CD4+ Helper-T, (D) CD3+ CD8+ Cytotoxic T-Cells, (E) CD11b+ F4/80 Hi resident macrophages, (F) CD11b+ F4/80 Lo infiltrating macrophages, (G) F4/80+ CD206+ M2 macrophages, and (H) CD11b+ Ly6c Hi inflammatory monocytes. Data are expressed as means ± SEM; n=5–15. Statistical significance was determined by an unpaired T-test. *p < 0.05, ***p<0.001

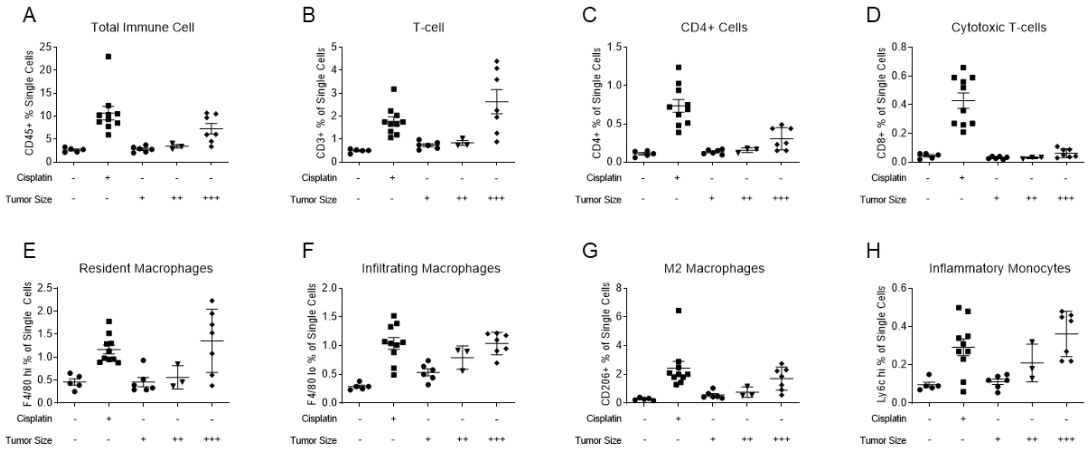

Figure 27. Elevated kidney immune cell infiltration with subcutaneous lung cancer grouped by tumor size.

Eight- to ten-week-old B6;129 male mice with and without subcutaneous cancer were treated with either 0 or 7 mg/kg cisplatin once a week for four weeks**.** Flow cytometric analysis of renal immune cells. Whole kidneys were homogenized, made into a single-cell suspension, and then stained with fluorescent antibodies. One million events were collected from each sample. The cancer + vehicle mice were grouped by tumor size. Analysis identified (A) CD45+ immune cells, (B) CD45+ CD3+ T-cells, (C) CD3+CD4+ Helper-T, (D) CD3+ CD8+ Cytotoxic T-Cells, (E) CD11b+ F4/80 Hi resident macrophages, (F) CD11b+ F4/80 Lo infiltrating macrophages, (G) F4/80+ CD206+ M2 macrophages, and (H) CD11b+ Ly6c Hi inflammatory monocytes. Data are expressed as means ± SEM; n=5–15.

Subcutaneous lung tumors alter makers of kidney function, injury, fibrosis, and inflammation in immunocompromised mice even without cisplatin treatment. After the observations that cancer alone without cisplatin can produce significant changes in the kidney, we wanted to determine how much of this can be attributed to the immune system. The immune system is a crucial player in other models of AKI [244-246], and loss of T-cells is protective in other models of AKI [247, 248]. To assess how the loss of a functional immune system contributes to the phenotype, we utilized an IXM with NRGS mice, which have no mature B- or T-cells and functionally immature macrophages [233]. NRGS mice were injected subcutaneously with the 238N1 cells and allowed to grow over the same timeframe as in the SXM model (Figure 17A) NRGS mice with cancer had increased levels of BUN and urinary NGAL even without treatment with cisplatin (Figure 28A-B). There was no change in KIM-1 expression (Figure 28C). These results suggest that subcutaneous lung cancer affects kidney function and injury regardless of an intact immune system, but the KIM-1 expression may in part require crosstalk with functional immune cells.

We assessed kidney fibrosis in these mice using multiple methods. Cancer increased mRNA expression of TIMP-1 and COL1A1 in the kidneys, albeit not significantly (Figure 29A-B). Kidney cortex protein levels of fibronectin and α-SMA were elevated in the cancer mice compared to non-cancer mice (Figure 29C). SR/FG staining of collagen was elevated in the tumor bearing mice as compared to non-cancer mice (Figure 29D). These data indicate that the development of kidney fibrosis from subcutaneous lung cancer does not require a fully functional immune system.

We hypothesized there would be little to no change in kidney inflammation or immune cell infiltration in the immunocompromised mice when subcutaneous lung tumors were present. We measured kidney inflammation using mRNA expression of NLRP3, TNF-α, and CXCL1 (Figure 29E-G). All three markers were increased in the cancer group,

and both NLRP3 and TNF-α were significantly elevated in the cancer groups compared to the non-cancer mice. We assessed immune cell infiltration in kidneys of immunocompromised mice with and without subcutaneous lung tumors. The tumor bearing mice had increased kidney populations of $CD45^{+}$, $Ly6C^{Lo}$, $Ly6C^{Hi}$, $F4/80^{Hi}$, $F4/80^{Lo}$, and $CD206^{+}$ immune cells compared to the non-cancer group (Figure 30A-F). These data suggest that in the immunocompromised mice, the immune cell populations are still being altered by a distant tumor, and functional B-cells and T-cells are not required for the development of kidney injury and fibrosis in this model.

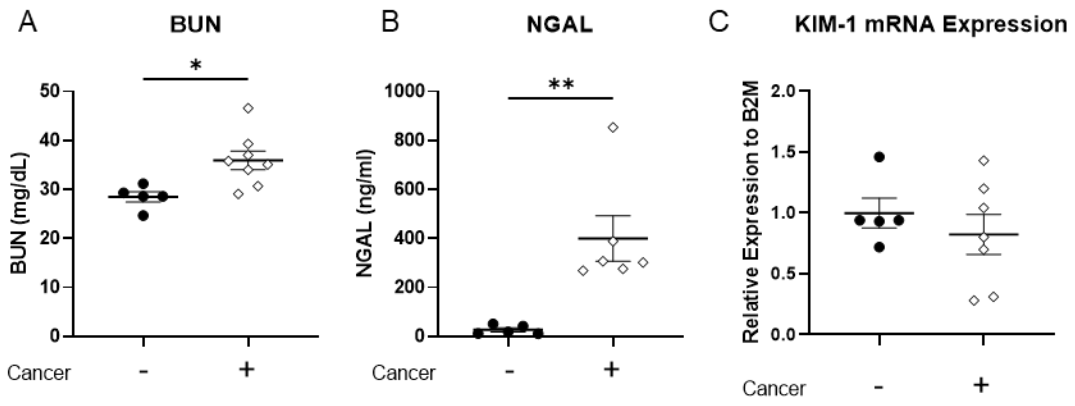

Figure 28. Kidney function and injury in immunocompromised mice with and without subcutaneous lung cancer.

Eight- to twelve-week-old NRGS mice were randomly assigned into two groups: 1. non-cancer, 2. cancer. (A) BUN levels from plasma and (B) Urine NGAL levels were measured 31 days after tumor implantation. (C) qRT-PCR of KIM-1 normalized to B2M. Data are expressed as means ± SEM; n=5–8. Statistical significance was determined by an unpaired T-test. *$p < 0.05$ **$p<0.01$, ****$p < 0.0001$

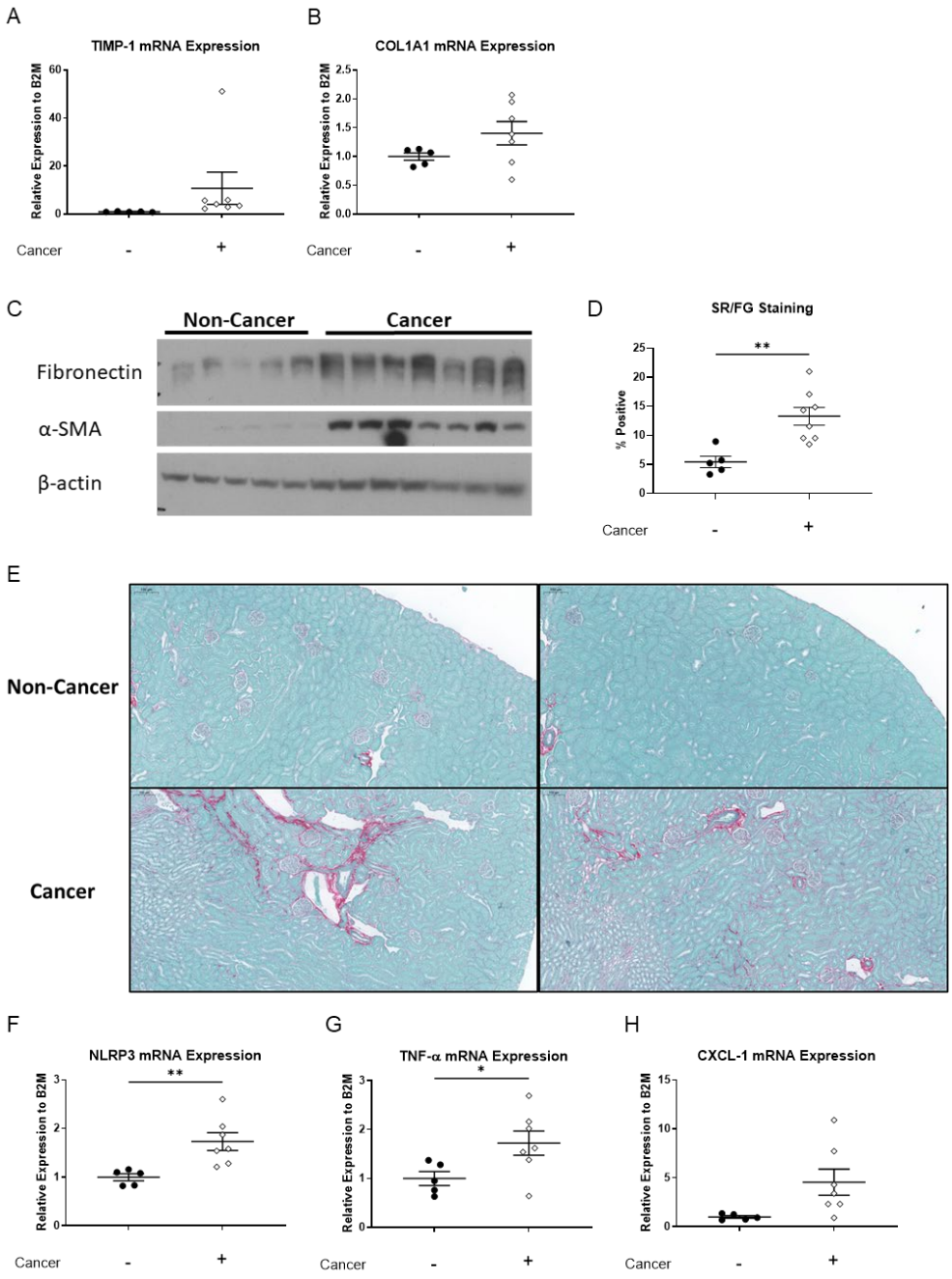

Figure 29. Kidney fibrosis and inflammation in immunocompromised mice with and without subcutaneous lung cancer.

Eight- to twelve-week-old NRGS mice were randomly assigned into two groups: 1. non-cancer, 2. cancer. mRNA expression via qRT-PCR of (A) TIMP-1, (B) COL1A1, (F) NLRP3, (G) TNF-α, and (H) CXCL1 normalized to B2M. (C) Protein levels of Fibronectin, α-SMA, and β-Actin in kidney cortex homogenates were determined by Western blot. (D) Quantification of SR/FG stain for total collagen levels on 5-μm-thick paraffin-embedded kidney sections and the representative images (E). Data are expressed as means ± SEM; n=5–7. Statistical significance was determined by an unpaired T-test.

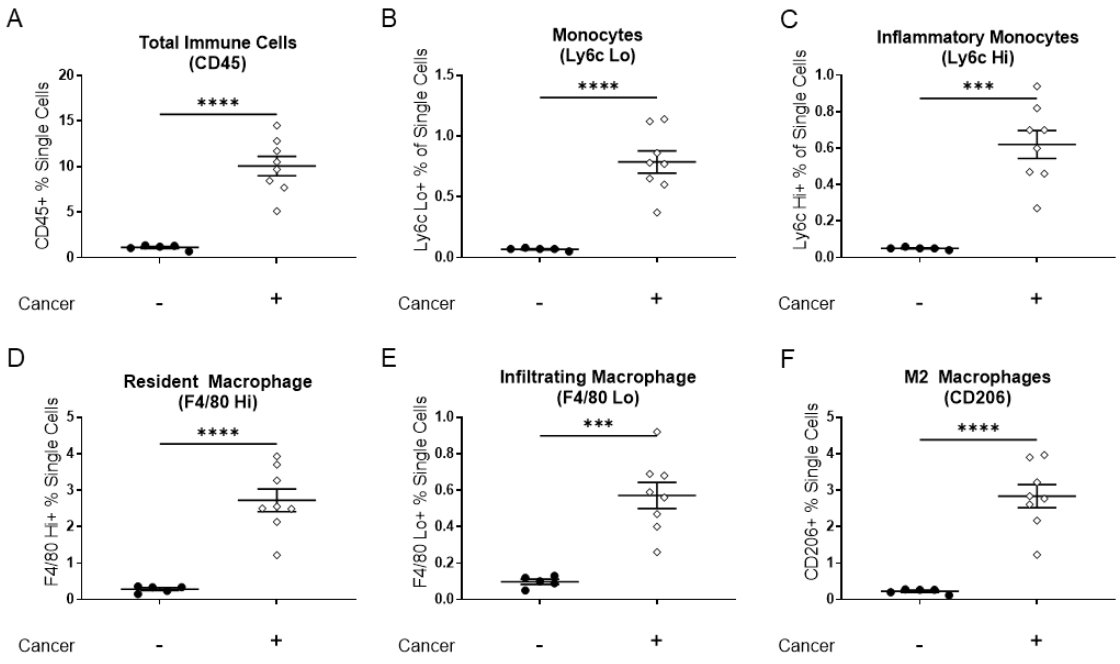

Figure 30. Elevated immune cell infiltration in immunocompromised mice with subcutaneous lung cancer.

Eight- to twelve-week-old NRGS mice were randomly assigned into two groups: 1. non-cancer, 2. cancer. Flow cytometric analysis of renal immune cells. Whole kidneys were homogenized, made into a single-cell suspension, and then stained with fluorescent antibodies. Analysis identified (A) CD45+ immune cells, (B) CD11b+ Ly6c Lo resident monocytes, (C) CD11b+ Ly6c Hi inflammatory monocytes. (D) CD11b+ F4/80 Hi resident macrophages, (E) CD11b+ F4/80 Lo infiltrating macrophages, and (F) F4/80+ CD206+ M2 macrophages. Data are expressed as means ± SEM; n=5–8. Statistical significance was determined by an unpaired T-test. ***p<0.001, and ****p<0.0001.

Subcutaneous lung tumors increased liver fibrosis. Lung can cancer has been shown to alter liver metabolism [249]. Thus, we determined if the fibrotic effects from cancer were unique to the kidney. The development of liver fibrosis was assessed by protein levels of fibronectin by western analysis. The treatment of cisplatin in non-cancer mice (non-cancer/cisplatin) had no effect on fibronectin protein levels (Figure 31A). In contrast, the cancer/vehicle and cancer/cisplatin group had increased liver fibronectin levels compared to the non-cancer/vehicle mice (Figure 31A). There was also increased liver expression in the cancer/vehicle group of the fibrotic marker Timp-1with increasing tumor size (Figure 31B-C). These data suggest that cisplatin alone has no effects on liver fibrosis, but lung cancer does induce fibrosis in the liver.

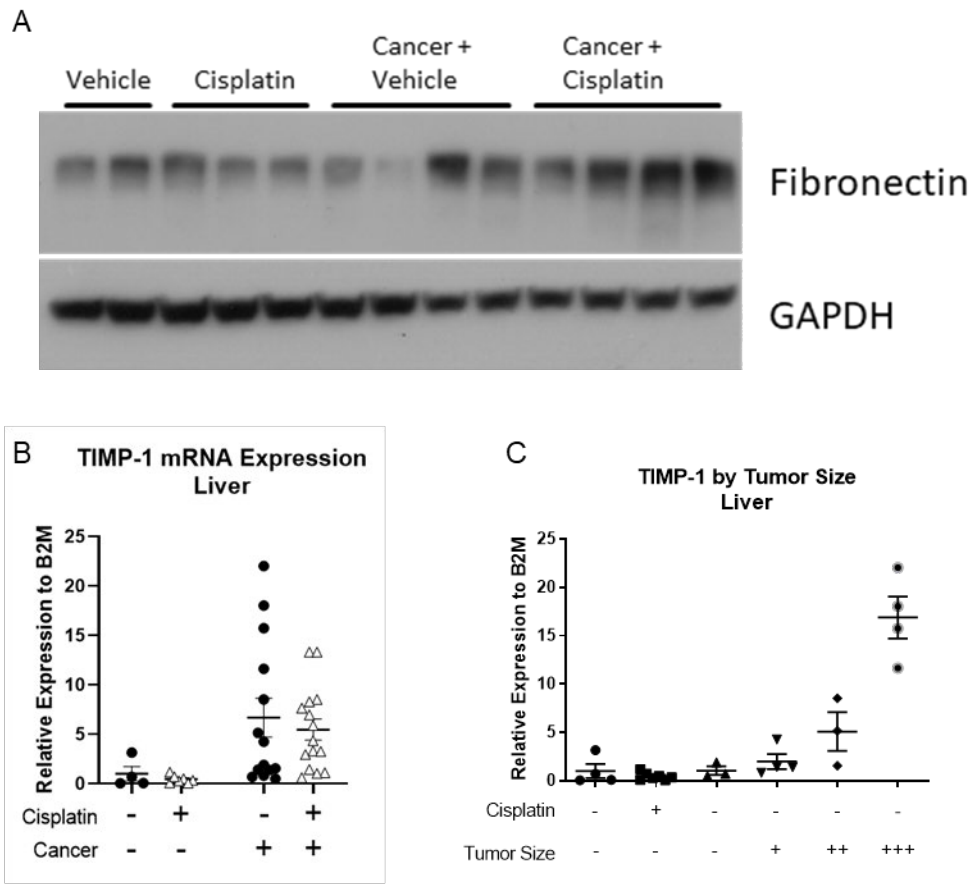

Figure 31. Mice with subcutaneous lung cancer had increased development of liver fibrosis compared to non-cancer mice.

Eight- to ten-week-old B6;129 male mice with and without subcutaneous cancer were treated with either 0 or 7 mg/kg cisplatin once a week for four weeks. (A) Protein levels of fibronectin in liver homogenates were determined by Western blot. mRNA expression via qRT-PCR of TIMP-1 (B) normalized to B2M. (C) TIMP-1 mRNA levels grouped by tumor size for the Cancer/Vehicle group. Data are expressed as means ± SEM; n=5–10. Statistical significance was determined by Two-Way ANOVA followed by Tukey post-test.

Elevated liver inflammation in mice with subcutaneous lung cancer independent of cisplatin treatment. We measured mRNA expression of NLRP3, TNF-α, CXCL1, and IL-6 in the liver. The treatment of cisplatin in non-cancer mice (non-cancer/cisplatin) had no effect on the liver inflammatory markers that we measured compared to non-cancer/vehicle group (Figure 32A-D). In the cancer/vehicle group, we observed significant increases in the markers NLRP3 and TNF-α (Figure 32A-D) compared to non-cancer/vehicle group. Breaking the cancer/ vehicle group up by tumor size allowed us to see increasing tumor size increased liver inflammatory expression (Figure 32E-H). In the cancer/cisplatin group, we saw increased expression of all four inflammatory markers (Figure 32A-D) compared to non-cancer/vehicle, but none were significant. These data suggest that cisplatin alone has no effects on liver inflammation, but lung cancer does induce inflammation in the liver.

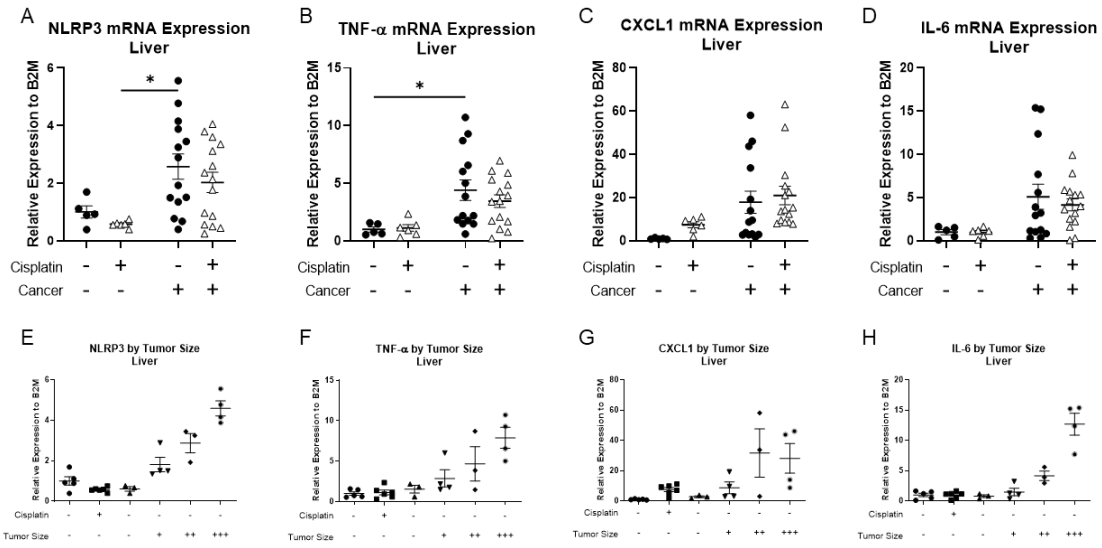

Figure 32. Elevated liver inflammatory cytokine and chemokine levels following RLDC in mice with subcutaneous lung cancer.

Eight- to ten-week-old B6;129 male mice with and without subcutaneous cancer were treated with either 0 or 7 mg/kg cisplatin once a week for four weeks**.** mRNA expression via qRT-PCR of (A) NLRP3, (B) TNF-α , (C) CXCL1, and (D) IL-6 were measured in the liver. Figures (E-F) show mRNA expression grouped by tumor size for the Cancer + Vehicle group. Data are expressed as means ± SEM; n=5–15. Statistical significance was determined by Two-Way ANOVA followed by Tukey post-test. * $p < 0.05$.

KIDNEY MITOCHONDRIAL CONTENT AND BIOGENESIS ARE ALTERED BY LUNG CANCER

In our study, we have demonstrated that subcutaneous lung cancer triggers kidney fibrosis, which in turn creates a pro-inflammatory and pro-fibrotic microenvironment. Both of these pathways suppress PGC-1α, as supported by previous research [140, 179, 207]. Furthermore, subcutaneous lung cancer leads to decreased kidney function and increased kidney injury, as indicated by Figures 19 and 29. As proper kidney function relies on adequate mitochondrial function, we were intrigued by the potential correlation between lung cancer and kidney mitochondrial content and biogenesis. Inherited genetic mitochondrial diseases have been shown to coincide with renal impairment [168-171], and tissue repair is also highly dependent on mitochondrial mass and respiration [94]. Thus, our results from CHAPTER 2 & 3 led us to investigate the effects of lung cancer on kidney mitochondrial content and biogenesis in the SXM mice.

Our analysis involved assessing the mitochondrial content through mtDNA/nDNA ratio and measuring mitochondrial biogenesis (MB) through PGC-1α mRNA expression and protein levels. We speculate that cancer serves as the first hit of injury to the kidney, reducing mitochondrial content and biogenesis, and potentially priming the kidney for further damage.

Decreased kidney mitochondrial content and biogenesis following RLDC in mice with lung cancer. The kidneys of mice in the cisplatin/vehicle group significantly lower mitochondrial content when compared to non-cancer/vehicle group as measured by mtDNA/nDNA (Figure 33A). There was a large amount of variability in the tumor sizes between mice (Figure 16D-F). Mice with subcutaneous lung cancer were grouped by their tumor weight. Data indicate as tumor size increases there is lower amount of kidney mitochondria as detected by mtDNA/nDNA assay (Figure 33B). Mice with medium and large tumors in the cancer/vehicle group have suppressed levels of mtDNA/nDNA that are

comparable to non-cancer/cisplatin treated mice. These data suggest that both cisplatin and cancer are suppressing kidney mitochondrial content and the effect appears to be additive in the cancer/cisplatin group (Figure 33B).

Mitochondrial biogenesis (MB) was measured through PGC-1α mRNA expression and protein levels. The mice in the non-cancer/cisplatin group had significantly lower PGC-1α mRNA expression compared to non-cancer/vehicle mice (Figure 33C). The downstream targets of PGC-1α, Nrf-1 and Tfam which are involved in MB were also significantly lowered in the non-cancer/cisplatin group compared to the non-cancer/vehicle group (Figure 33D-E). Data indicate as tumor size increases PGC-1α expression is suppressed (Figure 33F) and so are Nrf-1 and Tfam (Figure 33G-H). Mice with medium and large tumors in the cancer/vehicle group have suppress of the MB pathway (PGC-1, Nrf-1, and Tfam) comparable to non-cancer/cisplatin treated mice (Figure 33F-H). The combination of cancer and cisplatin does not further suppress MB gene expression when compared to non-cancer/cisplatin and cancer/vehicle.

The suppression of PGC-1α in the non-cancer/cisplatin group is also supported by the increase in inhibitory regulators p-SMAD3 and p-ERK1/2 when compared to non-cancer/vehicle group (Figure 33I). p-SMAD3 and p-ERK1/2 are also elevated in the cancer/vehicle when compared to non-cancer/vehicle group (Figure 33I). The highest levels of p-SMAD3 and p-ERK1/2 are found in the cancer/cisplatin group suggesting there is an additive effect on PGC-1α suppression (Figure 33I).

The protein levels of PGC-1α were also reduced by cisplatin in the non-cancer/cisplatin group compared to non-cancer/vehicle group (Figure 33I). The cancer/vehicle group only a few of the sample had detectable levels of PGC-1α protein compared to non-cancer/vehicle and in the cancer/cisplatin group none of the kidneys had any detectable level of PGC-1α protein (Figure 33I). Again, these data suggest an additive effect between cisplatin and cancer on PGC-1α protein suppression. Additionally, AKT

can phosphorylate PGC-1α and reduce its activity. The use of cisplatin increased p-AKT levels in the non-cancer/cisplatin group compared to the non-cancer/vehicle group.

p-AKT levels were elevated in the cancer/vehicle group compared to non-cancer/vehicle group and cancer/cisplatin group had elevated p-AKT levels compared to non-cancer/vehicle group (Figure 33I). The use of LY344864 in the vehicle/LY344864 group had no effect on kidney mitochondrial content or biogenesis (Figure 14A-F). These data suggest cisplatin reduces kidney mitochondrial content and biogenesis and cancer independently reduces kidney mitochondrial content and biogenesis. The effects of cisplatin and cancer on kidney mitochondrial content and biogenesis suppression appear to be additive, though not significant and maybe be the driving mechanism of enhanced toxicity in tumor bearing mice from cisplatin. Further studies need to be completed to determine if altering kidney mitochondrial content and biogenesis will prevent cancer and cisplatin induced nephrotoxicity.

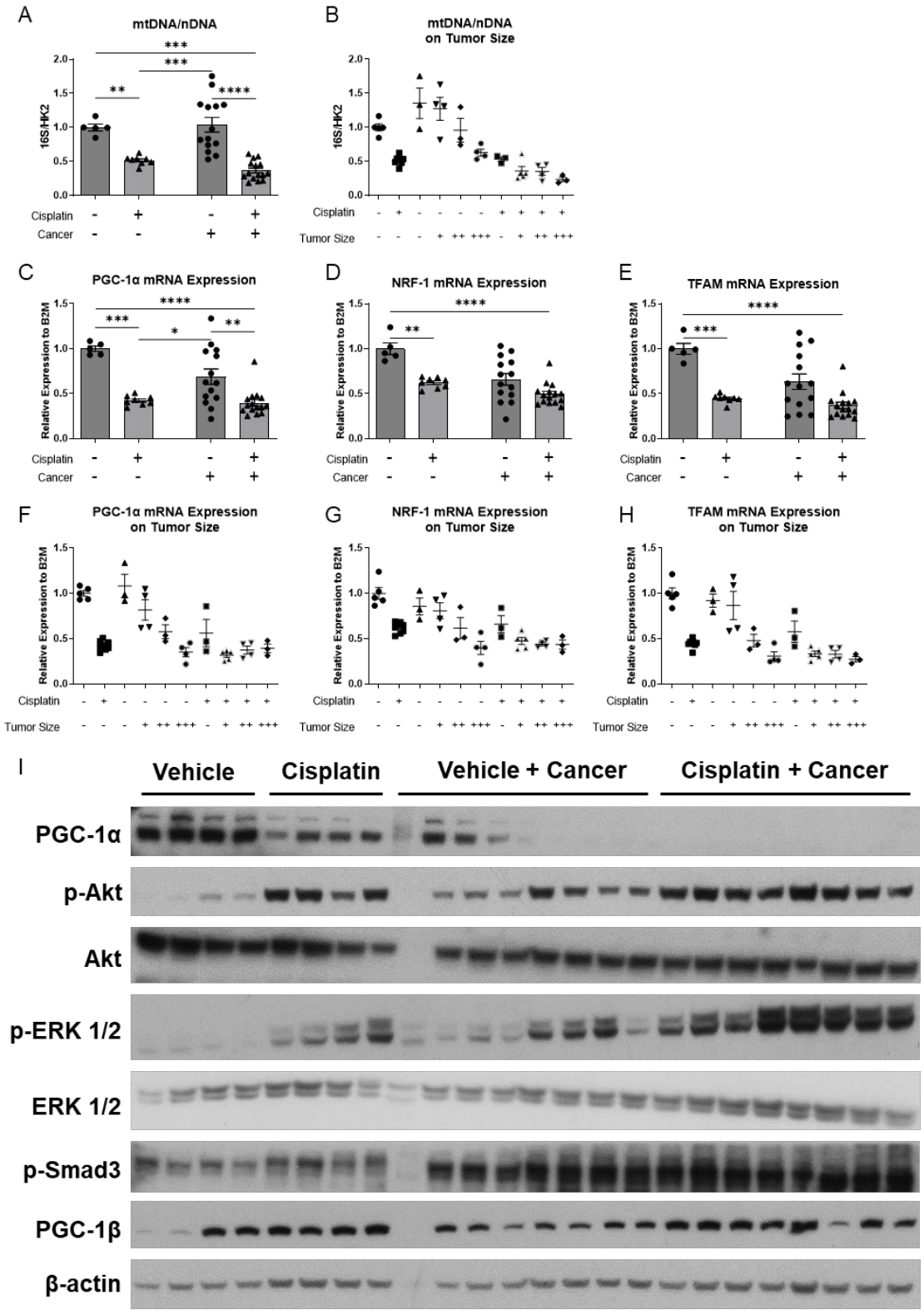
A
mtDNA/nDNA
16S/HK2
Cisplatin
Cancer
B
mtDNA/nDNA
on Tumor Size
Tumor Size
C
PGC-1α mRNA Expression
Relative Expression to B2M
D
NRF-1 mRNA Expression
E
TFAM mRNA Expression
F
PGC-1α mRNA Expression
on Tumor Size
G
NRF-1 mRNA Expression
on Tumor Size
H
TFAM mRNA Expression
on Tumor Size
I
Vehicle
Cisplatin
Vehicle + Cancer
Cisplatin + Cancer
PGC-1α
p-Akt
Akt
p-ERK 1/2
ERK 1/2
p-Smad3
PGC-1β
β-actin

Figure 33. Decreased kidney mitochondrial content and biogenesis following RLDC in mice with and without subcutaneous lung cancer.

(A) qPCR on nuclear-encoded HK2 and mitochondrial-encoded 16S were used to calculate the ratio between mtDNA to nDNA, normalized to vehicle-treated kidneys. (B) mtDNA/nDNA with the cancer groups separated by tumor size. (C-E) qRT-PCR of PGC-1α, NRF-1, and TFAM in kidney cortex homogenates is normalized to B2M and separated by tumor size (F-H). Immunoblotting for PGC-1α, p-AKT, AKT, p-ERK1/2, total ERK1/2, p-Smad3, PGC-1β, and β-actin on kidney cortex homogenates (I).

Liver mitochondrial content and biogenesis altered by lung cancer independent of cisplatin treatment.

The livers of mice in the cisplatin/vehicle group had slightly elevated, though not significantly mitochondrial content when compared to non-cancer/vehicle group as measured by mtDNA/nDNA (Figure 34A). The livers of mice in the cancer/vehicle group had reduced levels of mitochondrial content compared to the non-cancer/vehicle group (Figure 34A). There was a large amount of variability in the tumor sizes between mice (Figure 16D-F). Mice with subcutaneous lung cancer were grouped by their tumor weight. Data indicate as tumor size increases there is lower amount of liver mitochondria as detected by mtDNA/nDNA assay (Figure 34B). Unlike the kidney, in the liver cisplatin does not lower liver mitochondrial content, whereas tumor size does appear to correlate with reduced mtDNA/nDNA levels in the liver (Figure 34B). These data suggest cancer is able to reduce liver mitochondrial content and cisplatin does not alter liver mitochondrial content.

Mitochondrial biogenesis (MB) was measured through PGC-1α mRNA expression and protein levels. The mice in the non-cancer/cisplatin and cancer/cisplatin group had significantly elevated levels of PGC-1α mRNA expression compared to non-cancer/vehicle mice (Figure 34C). These data suggest that cisplatin induces PGC-1α expression in the liver, the opposite of what occurs in the kidney. The expression of liver Nrf-1 and Tfam expression are not changed in the any of the groups (Figure 34D-E). These data suggest that neither cisplatin nor cancer alter the downstream targets of PGC-1α in the liver, contrary to what occurs in the kidney.

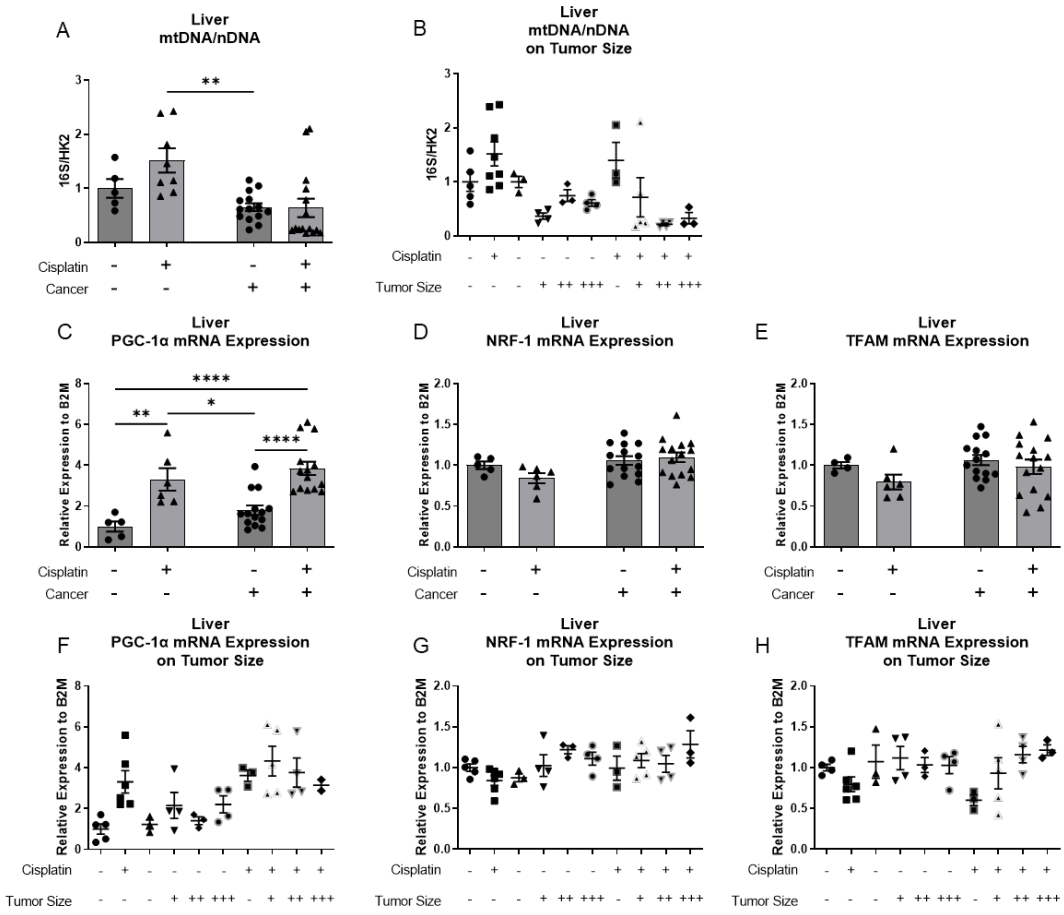

Figure 34. Liver mitochondrial content and biogenesis in mice with cancer following RLDC.

(A) qPCR on nuclear-encoded HK2 and mitochondrial-encoded 16S were used to calculate the ratio between mtDNA to nDNA, normalized to vehicle-treated kidneys. (B) mtDNA/nDNA with the cancer groups separated by tumor size. (C-E) qRT-PCR of PGC-1α, NRF-1, and TFAM in kidney cortex homogenates is normalized to B2M and separated by tumor size (F-H). Data are expressed as means ± SEM; n=5–10. Statistical significance was determined by TWO-Way ANOVA followed by a Tukey post-test. *p < 0.05, **p<0.01, ***p<0.001, ****p < 0.0001

DISCUSSION

Cisplatin toxicity in preclinical mouse models has traditionally been studied in mice without cancer. Since all patients receiving cisplatin have cancer, cancer was incorporated into the RLDC model. We found that in tumor bearing mice, cisplatin nephrotoxicity and kidney fibrosis are significantly worsened. This is the first published data that we are aware of that specifically assesses the impacts of cancer on the kidney and its response to the nephrotoxicity of cisplatin. We believe the comorbidity of cancer has been a missing variable in previous work. Optimizing preclinical models to more accurately represent the dosing and comorbidities present in cancer patients will allow us to better understand the pathophysiology and potentially develop more successful preventative and/or interventional strategies. We believe cancer delivers the first hit to the kidney and the subsequent doses of cisplatin become too burdensome, increasing kidney injury and fibrosis.

In addition to our main findings, the data presented here shows that the presence of lung cancer induces kidney injury, inflammation, and fibrosis even in the absence of cisplatin treatment. The GEMM did not show this overt phenotype, but we believe this can be explained by type of the cancer generated [250]. The tumors are driven solely by mutant $Kras^{G12D}$, producing a less aggressive lung adenoma, as compared to the metastatic lung adenocarcinoma cell line 238N1, which expressed a mutant $Kras^{G12D}$ and was deficient in tumor suppressor, p53 [232, 250]. This cell line has been shown to metastasize [232], and is more characteristic of aggressive tumors in lung cancer patients.

The immune system is becoming increasingly recognized as an important component of cancer development, progression, metastasis, and response to therapeutics [251-253]. The immune system has been shown to play an important role in other models of kidney disease [244-246]. We utilized tumor-bearing immunocompromised mice to assess the contribution of the immune system on cancer

induced kidney injury, inflammation, and fibrosis. The tumor- bearing mice had elevated BUN and NGAL levels, but there was no change in KIM-1 expression. Recent data have shown the importance of crosstalk between the proximal tubule cells and macrophages [254], and the lack of proper crosstalk in the immunocompromised mice could help explain the lack of increased KIM-1 expression. The data presented here indicate that the presence of subcutaneous lung adenocarcinoma resulted in increased kidney fibrosis and inflammation even in the absence of T and B cells. Previous work from our lab and others has shown resident macrophages to be an important driver of kidney fibrosis [223, 255, 256]. We cannot rule out the contribution of macrophages in this strain of immunocompromised mice as there are still macrophages present that are elevated in the kidneys that could retain some function. Further analysis whereby the macrophages are eliminated [223] in this model will shed light on their contribution to the lung tumor-induced sensitization of the kidney to cisplatin.

Solid tumors were once thought of as multiple clones of a single cell. However, it is now recognized that solid tumors may more closely resemble complex organs [257] with many different cell types that can affect the biology of the entire organism [258]. We show that lung adenocarcinoma can alter kidney injury, inflammation, and fibrosis. Our study supports prior findings by Masri, S., et al. [249] that indicate lung cancer alters liver circadian rhythm, leading to changes in liver lipid metabolism that benefits the tumor. To determine if our phenotype was unique to the kidney, we looked at liver fibrosis and inflammation. We found that cisplatin had no effect on liver fibrosis or inflammation, while tumor-bearing mice did have elevated markers of liver fibrosis and inflammation (Figures 31-32). The data presented in this study suggest that cancer cells are secreting factors into systemic circulation that impact distant organs leading to inflammation, fibrosis, and immune cell infiltration. There is no evidence to suggest metastasis to the kidney creates this phenotype; however, we cannot rule it out.

Previous studies in the literature employed models of tumor xenografts in nude mice and syngeneic models to assess potential strategies of nephroprotection [259-261]. These studies did not assess the development of kidney fibrosis, immune cell infiltration, and the transition to CKD. $CD4^{+}$ knockout mice had no protection from cisplatin, worsen cancer growth [262], and until we fully understand the contribution of the immune system to the sensitizing effects of cancer, the use of mouse models with a competent immune system is critical to understanding the pathophysiology of cisplatin-induced CKD. We believe our study is the first to use the RLDC dosing in a syngeneic cancer model to show that cisplatin nephrotoxicity and kidney fibrosis are potentiated by cancer.

We utilized GEMM and SXM lung cancer models to investigate cancer-kidney crosstalk in the context of a nephrotoxic chemotherapy. The GEMM has several disadvantages over the SXM with a major concern being the low survivability of the mice. Additionally, the GEMM model requires the mice to be on doxycycline chow for over 6 months before the formation of tumors. Lastly, quantifying tumor burden is challenging which prevents us from examining the relationship between tumor size and nephrotoxicity. The SXM allowed us to quantify tumor size as well as allowed us to examine the variable of cancer independent of age. An additional advantage of the SXM that we employed is that it can be implanted into mice with intact immune systems or those immunocompromised to be able to dissect the contribution of specific immune cell subtypes to the development of fibrosis. Additional cancer types need to be examined to determine if this phenotype is specific to lung cancer. All studies employed here utilized tumors driven by mutant $Kras^{G12D}$. Future studies also need to be completed with cells lines that have different driver mutations to determine if the cancer-kidney crosstalk is specific to mutant $Kras^{G12D}$.

The toxicity from RLDC is a cumulative process [160]. We believe cancer delivers an initial injury hit to the kidney, which then primes the kidney for enhanced susceptibility

to cisplatin toxicity. Understanding the mechanism that drives this priming in cancer patients could be essential to understanding how to prevent cisplatin-induced nephrotoxicity and the progression to CKD. Finally, we firmly believe that any nephroprotective strategies developed for cisplatin must consider the comorbidity of cancer and be designed to maximize the effectiveness/efficacy of chemotherapy.

CHAPTER 5: LUNG CANCER-KIDNEY CROSSTALK PREVENTS PROTECTION FROM 5-HYDROTRYPTAMINE-1F RECEPTOR AGONIST IN REPEATED LOW DOSE CISPLATIN INDUCED NEPHROTOXICITY

INTRODUCTION

Cisplatin causes AKI in 30% of patients [30, 31, 39], and repeated cycles of cisplatin are associated with increased incidence of chronic kidney disease (CKD) [14]. AKI and CKD are interconnected syndromes [6] involving maladaptive repair processes [8]. Recent research has made significant strides in understanding the pathophysiology of kidney injury caused by repeated low-dose cisplatin (RLDC), including the use of single-nucleus transcriptional profiling analysis, which uncovered a unique population of proximal tubule cells in an injury/repair phase [159]. In addition, cisplatin-induced injury produces a proinflammatory tubule cell population that fails to repair, and repeated administration of cisplatin exacerbates kidney injury by causing DNA damage accumulation in tubule cells attempting to repair from previous rounds of injury [160].

Although, cisplatin-induced nephrotoxicity has been studied extensively, most of this work has been completed in mouse models without cancer [39, 115, 121, 210, 211], The addition of cancer to the RLDC model of nephrotoxicity further improves the clinical relevancy of this preclinical model. We have shown that subcutaneous lung cancer alone alters kidney physiology, inducing kidney injury, inflammation, and fibrosis [226]. The advancement of the RLDC model to include the comorbidity of cancer requires reassessment of previously discovered protective strategies.

One such protective strategy is the use of the 5HT-$_{1F}$ agonist LY344864. Our laboratory recently used LY344864 to prevent cisplatin-induced nephrotoxicity. The

results suggest LY34486 protects from RLDC induced kidney injury, interstitial fibrosis, and inflammation by increasing mitochondrial content in mice without cancer. The 5HT-$_{1F}$ receptor is a G-protein coupled receptor (GPCR) whose functions outside of the central nervous system are not completely characterized [217-221]. The 5HT-$_{1F}$ receptor has been found on freshly isolated tubule cells and on cultured renal proximal tubule epithelial cells [215]. Additionally, the knockout of 5HT-$_{1F}$ receptor in mice impairs the injury repair process in the kidney and worsens AKI events [222].

The 5HT-$_{1F}$ agonist, LY344864 has been shown to provide protection from AKI [215] and from spinal cord injury [216] through increased PGC-1α and mitochondrial biogenesis. In line with other published research increasing PGC-1α expression protects in other models of AKI including; ischemia-reperfusion injury, sepsis, folic acid toxicity, and single high-dose cisplatin-induced nephrotoxicity [179, 192, 194-201, 203-206]. More recently, PGC-1α has been shown to be a key mediator in renal fibrosis and CKD development [140, 141, 163, 176, 180, 193]. PGC-1α is a unique target for the RLDC model because of its role in both AKI, CKD, and it is suppressed in the kidneys by cancer.

This study was designed to determine if 5HT-1F agonist LY344864 will protect from cisplatin induced nephrotoxicity in mice with subcutaneous lung cancer. Our work has shown that both cisplatin and cancer suppress kidney mitochondrial content and the effect appears to be additive in the cancer/cisplatin group. We hypothesize that increasing PGC-1α expression through the 5HT-$_{1F}$ receptor will protect from both cancer-induced, and cisplatin-induced nephrotoxicity. We believe increasing mitochondrial biogenesis and mitochondrial content will reduce the injured/failed-repair tubule cell population resulting in improved renal function and reduced fibrosis.

MATERIALS AND METHODS

ANIMALS

All mice were maintained on a 12-hour/12-hour light/dark cycle and provided with food and water *ad libitum*. Animals were maintained under standard laboratory conditions. All animal procedures were approved by the Institutional Animal Care and Use Committee of the University of Louisville (Protocol ID 19568) and followed the guidelines of the American Veterinary Medical Association.

SYNGENEIC XENOGRAFT MODEL OF LUNG CANCER

In the syngeneic xenograft model (SXM) of lung cancer, the mouse lung adenocarcinoma cell line (238N1) previously developed [232] was injected subcutaneously into B6129SF1/J mice. Eight- to ten-week-old male B6129SF1/J (B6129) mice were purchased from The Jackson Laboratory. Mice were randomly assigned into four treatment groups: 1. cancer/vehicle, 2. cancer/LY344864, 3. cancer/cisplatin, and 4. cancer/cisplatin/LY344864 (cancer/cis/LY). In the cancer groups, 10,000 lung adenocarcinoma cells (238N1) were injected subcutaneously in the right rear flank seven days before the start of cisplatin treatment. Experimental Design is shown in Figure 35A. Pharmaceutical grade cisplatin (NDC 16729-288-38, 1 mg/ml) or saline vehicle (0.9% normal saline) was administered via intraperitoneal (i.p.) injection once a week between 8-9AM for four weeks. In the vehicle group, 400 µL normal saline was administered via i.p. injection. In the cisplatin treatment group, 7mg/kg of cisplatin in normal saline in a total volume of 400 µL was administered via i.p. injection. Animals were euthanized 72 hours following their final cisplatin injection.

LY344864 DOSING REGIMEN

The serotonin receptor (5HT) subtype 1F agonist (5HT-$_{1F}$), LY344864 (item #, 29496, CAS # 1217756-94-9) was purchased from Cayman Chemical Company (Ann Arbor, Michigan; United States). LY344864 was dissolved in normal saline, mice were administered vehicle

or LY344864 via intraperitoneal (i.p.). All mice were administered 10 doses of saline or LY344864 in a final volume of 200 µL to control for fluid delivery. Starting 5 days after the second dose of cisplatin on day 12 of the experiment mice were administered saline or LY344864 daily. Experimental Design is shown in Figure 35A.

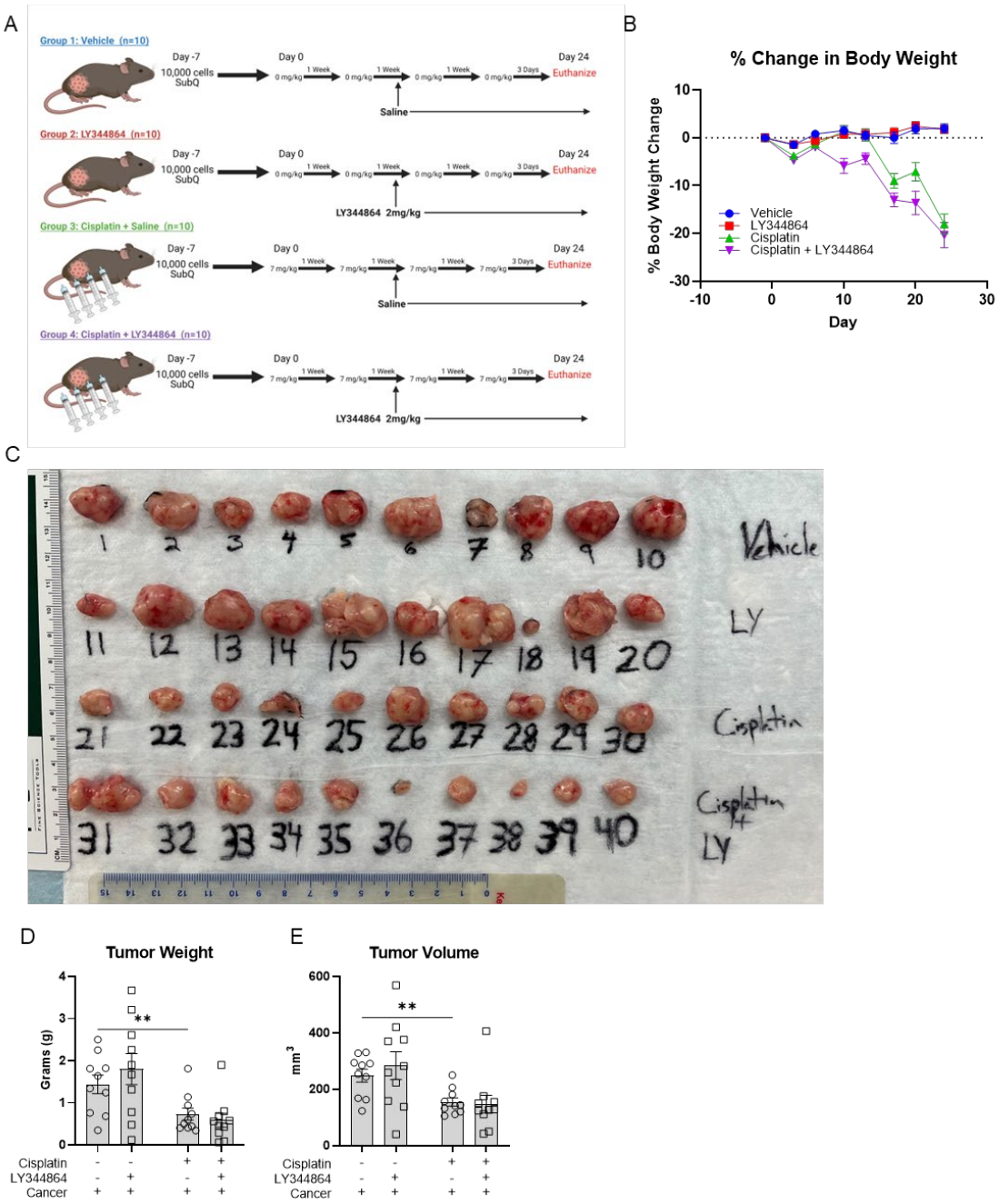

Figure 35. Experimental design for RLDC in mice with subcutaneous lung cancer treated with LY344864 study.

Eight- to ten-week-old B6;129 male mice were randomly assigned into four treatment groups: 1. Cancer/vehicle, 2. Cancer/LY344864, 3. Cancer/cisplatin, and 4. Cancer/cisplatin/LY344864. The cancer groups were injected with 10,000 lung adenocarcinoma cells subcutaneously seven days prior to the start of cisplatin treatment. Cisplatin or saline was administered via intraperitoneal injection once a week for four weeks. Additionally, mice were treated with vehicle (normal saline) or LY344864 via IP injection starting 5 days after the second dose of cisplatin for a total of 10 doses. Animals

were euthanized 72 hours following their final cisplatin injection. (A) Experimental Design. (B) Change in body weight. (C) Tumor photo, (D) tumor weight, and (E) tumor volume. Data are expressed as means ± SEM; n=5–10. Statistical significance was determined by TWO-Way ANOVA followed by Tukey post-test. **p<0.01.

BLOOD UREA NITROGEN (BUN) AND NEUTROPHIL GELATINASE ASSOCIATED LIPOCALIN (NGAL) DETERMINATION

BUN (AMS Diagnostics, 80146) levels were measured from plasma samples using the indicated kits following the manufacturer's instructions. ELISAs for NGAL (R&D Systems, DY1857) were performed on the urine as directed by the manufacturer, as previously published [152].

PROTEIN QUANTIFICATION AND WESTERN BLOT ANALYSIS

Kidney tissues were homogenized in cell extraction buffer (Thermo Fisher Scientific) containing a Complete Protease Inhibitor Cocktail Tablet and Phosphatase Inhibitor Cocktail Tablet (Roche). Homogenates were centrifuged at 15,000 X g for 10 min at 4° C. Supernatants were removed and stored at -80°C. Protein concentrations were determined using BCA reagent (Thermo Fisher Scientific). 40 µg of kidney homogenate protein were loaded and separated on 4–12% gradient Tris-Glycine-SDS polyacrylamide gels. Protein was then transferred to PVDF membranes that were blocked in 5% (w/v) dried milk in tris buffered saline 0.1% Tween 20 (TBST) for 1 hour. Membranes were incubated with primary antibody overnight at 4°C. The following day, membranes were washed three times for 5 min each with TBST containing 5% (w/v) dried milk. Membranes were then incubated for 2 hours at room temperature with secondary antibodies conjugated with horseradish peroxidase (1:20,000) in TBST containing 1% (w/v) dried milk. Following two washes with 1% (w/v) dried milk and one wash in TBST membrane proteins were detected by chemiluminescence substrate.

ANTIBODIES

The following antibodies were purchased from Cell Signaling Technology (Beverly, MA): p44/42 MAP Kinase (Erk1/2) #4695, Phospho-p44/42 MAP Kinase (Erk1/2) (Thr202/Tyr204) #4370, Transforming growth factor-beta (TGF-β) #3711, Mothers against

decapentaplegic homolog 2/3 (SMAD 2/3) #8685, Phospho-Smad3 (Ser423/425) #9520, Phospho-Akt (Ser473) Antibody #9271, total Akt Antibody #9272, and GAPDH (D16H11) #5174. The following antibodies were purchased from Abcam (Cambridge, CB2 0AX, UK): Peroxisome proliferative activated receptor, gamma, coactivator 1 alpha (PGC-1α, abcam, ab54481) and α-Smooth Muscle Actin (α-SMA, abcam, ab5694). The remaining antibodies include fibronectin (F3648, Sigma-Aldrich), and α-tubulin (SC-5286, Santa Cruz Biotechnology).

Rodent Total OXPHOS Antibody Cocktail (abcam, ab110413) contains 5 mouse mAbs, one each against Complex I subunit NDUFB8 (ab110242), Complex II-30kDa (ab14714), Complex III-Core protein 2 (ab14745), Complex IV subunit I (ab14705) and Complex V alpha subunit (ab14748) as an optimized premixed cocktail.

GENE EXPRESSION

RNA was isolated from kidney tissue using E.Z.N.A. Total RNA Kit 1 (OMEGA) per manufacturer's protocol. cDNA was synthesized with High-Capacity cDNA Reverse Transcriptase PCR (Thermo Fisher Scientific) per manufacturer's instructions. Gene-specific cDNA was quantified with real-time qRT-PCR using either predesigned TAQman assays or self-designed SYBR assays. The following TAQman primers were purchased from Thermo FisherScientific: tumor necrosis factor alpha (*Tnf-α*, Mm00443258_m1), chemokine (C-X-C Motif) ligand 1 (*Cxcl1*, Mm04207460_m1), and the housekeeping gene beta-2-microglobulin (*B2m*, Mm00437762_m1). The following primers were self-designed: kidney injury molecule-1 (*Kim-1*, Invitrogen, forward: AGATCCACACATGTACCAACATCAA, reverse: CAGTGCCATTCCAGTCTGGTTT), Peroxisome proliferative activated receptor, gamma, coactivator 1 alpha (*Pgc-1α*, Invitrogen, forward: AACAATGAGCCTGCGAACATATT, reverse:

TAGCAAGTTTGCCTCATTCTCTTC), Nuclear Respiratory Factor 1 (*Nrf-1*, Invitrogen, forward: GGATTCCAGTCTCTGTGGACAAA, reverse: CCCCCGACCTGTGGAATACT), Transcription factor A, mitochondrial (*Tfam*, Eurofins, forward: TTTAAAGCTAAACACCCAGATGCA, reverse: TTCTGGTAGCTCCCTCCACAG), *Timp-1*, Invitrogen forward: GCAACTCGGACCTGGTCATAA, reverse: TTAGTCATCTTGATCTTATAACGCTGGTA), *Nlrp3*, Invitrogen, forward: AAGATGAAGGACCCACAGTGTAACTT, reverse: CAGATTGAAGTAAGGCCGGAATT), and *Col1a1*, Invitrogen, forward: CGATGGATTCCCGTTCGAGTA, reverse: GTGGACATTAGGCGCAGGAA) qRT-PCR was done with either iTaq Universal Probes Supermix (172-5134, Bio-Rad) or iTaq Universal SYBR Green Supermix (172–5124, Bio-Rad).

MITOCHONDRIAL DNA TO NUCLEAR DNA ASSAY

DNA was isolated from kidney tissue using E.Z.N.A. Tissue DNA Kit 1 (OMEGA) per the manufacturer's protocol. DNA was quantified using Nanodrop, and 5 ng/µl solutions were prepared for each sample. 20ng of DNA was loaded into each well, followed by quantitative PCR using primers designed for specific amplification of particular mtDNA encoded and nuclear-encoded fragments. Primers were designed to evaluate the relative copy number of mtDNA and nDNA. The mitochondrially encoded genes selected were *16s rRNA* and *Nd1*, and the nuclear-encoded gene was Hexokinase 2 (*Hk2*) along with the adaptation of the protocol according to previously published work [212]. Forward and reverse primers *16s rRNA*, Invitrogen, forward: CCGCAAGGGAAAGATGAAAGAC, reverse: TCGTTTGGTTTCGGGGTTTC, *Nd1*, Invitrogen, forward: CTAGCAGAAACAAACCGGGC, reverse: CCGGCTGCGTATTCTACGTT, *Hk2*, Invitrogen, forward: GCCAGCCTCTCCTGATTTTAGTGT, reverse

GGGAACACAAAAGACCTCTTCTGG. qPCR was done with iTaq Universal SYBR Green Supermix (172–5124, Bio-Rad).

HISTOLOGY: SIRIUS RED/FAST GREEN STAINING

Following formalin fixation, kidney tissue was processed and embedded in paraffin. Sirius Red/Fast Green performed on formalin-fixed paraffin-embedded (FFPE) kidney sections (5 μm thick) for total collagen deposition as previously published [152, 223]. Kidney sections were rehydrated in Histoclear followed by an ethanol gradient. Slides were then dipped in PBS with 0.1% Tween 20 and incubated for 5 minutes. Slides were washed with distilled water twice for 5 minutes each and then incubated in 1.2% (w/v) saturated picric acid (#5860-32, Ricca Chemicals) containing 0.1% sirius red/direct red 80 (#365548, Sigma) and 0.1% fast green FCF (#F7258, Sigma). Slides were then washed with 5% glacial acetic water until the water ran clear. Tissue samples were then dehydrated and fixed using Permount (#17986-01, Electron Microscopy Sciences).

QUANTIFICATION OF TISSUE HISTOLOGY

Orbit Image Analysis software [224] (version 3.64) was used to quantify positive staining of kidney histology. The Tissue Quantification feature was used to quantify collagen staining. The software developers' protocol was followed for training the software to correctly identify collagen over normal tissue [224, 225]. In the training step the images were labeled by manually drawing several annotations per tissue class (e.g., collagen, normal tissue,). After training the software images were tested to verify correct determination of positive staining. Digital scans of kidney sections were divided into 5-8 sections and the classification (e.g., collagen, normal tissue) of the tissue sections were

assigned by the software. The percentage of collagen per image was used to quantify positive staining.

STATISTICAL ANALYSIS DATA

Quantitative data are expressed as the mean ± SEM for all experiments. Statistical significance was determined using GraphPad Prism software 9.4.1. Statistically significant differences were determined by Two-Way ANOVA followed by Tukey post-test. The criterion for the statistical difference was $P < 0.05$.

RESULTS

Kidney function and kidney injury are not protected in mice with lung cancer following RLDC treated with LY344864.

The experiment design for this study is shown in Figure 35A. Briefly mice were randomly assigned into 4 groups: 1. cancer/vehicle, 2. cancer/LY344864, 3. cancer/cisplatin, and 4. cancer/cisplatin/LY344864 (cancer/cis/LY). Ten-thousand lung cancer cells were injected into the right flank of each mouse and allowed to engraft for 7 days prior to starting the cisplatin regimen. Starting 5 days after the second dose of cisplatin on day 12 of the experiment mice were administered saline or LY344864 daily. Mice were euthanized 3 days following the fourth dose of cisplatin.

We have previously shown that subcutaneous lung cancer alters kidney function and induces injury (CHAPTER 4). The cancer/vehicle group from CHAPTER 5 was compared to the non-cancer/vehicle group from CHAPTER 3 (Figure 36). This was done to help visualize and understand the degree of injury and inflammation already occurring in these mice just from cancer. There was a significant elevation in BUN, urinary NGAL, and kidney Kim-1 expression (Figure 36A-C) between non cancer and cancer mice. The cancer/vehicle group is represented in Figure 37 as the first column of data. The treatment of LY344864 in the cancer/LY344864 group compared to the cancer/vehicle group had no effect on BUN, NGAL, or kidney Kim-1 expression (Figure 37 A-C). These data suggest the mechanism through which cancer reduces kidney function and induces kidney injury is not protected by LY344864. The use of cisplatin in the cancer/cisplatin group elevated BUN, NGAL, and kidney Kim-1 expression compared to the cancer/vehicle groups confirming previous results that lung cancer exacerbates the nephrotoxicity of cisplatin (CHAPTER 4). The use of LY344864 in the RLDC has previously been shown to be protective by improving markers of kidney function and reducing markers of kidney injury (CHAPTER 3). The use of LY344864 in mice with cancer did not provide the same

protection from cisplatin. Comparing the cancer/cisplatin group to the cancer/cisplatin/LY group shows that LY344864 does not provide protection from cisplatin induced nephrotoxicity in mice with subcutaneous lung cancer as there is no reduction in BUN, NGAL, or kidney Kim-1 expression (Figure 37A-C).

There was no significant difference in tumor weight or tumor volume between the cancer/vehicle and cancer/LY344864 group (Figure 35C-E). The use of cisplatin in the cancer/cisplatin group significantly reduced the size of tumors (weight and volume) when compared to the cancer/vehicle group (Figure 35C-E). The use of LY344864 in the cancer/cisplatin/LY group did not significantly change tumor weight or volume compared to cancer/cisplatin group (Figure 35C-E). Our results suggest that LY344864 does not alter the therapeutic efficacy of cisplatin to reduce tumor size. Additional work needs to be completed to confirm tumor angiogenesis and distant organ metastasis are not being stimulated by LY344864.

In total these data indicate that while LY344864 provides protection from RLDC induced nephrotoxicity in mice without cancer, these effects are nullified in mice with subcutaneous lung cancer.

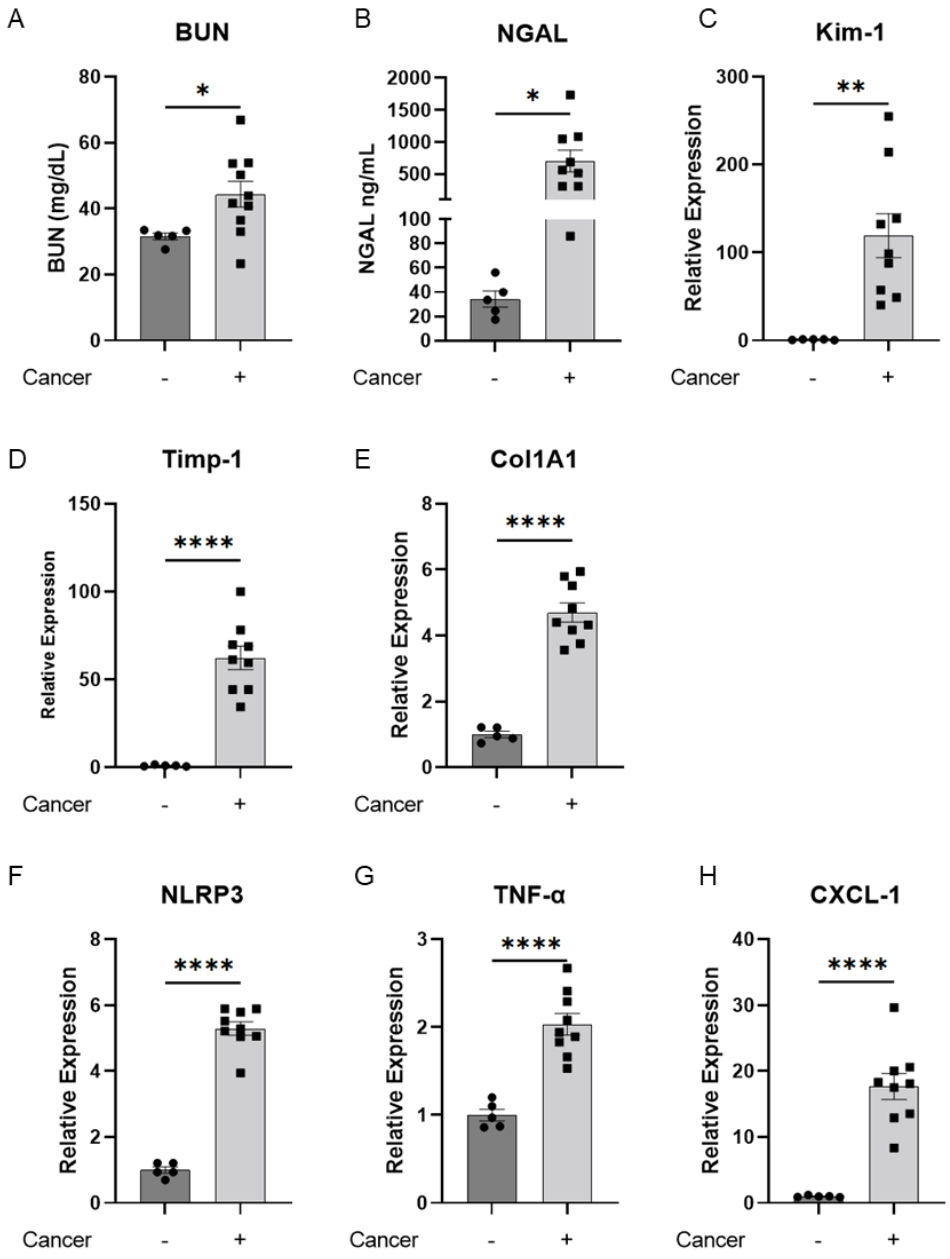

Figure 36. Kidney function, injury, fibrosis, and inflammation in mice with and without subcutaneous lung cancer.

Eight- to ten-week-old B6;129 male mice with and without subcutaneous cancer. Non-cancer mice are from CHAPTER 3 non-cancer vehicle/vehicle group and cancer mice are from CHAPTER 5 cancer/vehicle. (A) BUN levels from plasma and (B) Urine NGAL levels were measured following four doses of cisplatin on Day 24. qRT-PCR of (C) KIM-1, (D) TIMP-1, (E) COL1A1, (F) *NLRP3*, (G) TNF-α, and (H) CXCL-1 in kidney cortex homogenates is normalized to B2M. Data are expressed as means ± SEM; n=5–10. Statistical significance was determined by an unpaired t-test. *p < 0.05 **p<0.01, ****p < 0.0001

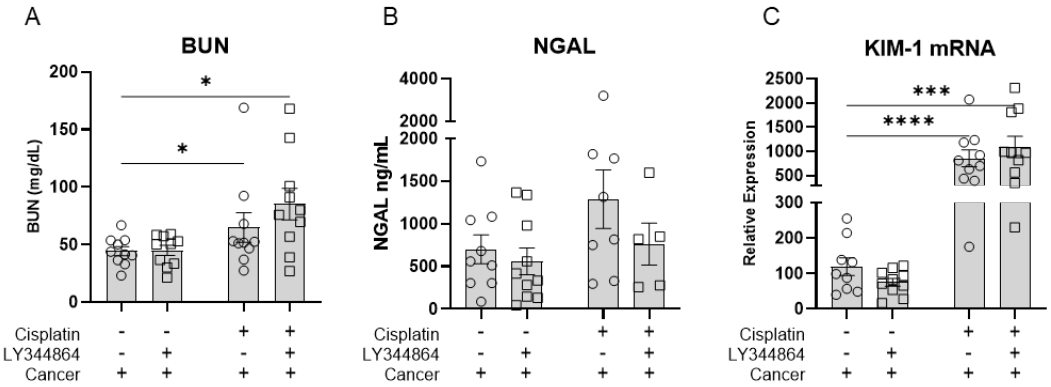

Figure 37. Kidney function and kidney injury in mice with lung cancer following RLDC treated with LY344864.

Eight- to ten-week-old B6;129 male mice with subcutaneous lung cancer were treated with 0 or 7 mg/kg cisplatin once a week for four weeks and vehicle or LY344864 daily. (A) BUN levels from plasma and (B) Urine NGAL levels were measured following four doses of cisplatin on Day 24. (C) qRT-PCR of KIM-1 in kidney cortex homogenates is normalized to non-cancer vehicle-treated kidneys. Data are expressed as means ± SEM; n=5–10. Statistical significance was determined by TWO-Way ANOVA followed by Tukey post-test. *p < 0.05, ***p<0.001, ****p<0.0001

Kidney fibrosis in mice with lung cancer following RLDC treated with LY344864.

Subcutaneous lung cancer alters kidney fibrosis (CHAPTER 4). We determined kidney cortex protein levels of fibronectin, and α-SMA, via immunoblotting analysis. Both markers are increased in the cancer/vehicle group as compared to the non-cancer/vehicle group (Figure 38A). The treatment of LY344864 in the cancer/LY344864 group compared to the cancer/vehicle group had little to no effect on amount of fibronectin or α-SMA detected (Figure 38A). These data suggest the mechanism through which cancer induces kidney fibrosis is not protected by LY344864. The use of cisplatin in the cancer/cisplatin group elevated fibronectin or α-SMA protein levels compared to the cancer/vehicle groups similar to results in (CHAPTER 4). The use of LY344864 in the RLDC has previously been shown to be protective by reducing markers of kidney fibrosis (CHAPTER 3). The use of LY344864 in mice with cancer did not provide the same protection from cisplatin. Comparing the cancer/cisplatin group to the cancer/cisplatin/LY group shows that LY344864 does not provide protection from cisplatin induced kidney fibrosis in mice with subcutaneous lung cancer as there is only a slight change in fibronectin or α-SMA protein levels (Figure 38A).

We determined the development of interstitial fibrosis on FFPE kidney sections using SR/FG. The treatment of LY344864 in the cancer/LY344864 group compared to the cancer/vehicle group had no effect on SR staining (Figure 38B). The use of cisplatin in the cancer/cisplatin group elevated SR staining levels though non-significantly compared to the cancer/vehicle groups (Figure 38B). Comparing the cancer/cisplatin group to the cancer/cisplatin/LY group shows that LY344864 does not provide protection from cisplatin induced kidney fibrosis in mice with subcutaneous lung cancer as there is no reduction in SR staining levels (Figure 38B).

Subcutaneous lung cancer alters kidney fibrosis (CHAPTER 4). The cancer/vehicle group from CHAPTER 5 was compared to the non-cancer/vehicle group

from CHAPTER 3 (Figure 36). This was done to help visualize and understand the degree of kidney fibrosis occurring in these mice just from cancer. There was a significant increase in Timp-1 and Col1a1 expression between non-cancer and cancer mice kidneys (Figure 36D-E). The treatment of LY344864 in the cancer/LY344864 group compared to the cancer/vehicle group had no effect on Timp-1 or Col1a1 kidney expression (Figure 38C-D). The use of cisplatin in the cancer/cisplatin group elevated kidney Timp-1 and had no effect on Col1a1 expression levels compared to the cancer/vehicle groups. The use of LY344864 in the RLDC model has previously been shown to be protective by reducing markers of kidney fibrosis (CHAPTER 3). The use of LY344864 in mice with cancer did not provide the same protection from cisplatin. Comparing the cancer/cisplatin group to the cancer/cisplatin/LY group shows that LY344864 does not provide protection from cisplatin induced kidney fibrosis in mice with subcutaneous lung cancer as there is no change in kidney Timp-1 and Col1a1 expression (Figure 38C-D).

The mechanism through which cancer induces kidney fibrosis is not protected by LY344864. The use of LY344864 in mice with cancer did not provide the same protection from cisplatin induced kidney fibrosis. Together these data indicate that while LY344864 provides protection from RLDC induced kidney fibrosis in mice without cancer, these effects are nullified in mice with subcutaneous lung cancer.

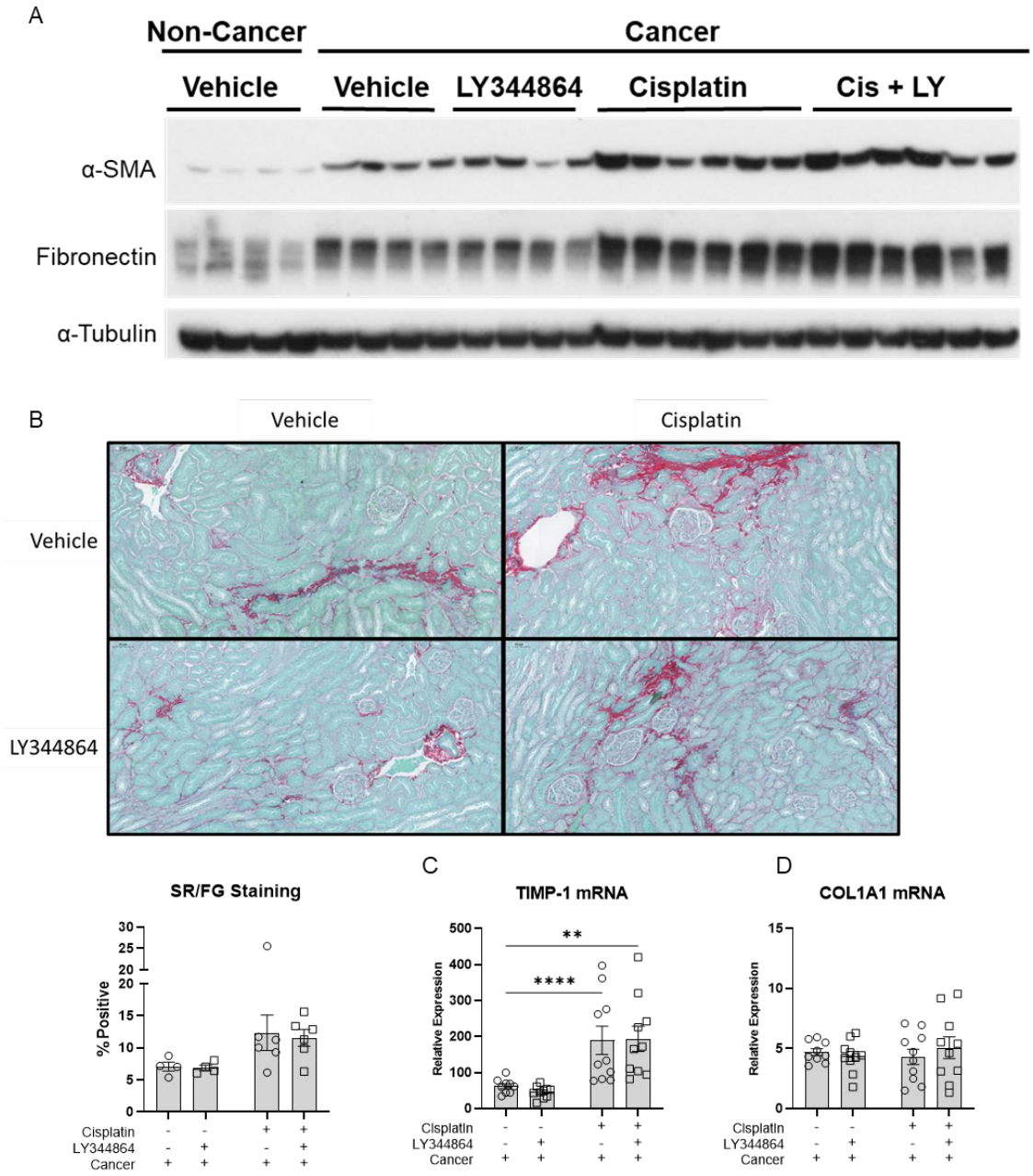

Figure 38. Kidney fibrosis in mice with lung cancer following RLDC treated with LY344864.

Eight- to ten-week-old B6;129 male mice with subcutaneous lung cancer were treated with 0 or 7 mg/kg cisplatin once a week for four weeks and vehicle or LY344864 daily. (A) Immunoblotting from kidney cortex homogenates for Fibronectin, α-SMA, and α-Tubulin. (B) SR/FG stain for total collagen levels on 5-µm-thick paraffin-embedded kidney sections and the quantifications. (C-D) qRT-PCR of *Timp-1* and *Col1a1* in kidney cortex homogenates is normalized to non-cancer vehicle-treated kidneys. Data are expressed as means ± SEM; n=5–10. Statistical significance was determined by TWO-Way ANOVA followed by a Tukey post-test. **p < 0.01, ***p<0.001

Kidney inflammation in mice with lung cancer following RLDC treated with LY344864.

Subcutaneous lung cancer increases kidney inflammation (CHAPTER 4). The cancer/vehicle group from CHAPTER 5 was compared to the non-cancer/vehicle group from CHAPTER 3 (Figure 36). This was done to help visualize and understand the degree of kidney inflammation occurring in these mice just from cancer. There was a significant increase in *Nlrp3, Tnf-α*, and *Cxcl1* expression between non-cancer and cancer mice kidneys (Figure 36F-H). The cancer/vehicle group is represented in Figure 39 as the first column of data. The treatment of LY344864 in the cancer/LY344864 group compared to the cancer/vehicle group had no effect on *Tnf-α, Cxcl1, Il-6, and Nlrp3* kidney expression (Figure 39A-D). The use of cisplatin in the cancer/cisplatin group elevated kidney *Tnf-α, and Cxcl1* and had no effect on *Il-6 and Nlrp3* expression levels compared to the cancer/vehicle groups (Figure 39A-D). The use of LY344864 in the RLDC model has previously been shown to be protective by reducing markers of kidney inflammation (CHAPTER 3). The use of LY344864 in mice with cancer did not provide the same protection from cisplatin. Comparing the cancer/cisplatin group to the cancer/cisplatin/LY group shows that LY344864 does not provide protection from cisplatin induced kidney inflammation in mice with subcutaneous lung cancer as there is no change in kidney *Tnf-α, Cxcl1, Il-6, and Nlrp3* expression (Figure 39A-D).

The mechanism through which cancer induces kidney inflammation is not protected by LY344864. The use of LY344864 in mice with cancer did not provide the same protection from cisplatin induced kidney inflammation. Together these data indicate that while LY344864 provides protection from RLDC induced kidney inflammation in mice without cancer, these effects are nullified in mice with subcutaneous lung cancer.

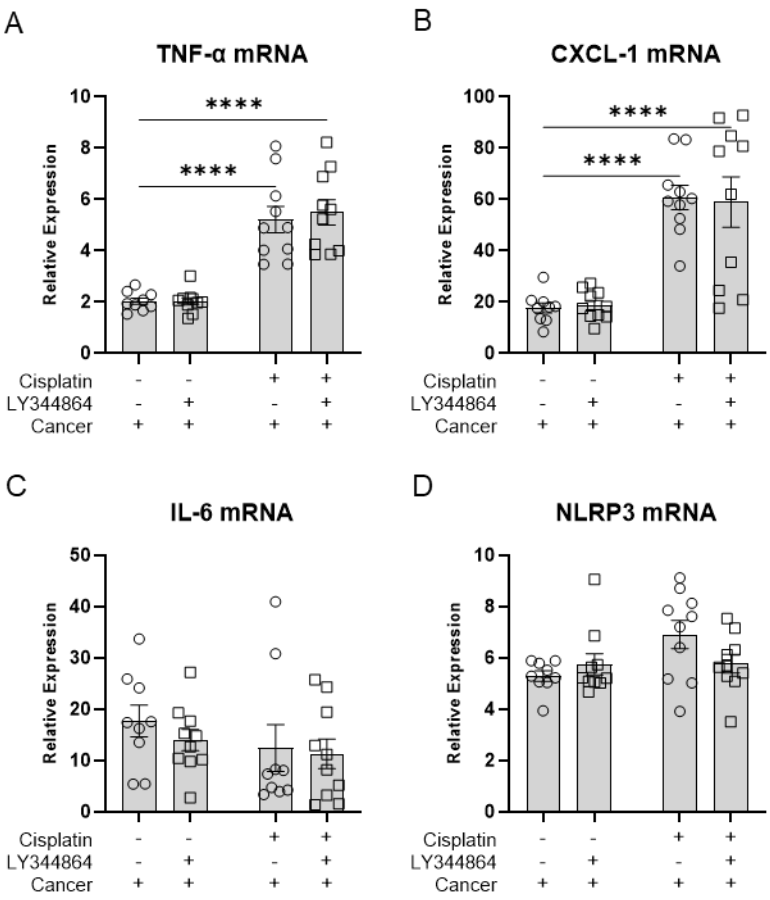

Figure 39. Kidney inflammation in mice with lung cancer following RLDC treated with LY344864.

Eight- to ten-week-old B6;129 male mice with subcutaneous lung cancer were treated with 0 or 7 mg/kg cisplatin once a week for four weeks and vehicle or LY344864 daily. (A-D) qRT-PCR of *Tnf-α, Cxcl-1, Il-6*, and *Nlrp3* in kidney cortex homogenates is normalized to non-cancer vehicle-treated kidneys. Data are expressed as means ± SEM; n=5–10. Statistical significance was determined by TWO-Way ANOVA followed by a Tukey post-test. ****$p < 0.0001$

Kidney mitochondrial content and biogenesis in mice with lung cancer following RLDC treated with LY344864.

Subcutaneous lung cancer reduces kidney mitochondrial content and biogenesis (CHAPTER 4). The cancer/vehicle group from CHAPTER 5 was compared to the non-cancer/vehicle group from CHAPTER 3 (Figure 40). This was done to help visualize and understand the magnitude of reduction in kidney mitochondrial content and biogenesis occurring in these mice from cancer. There was a significant reduction in kidney mtDNA/nDNA ratio between non-cancer and cancer mice (Figure 40A). The cancer/vehicle group is represented in Figure 41 as the first column of data. The treatment of LY344864 in the cancer/LY344864 group compared to the cancer/vehicle group had no effect on kidney mitochondrial content as assessed mtDNA/nDNA ratio and immunoblotting for ETC subunit proteins (Figure 41A-B). The use of cisplatin in the cancer/cisplatin group had slight reduction on mtDNA/nDNA ratio and ETC subunit proteins compared to the cancer/vehicle groups (Figure 41A-B). The use of LY344864 in the RLDC model has previously been shown to be protective by increasing kidney mitochondrial content (CHAPTER 3). The use of LY344864 in mice with cancer did not provide the same protection from cisplatin. Comparing the cancer/cisplatin group to the cancer/cisplatin/LY group shows that LY344864 does not increase mtDNA/nDNA ratio in mice with subcutaneous lung cancer (Figure 41A). The only marker to show benefit between cancer/cisplatin group and cancer/cisplatin/LY group is an increase in Complex 5 of ETC subunit proteins (Figure 41B).

Mitochondrial biogenesis (MB) was measured through PGC-1α mRNA expression and protein levels. Subcutaneous lung cancer reduces kidney mitochondrial biogenesis (CHAPTER 4). The cancer/vehicle group from CHAPTER 5 was compared to the non-cancer/vehicle group from CHAPTER 3 (Figure 36). This was done to help visualize and understand the magnitude of reduction in kidney mitochondrial biogenesis occurring in

these mice from cancer. There was a significant reduction in *PGC-1α, Nrf-1*, and *Tfam* kidney expression (Figure 40B-D) between non-cancer and cancer mice. The cancer/vehicle group is represented in Figure 41 as the first column of data. The treatment of LY344864 in the cancer/LY344864 group compared to the cancer/vehicle group had no effect on kidney mitochondrial biogenesis as assessed *PGC-1α, Nrf-1*, and *Tfam* kidney expression (Figure 41C-E). The use of cisplatin in the cancer/cisplatin group had no additional reduction on *PGC-1α, Nrf-1*, and *Tfam* kidney expression levels compared to the cancer/vehicle groups (Figure 41C-E). The use of LY344864 in the RLDC model has previously been shown to be protective by increasing markers of kidney mitochondrial biogenesis (CHAPTER 3). The use of LY344864 in mice with cancer did not provide the same protection from cisplatin. Comparing the cancer/cisplatin group to the cancer/cisplatin/LY group shows that LY344864 does not increase kidney mitochondrial biogenesis in mice with subcutaneous lung cancer as there is no change in kidney *PGC-1α, Nrf-1*, and *Tfam* kidney expression (Figure 41C-E).

The treatment of LY344864 in the cancer/LY344864 group compared to the cancer/vehicle group had no effect on kidney PGC-1α protein levels (Figure 41F). The use of cisplatin in the cancer/cisplatin group had no additional reduction on kidney PGC-1α protein levels compared to the cancer/vehicle groups (Figure 41F). The use of LY344864 in the RLDC model has previously been shown to be protective by increasing markers of kidney mitochondrial biogenesis (CHAPTER 3). The use of LY344864 in mice with cancer did not provide the same protection from cisplatin. Comparing the cancer/cisplatin group to the cancer/cisplatin/LY group shows that LY344864 does not increase kidney mitochondrial biogenesis in mice with subcutaneous lung cancer as there is no change in kidney PGC-1α protein levels (Figure 41F).

The mechanism through which cancer reduces kidney mitochondrial content and biogenesis is not protected by LY344864. The use of LY344864 in mice with cancer did not provide the same protection from cisplatin induced reduction in kidney mitochondrial content and biogenesis Together these data indicate that while LY344864 provides protection from RLDC induced reduction in kidney mitochondrial content and biogenesis in mice without cancer, these effects are nullified in mice with subcutaneous lung cancer.

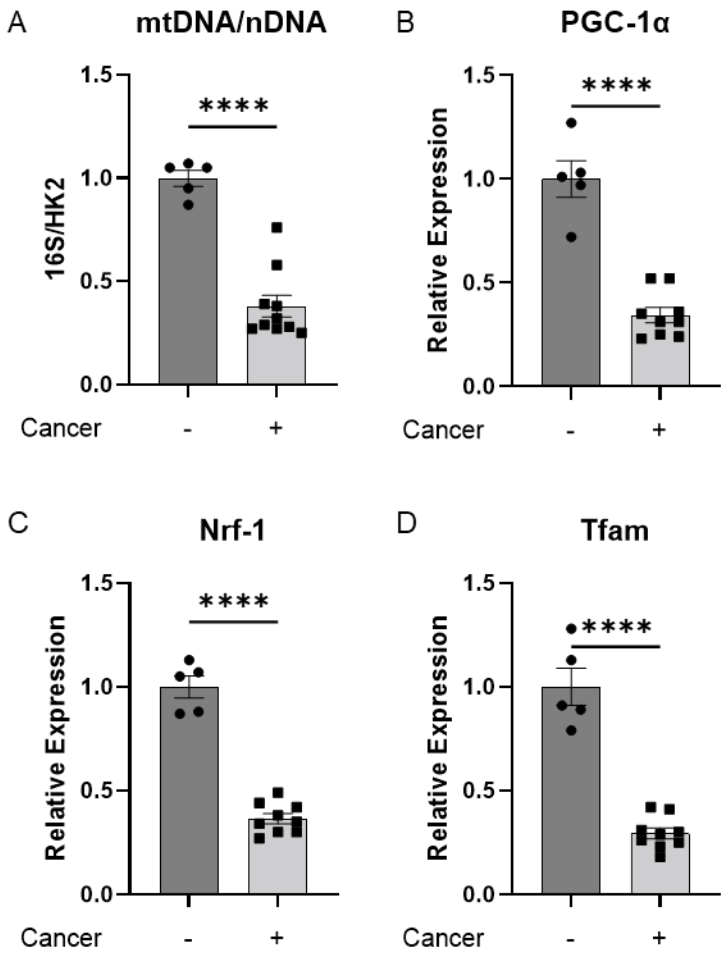

Figure 40. Kidney mitochondrial content and biogenesis in mice with and without subcutaneous lung cancer.

Eight- to ten-week-old B6;129 male mice with and without subcutaneous cancer. Non-cancer mice are from CHAPTER 3 non-cancer vehicle/vehicle group and cancer mice are from CHAPTER 5 cancer/vehicle. (A) qPCR on nuclear-encoded HK2 and mitochondrial-encoded 16S were used to calculate the ratio between mtDNA to nDNA, normalized to vehicle-treated kidneys. (B-D) qRT-PCR of PGC-1α, Nrf-1, and Tfam in kidney cortex homogenates is normalized to non-cancer vehicle-treated kidneys. Data are expressed as means ± SEM; n=5–10. Statistical significance was determined by an unpaired t-test. ****$p < 0.0001$

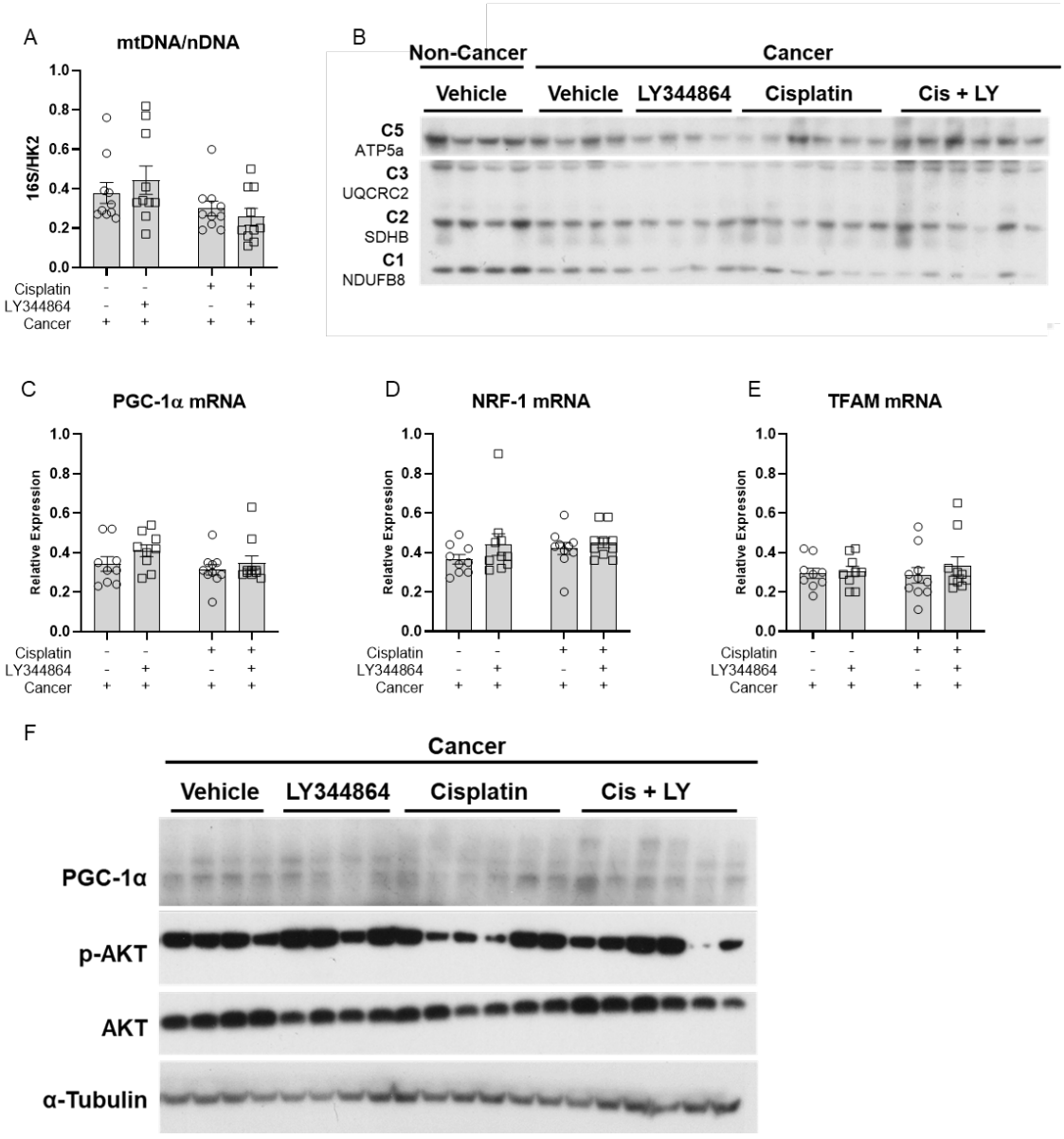

Figure 41. Kidney mitochondrial content and biogenesis in mice with lung cancer following RLDC treated with LY344864.

(A) qPCR on nuclear-encoded HK2 and mitochondrial-encoded 16S were used to calculate the ratio between mtDNA to nDNA, normalized to non-cancer vehicle-treated kidneys. (B) Immunoblotting for ETC subunit proteins: Complex 1 (NDUFB8), Complex 2 (SDHB) Complex 3 (UQCRC2), Complex 4 (MTCO1), and Complex 5 (ATP5a) of kidney cortex homogenates. (C-E) qRT-PCR of PGC-1α, NRF-1, and TFAM in kidney cortex homogenates is normalized to non-cancer vehicle-treated kidneys. (F) Immunoblotting for PGC-1α, p-AKT, AKT, and α-tubulin. Data are expressed as means ± SEM; n=5–10. Statistical significance was determined by TWO-way ANOVA followed by Tukey posttest.*P< 0.05, **P<0.01, and ****P < 0.0001.

DISCUSSION

Cisplatin nephrotoxicity has almost exclusively been studied in mice without cancer. Testing of nephroprotective agents in preclinical mouse models rarely includes the comorbidity of cancer. This is the first study to our knowledge to address nephroprotective agents in a clinically relevant cisplatin model that also includes the proper comorbidities. Our findings suggest that LY344864 provides some protection against cisplatin-induced nephrotoxicity in mice without cancer, as it reduces kidney function loss, injury, inflammation, and accumulation of fibrotic proteins. The protective effects of LY344864 are thought to be due to increased kidney mitochondrial biogenesis and content. However, when tested in mice with subcutaneous lung cancer, LY344864 had no effect on increasing kidney mitochondrial biogenesis and content. More importantly in mice with cancer LY344864 did not protect kidney function, injury, inflammation, or fibrosis.

An additional finding of this study is that cancer and cisplatin reduce kidney mitochondrial content and biogenesis through different pathways. The use of 5HT-1F agonist LY344864 in mice without cancer increases kidney mitochondrial content and biogenesis and helps prevent the reduction induced by cisplatin. However, mice with subcutaneous lung cancer also have reduced kidney mitochondrial content and biogenesis, and the use of LY344864 has no effect increasing kidney mitochondrial content and biogenesis. The suppression of kidney mitochondrial content and biogenesis from cancer appears to be a more powerful stimulus than cisplatin; and the combination of cancer and cisplatin does not significantly lower kidney mitochondrial content or biogenesis compared to cancer alone. The effects of cisplatin and cancer on kidney mitochondrial content and biogenesis suppression appear to be additive, though not significant, and maybe be the driving mechanism of enhanced toxicity in tumor bearing mice from cisplatin. Alternatively, cisplatin and cancer could be suppressing PGC-1α

through the same pathway and the dose of LY344864 used in this study was too low to overcome the combination. The evidence for this is shown by no change in PGC-1α expression or protein levels between cancer/vehicle and cancer/LY344864 groups. Further work needs to be completed to determine if cisplatin and cancer are working through the same pathway or are working independently of each other with an additive effect.

This study unable to determine the role of increased angiogenesis as the protective mechanism of 5HT-$_{1F}$ agonist LY344864 [263]. If angiogenesis is increased by LY344864, this could present a major problem for the clinical potential of this drug as angiogenesis is a hallmark of cancer and increasing angiogenesis in cancer patients could promote tumor growth and metastasis [251, 264]. The effects of 5HT-$_{1F}$ agonist on tumor growth needs to be fully characterized in preclinical models before any clinical studies should be conducted. Our results do not suggest that LY344864 increases tumor growth or inhibits the therapeutic effects of cisplatin. Additional work needs to be complete to confirm tumor angiogenesis and distant organ metastasis are not being stimulated by LY344864.

Historically, cisplatin nephrotoxicity has been studied in mice without cancer. This is the first study to our knowledge to demonstrate protection from cisplatin induced nephrotoxicity in non-cancer mice, but when tested in mice with lung cancer the nephroprotective effects are nullified. We believe any agents identified as potential therapeutic candidates for cisplatin nephrotoxicity must be extensively tested in preclinical models that more accurately represent the patient population they are being designed for. All clinical trials on nephroprotective agents have failed, and this study provides evidence that poorly representative mouse models may be misleading preclinical research to investigate agents that are bound to fail in clinical trials. The development of nephroprotective strategies for cancer patients must consider their primary comorbidity and be designed to maximize the effectiveness/efficacy of the chemotherapy.

CHAPTER 6: OVERALL DISCUSSION

SUMMARY

The results from this dissertation show that RLDC model reduce kidney function, induces kidney injury and the development of fibrosis, along with reducing mitochondrial content and PGC-1α expression. These findings are consistent with previous research that has shown reduced expression of PGC-1α in human renal biopsies from AKI/CKD patients compared to normal kidney tissue [140, 192, 193]. Lower PGC-1α expression is seen in other models of AKI and increasing PGC-1α expression has provided protection in other rodent models [179, 192, 194-201, 203-206]. Moreover, mitochondrial diseases associated with genetic inheritance have been found to coincide with renal impairment, particularly tubular defects [168-172]. The repeated insult of cisplatin produces a failed-repair tubule cell population [160], which can lead to a maladaptive repair process, and the development of kidney fibrosis/CKD. Tissue repair is energetically demanding, and adequate mitochondrial mass and mitochondrial respiration are required for proper healing [94]. The reduced kidney mitochondrial content and biogenesis during the RLDC model may be driving the maladaptive repair process.

We conducted experiments to explore whether increasing kidney mitochondrial content can mitigate cisplatin-induced nephrotoxicity and promote better recovery. Specifically, we investigated the potential of the 5HT-$_{1F}$ agonist, LY344864, to protect against cisplatin-induced kidney injury and fibrosis by enhancing kidney mitochondrial content and biogenesis. We found that LY344864 increases mitochondrial content and biogenesis, which is typically reduced by cisplatin treatment. Moreover, our results demonstrate that LY344864 provides protection against cisplatin-induced kidney injury,

interstitial fibrosis, and inflammation. LY344864 provides protection against cisplatin-induced kidney injury, interstitial fibrosis, and inflammation by increasing mitochondrial content in mice without cancer. These results are helpful in our understanding of the complex pathobiology of kidney fibrosis and help uncover potential driving mechanisms. It is particularly significant because current treatments for CKD are inadequate, and there are no options specifically targeting kidney fibrosis. This work, along with an extensive number of studies have investigated cisplatin-induced nephrotoxicity [39, 115, 121, 210, 211]. However, most of this work has been completed in mouse models without cancer and only patients with cancer will be exposed to cisplatin toxicity.

We argue that these models do not adequately reflect the altered physiology of cancer patients. Adding the comorbidity of cancer to this model will further our understanding of the pathophysiology and improves the clinical relevancy of this preclinical model. We used multiple mouse models of lung cancer in combination with the RLDC regimen to begin to understand the interplay between lung cancer and cisplatin-induced nephrotoxicity. Data indicate that lung cancer-bearing mice treated with RLDC have increased renal toxicity, injury, and fibrosis as compared to non-lung cancer-bearing mice. Additionally, lung cancer alone induced kidney injury and fibrosis prior to cisplatin treatment. Lung-kidney crosstalk is a known phenomenon [229, 230], and recent work has shown that during AKI events, the kidneys release cytokines that induce lung injury [231]. Further work is required to understand the mechanism driving this process. We believe the presence of lung cancer induces the first hit of injury in the kidney, which potentiates the nephrotoxicity of cisplatin. Additionally, we found that both cisplatin and cancer are suppressing kidney mitochondrial content and the effect appears to be additive in the cancer/cisplatin group.

The advancement of the RLDC model to include the comorbidity of cancer requires reassessment of previously discovered protective strategies. The data presented in this

study is the first to our knowledge to address nephroprotective agents in a clinically relevant cisplatin model that also includes the proper comorbidities. Our results show that the 5HT-$_{1F}$ agonist LY344864 is promising in protecting from RLDC induced nephrotoxicity in mice without cancer, but these protective effects are nullified by the presence of subcutaneous lung cancer. In non-cancer mice LY344864 provides protection against cisplatin-induced kidney injury, interstitial fibrosis, and inflammation by increasing mitochondrial content. However, in mice with cancer LY344864 had no effect on increasing kidney mitochondrial biogenesis and content. More importantly LY344864 usage in mice with cancer is unable to provide any protection to kidney function, injury, inflammation, or the development of fibrosis from cancer or cisplatin. This suggests that loss of kidney mitochondrial content is a driving mechanism of the maladaptive repair process seen from cisplatin and cancer.

Together this work highlights the importance of testing nephroprotective strategies to prevent cisplatin-induced nephrotoxicity in preclinical models that more accurately represent the patient population they are designed for. This is the first study to our knowledge to demonstrate protection from cisplatin induced nephrotoxicity in non-cancer mice, but when tested in mice with lung cancer the nephroprotective effects are nullified. Previous clinical trials on nephroprotective agents have failed, and we propose that poorly representative mouse models may be responsible for misleading preclinical research on agents that are bound to fail in clinical trials. Developing effective nephroprotective strategies for cancer patients requires considering their primary comorbidity and designing treatments to maximize the effectiveness and efficacy of chemotherapy.

STRENGTHS AND LIMITATIONS

The dissertation has several strengths. First, the RLDC model used in this study is more clinically relevant than other models of cisplatin-induced nephrotoxicity, which allows for more accurate translation of the findings to human patients. Second, this study is the first to demonstrate that repeated cycles of cisplatin lead to a reduction in kidney mitochondrial content and biogenesis, which may contribute to the development of kidney fibrosis. This novel pathway provides a new target for preventive and interventional strategies. Third, the inclusion of cancer in the RLDC model is a significant strength of this study. The data presented here demonstrate that cancer worsens cisplatin-induced nephrotoxicity and kidney fibrosis, which highlights the importance of considering comorbidities in preclinical models. Fourth, this study is the first to address nephroprotective agents in a clinically relevant chemotherapy model that includes the proper comorbidities. Fifth, the finding that the 5HT-1F agonist LY344864 provides protection from cisplatin-induced nephrotoxicity in non-cancer mice is a significant contribution to the field. However, the nullification of its effects in mice with lung cancer highlights the importance of extensive testing of potential therapeutic candidates in preclinical models that more accurately represent the patient population. Overall, this dissertation provides new insights into the pathophysiology of cisplatin-induced nephrotoxicity and highlights the need for more clinically relevant preclinical models and extensive testing of potential therapeutic candidates.

While this study provides valuable insights into the mechanisms underlying cisplatin-induced nephrotoxicity, the potential protective effects of 5HT-$_{1F}$ agonists, and discovered a Lung cancer-kidney crosstalk phenotype there are several limitations to this work that should be taken into consideration.

Firstly, all experiments were conducted in mice, which may not fully reflect what occurs in humans. The RLDC model used in this study is more representative of clinical

cisplatin administration than other mouse models, but there are still differences in dosing regimen and concomitant drug use between mice and humans. Patients receive cisplatin via slow I.V. infusion generally alongside fluids, and the dosing regimen can be multiple weeks in between each cycle. It is impossible to perfectly model this dosing regimen in mice. Additionally, most cancer patients are not on monotherapy and are receiving potentially multiple nephrotoxic agents at once. Therefore, the translatability of these findings to human patients may be limited.

Secondly, the only cancer type that was examined was lung-cancer and the lung cancer had the driver mutation of $Kras^{G12D}$.The data presented here could be a unique phenomenon to lung cancer driven by mutant $Kras^{G12D}$. Cisplatin is used clinically for a number of cancer types including head and neck cancers, testicular, small-cell, and NSCLC, ovarian, cervical cancer, and bladders. Mouse models of these different cancer types need to be assessed to determine if the cancer-kidney crosstalk phenomenon is exclusive to lung cancer.

Thirdly, the use of 5HT-1F agonist only caused slight increases in PGC-1α expression, suggesting that the protective effects observed may be due to off-target effects. Therefore, additional work is needed to determine the exact mechanism by which $5HT\text{-}_{1F}$ agonists protect against cisplatin-induced nephrotoxicity. The role of PGC-1α in RLDC also needs to be further elucidated, the use transgenic mouse models to remove the issue of off-target effects from pharmacological agents is required.

Overall, while this study provides important insights into the potential mechanisms underlying cisplatin-induced nephrotoxicity and the potential protective effects of $5HT\text{-}_{1F}$ agonists, further research is needed to determine the clinical relevance of these findings and to address the limitations outlined above.

FUTURE DIRECTIONS

This dissertation provides evidence to support future work to determine how distant cancer cells are altering kidney biology, inducing pathology, and enhancing cisplatin toxicity. Additional solid organ cancer types need to be examined to determine if this phenotype is specific to lung cancer. All studies employed here utilized tumors driven by mutant $Kras^{G12D}$, additional driver mutations in lung cancer cells need to be examined. This work needs to be repeated in humanized mice with tumors from PDX. These can be met with the following future directions.

1. **Determine if cancer-kidney crosstalk is specific to lung cancer, and if other cancer types enhance cisplatin nephrotoxicity.** Cisplatin is used clinically for a number of cancer types including head and neck cancers, testicular, small-cell, and NSCLC, ovarian, cervical cancer, and bladders. Mouse models of these different cancer types need to be assessed to determine if the cancer-kidney crosstalk phenomenon is exclusive to lung cancer. Each mouse model will have different stipulations, but the general experiment will involve mice with and without the particular cancer and mice that are treated with saline or cisplatin. Additionally, these studies will help us determine if other mouse models of cancer have increased nephrotoxicity from cisplatin as reported here.

2. **Determine if other driver mutations in NSCLC besides mutant $Kras^{G12D}$ are able to induce kidney injury, fibrosis and enhance cisplatin nephrotoxicity.** All studies employed here utilized tumors driven by mutant $Kras^{G12D}$. Future studies also need to be completed with cells lines that have different driver mutations to determine if the cancer-kidney crosstalk is specific to mutant $Kras^{G12D}$.

3. **Determine if lung cancer-kidney cross is only a mouse specific phenotype**. This work needs to be repeated in humanized mice with tumors from PDX. The NRGS mice strain can be humanized to have human immune cells. These humanized NRGS mice can then be implanted with patient derived xenografts (PDX) from multiple cancer types (see

future directions #1 for list). These PDX models are more representative of clinical tumors and will help determine if this phenotype is occurring in humans.

4. **Determine the role of PGC-1α and its protective potential from RLDC induced AKI-CKD**. The use of transgenic mouse experiments that knockout and overexpression PGC-1α will need to be conducted. Transgenic mice with tubule cell specific overexpression of PGC-1α and transgenic mice with tubule cell specific deletion of PGC-1α will be utilized to determine if the role of PGC-1α in RLDC induced nephrotoxicity. Additionally, to determine if the benefits of 5HT-$_{1F}$ agonists are through PGC-1α, the transgenic mice with tubule cell specific deletion of PGC-1α should show no benefit from LY344864 treatment. If 5HT-$_{1F}$ agonist provides protection in PGC-1α knockout mice an off-target mechanism is at work, nullifying the importance of PGC-1α as the mechanism of protection. To strengthen the clinical relevance of this work subsequent studies should be conducted with the FDA approved 5HT-$_{1F}$ agonist, Lasmiditan. The ideal study would be a clinical trial using Lasmiditan in cancer patients treated with cisplatin to prevent cisplatin toxicity.

5. **Investigate the potential mechanisms by which distant cancer cells alter kidney biology and induce pathology.** This can be done by examining the expression of signaling molecules, cytokines, and growth factors in the tumor microenvironment and their potential effects on the kidney. In vitro and ex vivo experiments can also be conducted to investigate the direct effects of cancer cell secretions on kidney cells. This will help identify potential targets for therapeutic intervention.

6. **Evaluate the potential of other nephroprotective agents in the context of cancer-induced kidney injury.** The current study found that the 5HT-$_{1F}$ agonist LY344864 provided protection in non-cancer mice but not in mice with lung cancer. Other agents with potential nephroprotective effects need to be reassessed in mouse models with cancer.

7. **Explore the potential of combination therapies to prevent or mitigate cisplatin-induced kidney injury in cancer patients.** The current study suggests that the presence of cancer exacerbates cisplatin-induced kidney injury and fibrosis. Combining cisplatin with other chemotherapy agents or targeted therapies may reduce the overall dose of cisplatin required and thus minimize kidney damage. Additionally, combining cisplatin with nephrotoxic agents may further increase kidney injury and needs to be investigated.

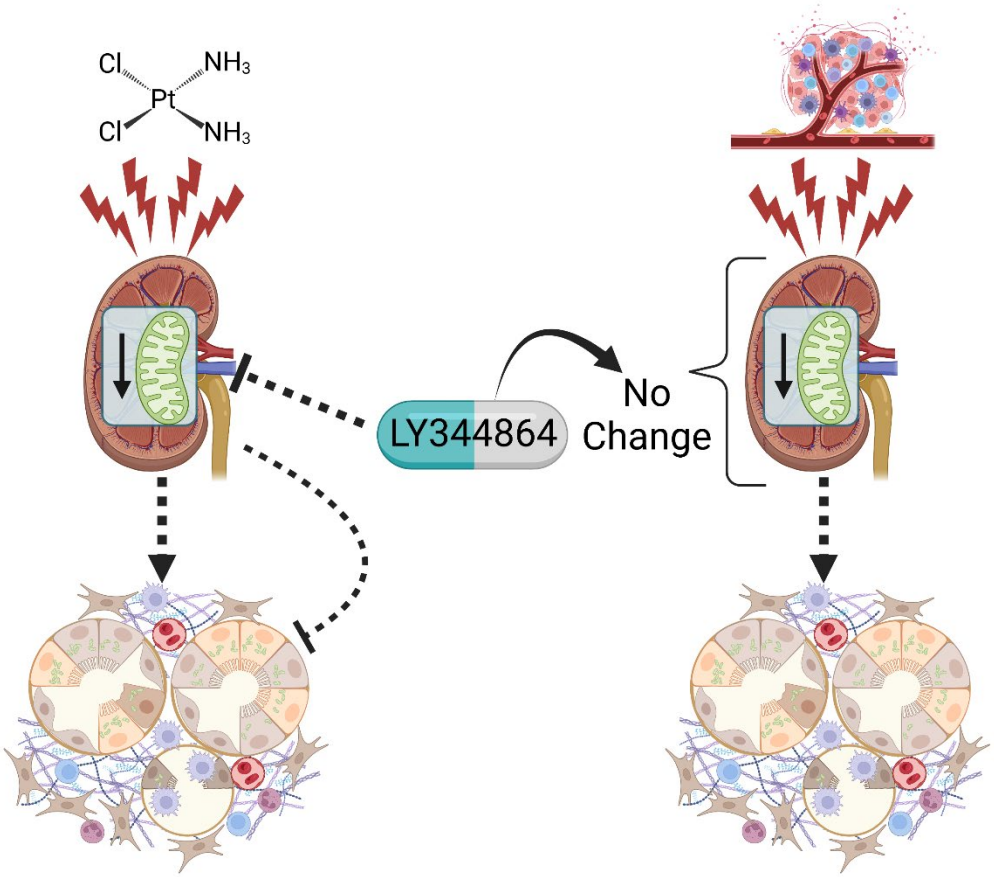

Figure 42. Graphical Summary

Graphical summary of the effects of LY344864 on RLDC and cancer induced nephrotoxicity. LY344864 increased kidney mitochondrial content and reduced loss of kidney function, kidney injury, inflammation, and development of fibrosis from RLDC in mice without cancer. Lung cancer alone without cisplatin reduced renal function, increased fibrosis, reduced mitochondrial content, and reduced PGC-1α of kidney cortices. The use of LY344864 in mice with cancer had no protective effects. Figure created using BioRender.com.

REFERENCES

1. Susantitaphong, P., et al., *World incidence of AKI: a meta-analysis.* Clin J Am Soc Nephrol, 2013. **8**(9): p. 1482-93.
2. United States Renal Data System, *2022 USRDS Annual Data Report: Epidemiology of kidney disease in the United States*. National Institutes of Health, National Institute of Diabetes and Digestive and Kidney Diseases, Bethesda, MD.
3. Webster, A.C., et al., *Chronic Kidney Disease.* Lancet, 2017. **389**(10075): p. 1238-1252.
4. Collaboration, G.B.D.C.K.D., *Global, regional, and national burden of chronic kidney disease, 1990-2017: a systematic analysis for the Global Burden of Disease Study 2017.* Lancet, 2020. **395**(10225): p. 709-733.
5. Chen, T.K., D.H. Knicely, and M.E. Grams, *Chronic Kidney Disease Diagnosis and Management: A Review*. JAMA, 2019. **322**(13): p. 1294-1304.
6. Chawla, L.S., et al., *Acute kidney injury and chronic kidney disease as interconnected syndromes.* N Engl J Med, 2014. **371**(1): p. 58-66.
7. Sohaney, R., et al., *In-Hospital and 1-Year Mortality Trends in a National Cohort of US Veterans with Acute Kidney Injury.* Clinical Journal of the American Society of Nephrology, 2022. **17**(2).
8. Ferenbach, D.A. and J.V. Bonventre, *Mechanisms of maladaptive repair after AKI leading to accelerated kidney ageing and CKD.* Nat Rev Nephrol, 2015. **11**(5): p. 264-76.
9. Chawla, L.S., et al., *The severity of acute kidney injury predicts progression to chronic kidney disease.* Kidney Int, 2011. **79**(12): p. 1361-9.
10. Coca, S.G., S. Singanamala, and C.R. Parikh, *Chronic kidney disease after acute kidney injury: a systematic review and meta-analysis.* Kidney Int, 2012. **81**(5): p. 442-8.
11. Amdur, R.L., et al., *Outcomes following diagnosis of acute renal failure in U.S. veterans: focus on acute tubular necrosis.* Kidney Int, 2009. **76**(10): p. 1089-97.
12. Ishani, A., et al., *Acute kidney injury increases risk of ESRD among elderly.* J Am Soc Nephrol, 2009. **20**(1): p. 223-8.
13. Skinner, R., et al., *Persistent nephrotoxicity during 10-year follow-up after cisplatin or carboplatin treatment in childhood: relevance of age and dose as risk factors.* Eur J Cancer, 2009. **45**(18): p. 3213-9.
14. Latcha, S., et al., *Long-Term Renal Outcomes after Cisplatin Treatment.* Clin J Am Soc Nephrol, 2016. **11**(7): p. 1173-9.
15. Drawz, P. and M. Rahman, *Chronic kidney disease.* Ann Intern Med, 2015. **162**(11): p. Itc1-16.
16. Kim, K.M., et al., *Impact of chronic kidney disease on mortality: A nationwide cohort study.* Kidney Res Clin Pract, 2019. **38**(3): p. 382-390.
17. Humphreys, B.D., *Onco-nephrology: kidney disease in the cancer patient: introduction.* Semin Nephrol, 2010. **30**(6): p. 531-3.
18. Salahudeen, A.K. and J.V. Bonventre, *Onconephrology: the latest frontier in the war against kidney disease.* J Am Soc Nephrol, 2013. **24**(1): p. 26-30.
19. Perazella, M.A., J.S. Berns, and M.H. Rosner, *Cancer and the kidney: the growth of onco-nephrology.* Adv Chronic Kidney Dis, 2014. **21**(1): p. 4-6.

20. Capasso, A., et al., *Summary of the International Conference on Onco-Nephrology: an emerging field in medicine.* Kidney Int, 2019. **96**(3): p. 555-567.
21. Rosner, M.H., et al., *Onconephrology: The intersections between the kidney and cancer.* CA: A Cancer Journal for Clinicians, 2021. **71**(1): p. 47-77.
22. Jhaveri, K. and M. Trivedi, *Cancer, Cancer Therapy, and the Kidney 2022.* Kidney News, 2022. **14**(5): p. 17-17.
23. Perazella, M.A. and M.H. Rosner, *Cancer and Kidney Diseases Onconephrology Comes of Age.* Kidney News, 2022. **14**(6): p. 21-21.
24. Launay-Vacher, V., et al., *Prevalence of Renal Insufficiency in cancer patients and implications for anticancer drug management: the renal insufficiency and anticancer medications (IRMA) study.* Cancer, 2007. **110**(6): p. 1376-84.
25. Janus, N., et al., *Prevalence of renal insufficiency in cancer patients: Data from the IRMA-2 study.* Journal of Clinical Oncology, 2009. **27**(15_suppl): p. 9559-9559.
26. Janus, N., et al., *Cancer and renal insufficiency results of the BIRMA study.* British Journal of Cancer, 2010. **103**(12): p. 1815-1821.
27. Perazella, M.A., *Onco-nephrology: renal toxicities of chemotherapeutic agents.* Clin J Am Soc Nephrol, 2012. **7**(10): p. 1713-21.
28. Lam, A.Q. and B.D. Humphreys, *Onco-nephrology: AKI in the cancer patient.* Clin J Am Soc Nephrol, 2012. **7**(10): p. 1692-700.
29. Rosner, M.H. and M.A. Perazella, *Acute Kidney Injury in Patients with Cancer.* N Engl J Med, 2017. **377**(5): p. 500-501.
30. Santos, M.L.C., et al., *Nephrotoxicity in cancer treatment: An overview.* World J Clin Oncol, 2020. **11**(4): p. 190-204.
31. Jagiela, J., P. Bartnicki, and J. Rysz, *Nephrotoxicity as a Complication of Chemotherapy and Immunotherapy in the Treatment of Colorectal Cancer, Melanoma and Non-Small Cell Lung Cancer.* Int J Mol Sci, 2021. **22**(9).
32. Gupta, S., P. Gudsoorkar, and K.D. Jhaveri, *Acute Kidney Injury in Critically Ill Patients with Cancer.* Clin J Am Soc Nephrol, 2022.
33. Perazella, M.A. and M.H. Rosner, *Drug-Induced Acute Kidney Injury.* Clin J Am Soc Nephrol, 2022. **17**(8): p. 1220-1233.
34. Perazella, M.A., *Drug-induced acute kidney injury: diverse mechanisms of tubular injury.* Curr Opin Crit Care, 2019. **25**(6): p. 550-557.
35. Izzedine, H. and M.A. Perazella, *Anticancer Drug-Induced Acute Kidney Injury.* Kidney International Reports, 2017. **2**(4): p. 504-514.
36. Matsubara, T., et al., *Nephrotoxicity associated with anticancer agents: perspective on onconephrology from nephrologists.* International Journal of Clinical Oncology, 2023.
37. Garcia-Carro, C., J. Draibe, and M.J. Soler, *Onconephrology: Update in Anticancer Drug-Related Nephrotoxicity.* Nephron, 2023. **147**(2): p. 65-77.
38. National Cancer Institute. *The "Accidental" Cure—Platinum-based Treatment for Cancer: The Discovery of Cisplatin*. 2014; Available from: https://www.cancer.gov/research/progress/discovery/cisplatin.
39. Miller, R.P., et al., *Mechanisms of Cisplatin nephrotoxicity.* Toxins (Basel), 2010. **2**(11): p. 2490-518.
40. Kelland, L., *The resurgence of platinum-based cancer chemotherapy.* Nat Rev Cancer, 2007. **7**(8): p. 573-84.
41. Oun, R., Y.E. Moussa, and N.J. Wheate, *The side effects of platinum-based chemotherapy drugs: a review for chemists.* Dalton Trans, 2018. **47**(19): p. 6645-6653.

42. Burton, R. and P. Theodore, *Clinical Physiology of Acid-Base and Electrolyte Disorders*. 2001: McGraw-Hill Education. 992.
43. Skorecki, K., et al., *Brenner & Rector's the kidney*. Tenth edition. ed. 2016: Elsevier.
44. Rennke, H.G., B.M. Denker, and B.D. Rose, *Renal pathophysiology : the essentials*. 5th ed. 2019, Philadelphia: Lippincott Williams & Wilkins. xii, 382 p.
45. Ogobuiro, I. and F. Tuma, *Physiology, Renal*, in *StatPearls*. 2021: Treasure Island (FL).
46. Al-Awqati, Q. and J.A. Oliver, *Stem cells in the kidney.* Kidney Int, 2002. **61**(2): p. 387-95.
47. Palmer, L.G. and J. Schnermann, *Integrated control of Na transport along the nephron.* Clin J Am Soc Nephrol, 2015. **10**(4): p. 676-87.
48. Curthoys, N.P. and O.W. Moe, *Proximal tubule function and response to acidosis.* Clin J Am Soc Nephrol, 2014. **9**(9): p. 1627-38.
49. King J, L.D., *Physiology, Cardiac Output.* 2022, In: StatPearls [Internet]. Treasure Island (FL): StatPearls Publishing; 2022 Jan.
50. Dalal R, B.Z., Sehdev JS, *Physiology, Renal Blood Flow and Filtration.* 2022, In: StatPearls [Internet]. Treasure Island (FL): : StatPearls Publishing; 2022 Jan.
51. Kaufman DP, B.H., Knohl SJ., *Physiology, Glomerular Filtration Rate.* 2022, In: StatPearls [Internet]. : Treasure Island (FL): StatPearls Publishing; 2022 Jan.
52. Sharma, R. and S. Sharma, *Physiology, Blood Volume*, in *StatPearls*. 2021: Treasure Island (FL).
53. Rajasekaran, A.K. and S.A. Rajasekaran, *Role of Na-K-ATPase in the assembly of tight junctions.* Am J Physiol Renal Physiol, 2003. **285**(3): p. F388-96.
54. Rajasekaran, S.A., et al., *Na,K-ATPase activity is required for formation of tight junctions, desmosomes, and induction of polarity in epithelial cells.* Mol Biol Cell, 2001. **12**(12): p. 3717-32.
55. Rajasekaran, S.A., et al., *Na,K-ATPase subunits as markers for epithelial-mesenchymal transition in cancer and fibrosis.* Mol Cancer Ther, 2010. **9**(6): p. 1515-24.
56. Pagliarini, D.J., et al., *A mitochondrial protein compendium elucidates complex I disease biology.* Cell, 2008. **134**(1): p. 112-123.
57. Soltoff, S.P., *ATP and the regulation of renal cell function.* Annu Rev Physiol, 1986. **48**: p. 9-31.
58. Vallon, V., *Tubular Transport in Acute Kidney Injury: Relevance for Diagnosis, Prognosis and Intervention.* Nephron, 2016. **134**(3): p. 160-166.
59. Scholz, H., et al., *Kidney physiology and susceptibility to acute kidney injury: implications for renoprotection.* Nature Reviews Nephrology, 2021.
60. Clark, A.J. and S.M. Parikh, *Mitochondrial Metabolism in Acute Kidney Injury.* Semin Nephrol, 2020. **40**(2): p. 101-113.
61. Zager, R.A., A.C. Johnson, and K. Becker, *Renal cortical pyruvate depletion during AKI.* J Am Soc Nephrol, 2014. **25**(5): p. 998-1012.
62. Lan, R., et al., *Mitochondrial Pathology and Glycolytic Shift during Proximal Tubule Atrophy after Ischemic AKI.* J Am Soc Nephrol, 2016. **27**(11): p. 3356-3367.
63. Smith, J.A., L.J. Stallons, and R.G. Schnellmann, *Renal cortical hexokinase and pentose phosphate pathway activation through the EGFR/Akt signaling pathway in endotoxin-induced acute kidney injury.* Am J Physiol Renal Physiol, 2014. **307**(4): p. F435-44.
64. Levey, A.S. and M.T. James, *Acute Kidney Injury.* Ann Intern Med, 2017. **167**(9): p. ITC66-ITC80.
65. Ronco, C., R. Bellomo, and J.A. Kellum, *Acute kidney injury.* Lancet, 2019. **394**(10212): p. 1949-1964.

66. Hoste, E.A., et al., *Epidemiology of acute kidney injury in critically ill patients: the multinational AKI-EPI study.* Intensive Care Med, 2015. **41**(8): p. 1411-23.
67. Levy, E.M., C.M. Viscoli, and R.I. Horwitz, *The effect of acute renal failure on mortality. A cohort analysis.* Jama, 1996. **275**(19): p. 1489-94.
68. Chertow, G.M., et al., *Acute kidney injury, mortality, length of stay, and costs in hospitalized patients.* J Am Soc Nephrol, 2005. **16**(11): p. 3365-70.
69. Negi, S., et al., *Acute kidney injury: Epidemiology, outcomes, complications, and therapeutic strategies.* Semin Dial, 2018. **31**(5): p. 519-527.
70. Bellomo, R., et al., *Acute renal failure - definition, outcome measures, animal models, fluid therapy and information technology needs: the Second International Consensus Conference of the Acute Dialysis Quality Initiative (ADQI) Group.* Crit Care, 2004. **8**(4): p. R204-12.
71. Mehta, R.L., et al., *Acute Kidney Injury Network: report of an initiative to improve outcomes in acute kidney injury.* Crit Care, 2007. **11**(2): p. R31.
72. Khwaja, A., *KDIGO clinical practice guidelines for acute kidney injury.* Nephron Clin Pract, 2012. **120**(4): p. c179-84.
73. Mehta, R.L., et al., *Refining predictive models in critically ill patients with acute renal failure.* J Am Soc Nephrol, 2002. **13**(5): p. 1350-7.
74. Bell, M., et al., *Cystatin C is correlated with mortality in patients with and without acute kidney injury.* Nephrology Dialysis Transplantation, 2009. **24**(10): p. 3096-3102.
75. Basile, D.P., M.D. Anderson, and T.A. Sutton, *Pathophysiology of acute kidney injury.* Compr Physiol, 2012. **2**(2): p. 1303-53.
76. Kjeldsen, L., et al., *Isolation and primary structure of NGAL, a novel protein associated with human neutrophil gelatinase.* J Biol Chem, 1993. **268**(14): p. 10425-32.
77. Mishra, J., et al., *Identification of neutrophil gelatinase-associated lipocalin as a novel early urinary biomarker for ischemic renal injury.* J Am Soc Nephrol, 2003. **14**(10): p. 2534-43.
78. Mishra, J., et al., *Amelioration of ischemic acute renal injury by neutrophil gelatinase-associated lipocalin.* J Am Soc Nephrol, 2004. **15**(12): p. 3073-82.
79. Mårtensson, J. and R. Bellomo, *The rise and fall of NGAL in acute kidney injury.* Blood Purif, 2014. **37**(4): p. 304-10.
80. Castillo-Rodriguez, E., et al., *Kidney Injury Marker 1 and Neutrophil Gelatinase-Associated Lipocalin in Chronic Kidney Disease.* Nephron, 2017. **136**(4): p. 263-267.
81. Dai, X., et al., *Diagnostic value of neutrophil gelatinase-associated lipocalin, cystatin C, and soluble triggering receptor expressed on myeloid cells-1 in critically ill patients with sepsis-associated acute kidney injury.* Crit Care, 2015. **19**(1): p. 223.
82. Rizvi, M.S. and K.B. Kashani, *Biomarkers for Early Detection of Acute Kidney Injury.* J Appl Lab Med, 2017. **2**(3): p. 386-399.
83. Vijayan, A., et al., *Clinical Use of the Urine Biomarker [TIMP-2] × [IGFBP7] for Acute Kidney Injury Risk Assessment.* Am J Kidney Dis, 2016. **68**(1): p. 19-28.
84. Schinstock, C.A., et al., *Urinalysis is more specific and urinary neutrophil gelatinase-associated lipocalin is more sensitive for early detection of acute kidney injury.* Nephrology Dialysis Transplantation, 2012. **28**(5): p. 1175-1185.
85. Ichimura, T., et al., *Kidney injury molecule-1 (KIM-1), a putative epithelial cell adhesion molecule containing a novel immunoglobulin domain, is up-regulated in renal cells after injury.* J Biol Chem, 1998. **273**(7): p. 4135-42.
86. Han, W.K., et al., *Kidney Injury Molecule-1 (KIM-1): a novel biomarker for human renal proximal tubule injury.* Kidney Int, 2002. **62**(1): p. 237-44.

87. Rahman, M., F. Shad, and M.C. Smith, *Acute kidney injury: a guide to diagnosis and management.* Am Fam Physician, 2012. **86**(7): p. 631-9.
88. Bonventre, J.V. and L. Yang, *Cellular pathophysiology of ischemic acute kidney injury.* J Clin Invest, 2011. **121**(11): p. 4210-21.
89. Levey, A.S. and J. Coresh, *Chronic kidney disease.* Lancet, 2012. **379**(9811): p. 165-80.
90. Li, L., H. Fu, and Y. Liu, *The fibrogenic niche in kidney fibrosis: components and mechanisms.* Nat Rev Nephrol, 2022. **18**(9): p. 545-557.
91. Humphreys, B.D., *Mechanisms of Renal Fibrosis.* Annual Review of Physiology, 2018. **80**(1): p. 309-326.
92. Thakar, C.V., et al., *Acute kidney injury episodes and chronic kidney disease risk in diabetes mellitus.* Clin J Am Soc Nephrol, 2011. **6**(11): p. 2567-72.
93. Price, P.M., J. Megyesi, and R.L. Saf Irstein, *Cell cycle regulation: repair and regeneration in acute renal failure.* Kidney Int, 2004. **66**(2): p. 509-14.
94. Eming, S.A., T.A. Wynn, and P. Martin, *Inflammation and metabolism in tissue repair and regeneration.* Science, 2017. **356**(6342): p. 1026-1030.
95. Meng, X.M., D.J. Nikolic-Paterson, and H.Y. Lan, *TGF-β: the master regulator of fibrosis.* Nat Rev Nephrol, 2016. **12**(6): p. 325-38.
96. Yin, Q. and H. Liu, *Connective Tissue Growth Factor and Renal Fibrosis.* Adv Exp Med Biol, 2019. **1165**: p. 365-380.
97. Jun, J.I. and L.F. Lau, *Resolution of organ fibrosis.* J Clin Invest, 2018. **128**(1): p. 97-107.
98. Horowitz, J.C. and V.J. Thannickal, *Mechanisms for the Resolution of Organ Fibrosis.* Physiology (Bethesda), 2019. **34**(1): p. 43-55.
99. Ichimura, T., et al., *Kidney injury molecule-1 is a phosphatidylserine receptor that confers a phagocytic phenotype on epithelial cells.* J Clin Invest, 2008. **118**(5): p. 1657-68.
100. Humphreys, B.D., et al., *Chronic epithelial kidney injury molecule-1 expression causes murine kidney fibrosis.* J Clin Invest, 2013. **123**(9): p. 4023-35.
101. Zhou, D. and Y. Liu, *Renal fibrosis in 2015: Understanding the mechanisms of kidney fibrosis.* Nat Rev Nephrol, 2016. **12**(2): p. 68-70.
102. Fu, H., et al., *Tenascin-C Is a Major Component of the Fibrogenic Niche in Kidney Fibrosis.* J Am Soc Nephrol, 2017. **28**(3): p. 785-801.
103. Lippard, S.J., *New chemistry of an old molecule: cis-[Pt(NH3)2Cl2].* Science, 1982. **218**(4577): p. 1075-82.
104. Kauffman, G.B., *Alfred Werner, Founder of Coordination Chemistry*. 1966, Berlin: Springer-Verlag.
105. Smeaton, W., *THE STRUCTURE OF PLATINUM COMPLEXES.* Platinum Metals Review, 1966. **10**(4): p. 140-144.
106. Rosenberg, B., et al., *The inhibition of growth or cell division in Escherichia coli by different ionic species of platinum(IV) complexes.* J Biol Chem, 1967. **242**(6): p. 1347-52.
107. Rosenberg, B., et al., *Platinum compounds: a new class of potent antitumour agents.* Nature, 1969. **222**(5191): p. 385-6.
108. Rosenberg, B. and L. VanCamp, *The successful regression of large solid sarcoma 180 tumors by platinum compounds.* Cancer Res, 1970. **30**(6): p. 1799-802.
109. Pascoe, J.M. and J.J. Roberts, *Interactions between mammalian cell DNA and inorganic platinum compounds. I. DNA interstrand cross-linking and cytotoxic properties of platinum(II) compounds.* Biochem Pharmacol, 1974. **23**(9): p. 1359-65.
110. Wang, D. and S.J. Lippard, *Cellular processing of platinum anticancer drugs.* Nat Rev Drug Discov, 2005. **4**(4): p. 307-20.

111. Launay-Vacher, V., N. Janus, and G. Deray, *Renal insufficiency and cancer treatments.* ESMO Open, 2016. **1**(4): p. e000091.
112. Iff, S., et al., *Reduced estimated GFR and cancer mortality.* Am J Kidney Dis, 2014. **63**(1): p. 23-30.
113. Madias, N.E. and J.T. Harrington, *Platinum nephrotoxicity.* Am J Med, 1978. **65**(2): p. 307-14.
114. Yao, X., et al., *Cisplatin nephrotoxicity: a review.* Am J Med Sci, 2007. **334**(2): p. 115-24.
115. Pabla, N. and Z. Dong, *Cisplatin nephrotoxicity: mechanisms and renoprotective strategies.* Kidney Int, 2008. **73**(9): p. 994-1007.
116. Pabla, N., et al., *The copper transporter Ctr1 contributes to cisplatin uptake by renal tubular cells during cisplatin nephrotoxicity.* Am J Physiol Renal Physiol, 2009. **296**(3): p. F505-11.
117. Ciarimboli, G., et al., *Cisplatin nephrotoxicity is critically mediated via the human organic cation transporter 2.* Am J Pathol, 2005. **167**(6): p. 1477-84.
118. Ludwig, T., et al., *Nephrotoxicity of platinum complexes is related to basolateral organic cation transport.* Kidney Int, 2004. **66**(1): p. 196-202.
119. Filipski, K.K., et al., *Contribution of organic cation transporter 2 (OCT2) to cisplatin-induced nephrotoxicity.* Clin Pharmacol Ther, 2009. **86**(4): p. 396-402.
120. Ciarimboli, G., et al., *Organic cation transporter 2 mediates cisplatin-induced oto- and nephrotoxicity and is a target for protective interventions.* Am J Pathol, 2010. **176**(3): p. 1169-80.
121. Ozkok, A. and C.L. Edelstein, *Pathophysiology of cisplatin-induced acute kidney injury.* Biomed Res Int, 2014. **2014**: p. 967826.
122. Lau, J.K. and B. Ensing, *Hydrolysis of cisplatin--a first-principles metadynamics study.* Phys Chem Chem Phys, 2010. **12**(35): p. 10348-55.
123. Jamieson, E.R. and S.J. Lippard, *Structure, Recognition, and Processing of Cisplatin-DNA Adducts.* Chem Rev, 1999. **99**(9): p. 2467-98.
124. Alderden, R.A., M.D. Hall, and T.W. Hambley, *The Discovery and Development of Cisplatin.* Journal of Chemical Education, 2006. **83**(5): p. 728.
125. Burger, H., et al., *Lack of correlation between cisplatin-induced apoptosis, p53 status and expression of Bcl-2 family proteins in testicular germ cell tumour cell lines.* Int J Cancer, 1997. **73**(4): p. 592-9.
126. Olivero, O.A., et al., *Preferential binding of cisplatin to mitochondrial DNA of Chinese hamster ovary cells.* Mutat Res, 1995. **346**(4): p. 221-30.
127. Mandic, A., et al., *Cisplatin induces endoplasmic reticulum stress and nucleus-independent apoptotic signaling.* J Biol Chem, 2003. **278**(11): p. 9100-6.
128. Cullen, K.J., et al., *Mitochondria as a critical target of the chemotheraputic agent cisplatin in head and neck cancer.* J Bioenerg Biomembr, 2007. **39**(1): p. 43-50.
129. Townsend, D.M., et al., *Metabolism of Cisplatin to a nephrotoxin in proximal tubule cells.* J Am Soc Nephrol, 2003. **14**(1): p. 1-10.
130. Qian, W., et al., *Mitochondrial density determines the cellular sensitivity to cisplatin-induced cell death.* Am J Physiol Cell Physiol, 2005. **289**(6): p. C1466-75.
131. Hirama, M., et al., *Characterization of mitochondria in cisplatin-resistant human ovarian carcinoma cells.* Oncol Rep, 2006. **16**(5): p. 997-1002.
132. Errol, C.F., et al., *DNA Repair and Mutagenesis, Second Edition*. 2006: American Society of Microbiology.
133. Fu, Y., M. Tigano, and A. Sfeir, *Safeguarding mitochondrial genomes in higher eukaryotes.* Nat Struct Mol Biol, 2020. **27**(8): p. 687-695.

134. Fontana, G.A. and H.L. Gahlon, *Mechanisms of replication and repair in mitochondrial DNA deletion formation.* Nucleic Acids Research, 2020. **48**(20): p. 11244-11258.
135. Verlander, J.W., *Normal ultrastructure of the kidney and lower urinary tract.* Toxicol Pathol, 1998. **26**(1): p. 1-17.
136. Kruidering, M., et al., *Cisplatin-induced nephrotoxicity in porcine proximal tubular cells: mitochondrial dysfunction by inhibition of complexes I to IV of the respiratory chain.* J Pharmacol Exp Ther, 1997. **280**(2): p. 638-49.
137. Li, S., et al., *PPAR alpha ligand protects during cisplatin-induced acute renal failure by preventing inhibition of renal FAO and PDC activity.* Am J Physiol Renal Physiol, 2004. **286**(3): p. F572-80.
138. Li, S., et al., *PPAR-alpha ligand ameliorates acute renal failure by reducing cisplatin-induced increased expression of renal endonuclease G.* Am J Physiol Renal Physiol, 2004. **287**(5): p. F990-8.
139. Bhargava, P. and R.G. Schnellmann, *Mitochondrial energetics in the kidney.* Nature Reviews Nephrology, 2017. **13**(10): p. 629-646.
140. Kang, H.M., et al., *Defective fatty acid oxidation in renal tubular epithelial cells has a key role in kidney fibrosis development.* Nature Medicine, 2015. **21**(1): p. 37-46.
141. Li, S.Y. and K. Susztak, *The Role of Peroxisome Proliferator-Activated Receptor gamma Coactivator 1alpha (PGC-1alpha) in Kidney Disease.* Semin Nephrol, 2018. **38**(2): p. 121-126.
142. Houtkooper, R.H., et al., *Mitonuclear protein imbalance as a conserved longevity mechanism.* Nature, 2013. **497**(7450): p. 451-457.
143. Alborzinia, H., et al., *Real-Time Monitoring of Cisplatin-Induced Cell Death.* PLOS ONE, 2011. **6**(5): p. e19714.
144. Piccinini, A.M. and K.S. Midwood, *DAMPening inflammation by modulating TLR signalling.* Mediators of inflammation, 2010. **2010**: p. 672395.
145. Zhang, B., et al., *TLR4 signaling mediates inflammation and tissue injury in nephrotoxicity.* J Am Soc Nephrol, 2008. **19**(5): p. 923-32.
146. Ramesh, G. and W.B. Reeves, *TNF-alpha mediates chemokine and cytokine expression and renal injury in cisplatin nephrotoxicity.* J Clin Invest, 2002. **110**(6): p. 835-42.
147. Maekawa, H., et al., *Mitochondrial Damage Causes Inflammation via cGAS-STING Signaling in Acute Kidney Injury.* Cell Rep, 2019. **29**(5): p. 1261-1273 e6.
148. Al-Sarraf, M., et al., *Cisplatin hydration with and without mannitol diuresis in refractory disseminated malignant melanoma: a southwest oncology group study.* Cancer Treat Rep, 1982. **66**(1): p. 31-5.
149. Launay-Vacher, V., et al., *Prevention of cisplatin nephrotoxicity: state of the art and recommendations from the European Society of Clinical Pharmacy Special Interest Group on Cancer Care.* Cancer Chemother Pharmacol, 2008. **61**(6): p. 903-9.
150. Skrypnyk, N.I., et al., *Bridging translation for acute kidney injury with better preclinical modeling of human disease.* Am J Physiol Renal Physiol, 2016. **310**(10): p. F972-84.
151. Sharp, C.N. and L.J. Siskind, *Developing better mouse models to study cisplatin-induced kidney injury.* Am J Physiol Renal Physiol, 2017. **313**(4): p. F835-F841.
152. Sharp, C.N., et al., *Subclinical kidney injury induced by repeated cisplatin administration results in progressive chronic kidney disease.* Am J Physiol Renal Physiol, 2018. **315**(1): p. F161-F172.
153. Sharp, C.N., et al., *Repeated administration of low-dose cisplatin in mice induces fibrosis.* Am J Physiol Renal Physiol, 2016. **310**(6): p. F560-8.

154. Sharp, C.N., et al., *Moderate aging does not exacerbate cisplatin-induced kidney injury or fibrosis despite altered inflammatory cytokine expression and immune cell infiltration.* Am J Physiol Renal Physiol, 2019. **316**(1): p. F162-F172.
155. Black, L.M., et al., *Divergent effects of AKI to CKD models on inflammation and fibrosis.* Am J Physiol Renal Physiol, 2018. **315**(4): p. F1107-F1118.
156. Shi, M., et al., *Cisplatin nephrotoxicity as a model of chronic kidney disease.* Lab Invest, 2018. **98**(8): p. 1105-1121.
157. Landau, S.I., et al., *Regulated necrosis and failed repair in cisplatin-induced chronic kidney disease.* Kidney Int, 2019. **95**(4): p. 797-814.
158. Sears, S.M., et al., *C57BL/6 mice require a higher dose of cisplatin to induce renal fibrosis and CCL2 correlates with cisplatin-induced kidney injury.* Am J Physiol Renal Physiol, 2020. **319**(4): p. F674-F685.
159. Ma, Z., et al., *Single-Nucleus Transcriptional Profiling of Chronic Kidney Disease after Cisplatin Nephrotoxicity.* Am J Pathol, 2022. **192**(4): p. 613-628.
160. Yamashita, N., et al., *Cumulative DNA damage by repeated low-dose cisplatin injection promotes the transition of acute to chronic kidney injury in mice.* Sci Rep, 2021. **11**(1): p. 20920.
161. Tang, C., et al., *Mitochondrial quality control in kidney injury and repair.* Nature Reviews Nephrology, 2020.
162. Braga, P.C., et al., *Mitochondrial Pathophysiology on Chronic Kidney Disease.* Int J Mol Sci, 2022. **23**(3).
163. Galvan, D.L., N.H. Green, and F.R. Danesh, *The hallmarks of mitochondrial dysfunction in chronic kidney disease.* Kidney International, 2017. **92**(5): p. 1051-1057.
164. Bruni, F., R.N. Lightowlers, and Z.M. Chrzanowska-Lightowlers, *Human mitochondrial nucleases.* The FEBS Journal, 2017. **284**(12): p. 1767-1777.
165. Banoth, B. and S.L. Cassel, *Mitochondria in innate immune signaling.* Translational Research, 2018. **202**: p. 52-68.
166. Jiang, M., et al., *Mitochondrial dysfunction and the AKI-to-CKD transition.* Am J Physiol Renal Physiol, 2020. **319**(6): p. F1105-F1116.
167. O'Connor, P.M., *Renal oxygen delivery: matching delivery to metabolic demand.* Clin Exp Pharmacol Physiol, 2006. **33**(10): p. 961-7.
168. Niaudet, P. and A. Rötig, *Renal involvement in mitochondrial cytopathies.* Pediatr Nephrol, 1996. **10**(3): p. 368-73.
169. Emma, F., et al., *Renal involvement in mitochondrial cytopathies.* Pediatric Nephrology, 2012. **27**(4): p. 539-550.
170. O'Toole, J.F., *Renal manifestations of genetic mitochondrial disease.* Int J Nephrol Renovasc Dis, 2014. **7**: p. 57-67.
171. Emma, F., et al., *Mitochondrial dysfunction in inherited renal disease and acute kidney injury.* Nat Rev Nephrol, 2016. **12**(5): p. 267-80.
172. Govers, L.P., et al., *Mitochondrial DNA mutations in renal disease: an overview.* Pediatric Nephrology, 2021. **36**(1): p. 9-17.
173. Chevalier, R.L., *The proximal tubule is the primary target of injury and progression of kidney disease: role of the glomerulotubular junction.* Am J Physiol Renal Physiol, 2016. **311**(1): p. F145-61.
174. Bost, F. and L. Kaminski, *The metabolic modulator PGC-1α in cancer.* Am J Cancer Res, 2019. **9**(2): p. 198-211.
175. Fontecha-Barriuso, M., et al., *The Role of PGC-1alpha and Mitochondrial Biogenesis in Kidney Diseases.* Biomolecules, 2020. **10**(2).

176. Lynch, M.R., M.T. Tran, and S.M. Parikh, *PGC1alpha in the kidney.* Am J Physiol Renal Physiol, 2018. **314**(1): p. F1-F8.
177. Puigserver, P., et al., *A Cold-Inducible Coactivator of Nuclear Receptors Linked to Adaptive Thermogenesis.* Cell, 1998. **92**(6): p. 829-839.
178. Wu, Z., et al., *Mechanisms controlling mitochondrial biogenesis and respiration through the thermogenic coactivator PGC-1.* Cell, 1999. **98**(1): p. 115-24.
179. Ruiz-Andres, O., et al., *The inflammatory cytokine TWEAK decreases PGC-1α expression and mitochondrial function in acute kidney injury.* Kidney International, 2016. **89**(2): p. 399-410.
180. Han, S.H., et al., *PGC-1α Protects from Notch-Induced Kidney Fibrosis Development.* J Am Soc Nephrol, 2017. **28**(11): p. 3312-3322.
181. Long, J., et al., *Long noncoding RNA Tug1 regulates mitochondrial bioenergetics in diabetic nephropathy.* J Clin Invest, 2016. **126**(11): p. 4205-4218.
182. Ashabi, G., et al., *ERK and p38 inhibitors attenuate memory deficits and increase CREB phosphorylation and PGC-1α levels in Aβ-injected rats.* Behavioural Brain Research, 2012. **232**(1): p. 165-173.
183. Sano, M., et al., *Intramolecular control of protein stability, subnuclear compartmentalization, and coactivator function of peroxisome proliferator-activated receptor gamma coactivator 1alpha.* J Biol Chem, 2007. **282**(35): p. 25970-80.
184. Gai, Z., et al., *The Role of Mitochondria in Drug-Induced Kidney Injury.* Frontiers in Physiology, 2020. **11**(1079).
185. Bonekamp, N.A. and N.-G. Larsson, *SnapShot: Mitochondrial Nucleoid.* Cell, 2018. **172**(1): p. 388-388.e1.
186. Ngo, H.B., et al., *Distinct structural features of TFAM drive mitochondrial DNA packaging versus transcriptional activation.* Nature Communications, 2014. **5**(1): p. 3077.
187. Larsson, N.-G., et al., *Mitochondrial transcription factor A is necessary for mtDNA maintance and embryogenesis in mice.* Nature Genetics, 1998. **18**(3): p. 231-236.
188. Chung, K.W., et al., *Mitochondrial Damage and Activation of the STING Pathway Lead to Renal Inflammation and Fibrosis.* Cell Metab, 2019. **30**(4): p. 784-799.e5.
189. Valle, I., et al., *PGC-1alpha regulates the mitochondrial antioxidant defense system in vascular endothelial cells.* Cardiovasc Res, 2005. **66**(3): p. 562-73.
190. Chen, S.D., et al., *Roles of oxidative stress, apoptosis, PGC-1alpha and mitochondrial biogenesis in cerebral ischemia.* Int J Mol Sci, 2011. **12**(10): p. 7199-215.
191. Portilla, D., et al., *Alterations of PPARalpha and its coactivator PGC-1 in cisplatin-induced acute renal failure.* Kidney Int, 2002. **62**(4): p. 1208-18.
192. Tran, M.T., et al., *PGC1α drives NAD biosynthesis linking oxidative metabolism to renal protection.* Nature, 2016. **531**(7595): p. 528-32.
193. Sharma, K., et al., *Metabolomics reveals signature of mitochondrial dysfunction in diabetic kidney disease.* J Am Soc Nephrol, 2013. **24**(11): p. 1901-12.
194. Oh, C.J., et al., *Pyruvate dehydrogenase kinase 4 deficiency attenuates cisplatin-induced acute kidney injury.* Kidney International, 2017. **91**(4): p. 880-895.
195. Morigi, M., et al., *Sirtuin 3–dependent mitochondrial dynamic improvements protect against acute kidney injury.* The Journal of Clinical Investigation, 2015. **125**(2): p. 715-726.
196. Whitaker, R.M., et al., *cGMP-selective phosphodiesterase inhibitors stimulate mitochondrial biogenesis and promote recovery from acute kidney injury.* J Pharmacol Exp Ther, 2013. **347**(3): p. 626-34.

197. Fontecha-Barriuso, M., et al., *PGC-1alpha deficiency causes spontaneous kidney inflammation and increases the severity of nephrotoxic AKI.* J Pathol, 2019. **249**(1): p. 65-78.
198. Guan, Y., et al., *Nicotinamide Mononucleotide, an NAD⁺ Precursor, Rescues Age-Associated Susceptibility to AKI in a Sirtuin 1–Dependent Manner.* Journal of the American Society of Nephrology, 2017. **28**(8): p. 2337-2352.
199. Ruiz-Andres, O., et al., *Histone lysine crotonylation during acute kidney injury in mice.* Disease Models & Mechanisms, 2016. **9**(6): p. 633-645.
200. Smith, J.A., et al., *Suppression of Mitochondrial Biogenesis through Toll-Like Receptor 4–Dependent Mitogen-Activated Protein Kinase Kinase/Extracellular Signal-Regulated Kinase Signaling in Endotoxin-Induced Acute Kidney Injury.* Journal of Pharmacology and Experimental Therapeutics, 2015. **352**(2): p. 346-357.
201. Khader, A., et al., *SRT1720, a sirtuin 1 activator, attenuates organ injury and inflammation in sepsis.* Journal of Surgical Research, 2017. **219**: p. 288-295.
202. Collier, J.B., et al., *Rapid Renal Regulation of Peroxisome Proliferator-activated Receptor γ Coactivator-1α by Extracellular Signal-Regulated Kinase 1/2 in Physiological and Pathological Conditions.* J Biol Chem, 2016. **291**(52): p. 26850-26859.
203. Khader, A., et al., *Sirtuin 1 activation stimulates mitochondrial biogenesis and attenuates renal injury after ischemia-reperfusion.* Transplantation, 2014. **98**(2): p. 148-56.
204. Lempiäinen, J., et al., *Caloric restriction ameliorates kidney ischaemia/reperfusion injury through PGC-1α-eNOS pathway and enhanced autophagy.* Acta Physiol (Oxf), 2013. **208**(4): p. 410-21.
205. Jesinkey, S.R., et al., *Formoterol restores mitochondrial and renal function after ischemia-reperfusion injury.* J Am Soc Nephrol, 2014. **25**(6): p. 1157-62.
206. Lynch, M.R., et al., *TFEB-driven lysosomal biogenesis is pivotal for PGC1α-dependent renal stress resistance.* JCI insight, 2019. **5**(8): p. e126749.
207. Tran, M., et al., *PGC-1α promotes recovery after acute kidney injury during systemic inflammation in mice.* J Clin Invest, 2011. **121**(10): p. 4003-14.
208. Rasbach, K.A. and R.G. Schnellmann, *Signaling of mitochondrial biogenesis following oxidant injury.* J Biol Chem, 2007. **282**(4): p. 2355-62.
209. Van Biesen, W., R. Vanholder, and N. Lameire, *Defining acute renal failure: RIFLE and beyond.* Clin J Am Soc Nephrol, 2006. **1**(6): p. 1314-9.
210. Fu, Y., et al., *Rodent models of AKI-CKD transition.* Am J Physiol Renal Physiol, 2018. **315**(4): p. F1098-F1106.
211. Sears, S. and L. Siskind, *Potential Therapeutic Targets for Cisplatin-Induced Kidney Injury: Lessons from Other Models of AKI and Fibrosis.* J Am Soc Nephrol, 2021.
212. Quiros, P.M., et al., *Analysis of mtDNA/nDNA Ratio in Mice.* Current protocols in mouse biology, 2017. **7**(1): p. 47-54.
213. Clayton, D.A., J.N. Doda, and E.C. Friedberg, *The absence of a pyrimidine dimer repair mechanism in mammalian mitochondria.* Proc Natl Acad Sci U S A, 1974. **71**(7): p. 2777-81.
214. Gammage, P.A. and C. Frezza, *Mitochondrial DNA: the overlooked oncogenome?* BMC Biology, 2019. **17**(1): p. 53.
215. Garrett, S.M., et al., *Agonism of the 5-hydroxytryptamine 1F receptor promotes mitochondrial biogenesis and recovery from acute kidney injury.* J Pharmacol Exp Ther, 2014. **350**(2): p. 257-64.

216. Simmons, E.C., et al., *5-hydroxytryptamine 1F Receptor Agonist Induces Mitochondrial Biogenesis and Promotes Recovery from Spinal Cord Injury.* J Pharmacol Exp Ther, 2020. **372**(2): p. 216-223.
217. Adham, N., et al., *Cloning of another human serotonin receptor (5-HT1F): a fifth 5-HT1 receptor subtype coupled to the inhibition of adenylate cyclase.* Proc Natl Acad Sci U S A, 1993. **90**(2): p. 408-12.
218. Adham, N., et al., *Cloning and characterization of the guinea pig 5-HT1F receptor subtype: a comparison of the pharmacological profile to the human species homolog.* Neuropharmacology, 1997. **36**(4-5): p. 569-76.
219. Phebus, L.A., et al., *Characterization of LY344864 as a pharmacological tool to study 5-HT1F receptors: binding affinities, brain penetration and activity in the neurogenic dural inflammation model of migraine.* Life Sci, 1997. **61**(21): p. 2117-26.
220. Nelson, D.L., et al., *Preclinical pharmacological profile of the selective 5-HT1F receptor agonist lasmiditan.* Cephalalgia, 2010. **30**(10): p. 1159-69.
221. Clemow, D.B., et al., *Lasmiditan mechanism of action - review of a selective 5-HT1F agonist.* J Headache Pain, 2020. **21**(1): p. 71.
222. Gibbs, W.S., et al., *5-HT(1F) receptor regulates mitochondrial homeostasis and its loss potentiates acute kidney injury and impairs renal recovery.* Am J Physiol Renal Physiol, 2018. **315**(4): p. F1119-f1128.
223. Sears, S.M., et al., *F4/80^{hi} Resident Macrophages Contribute to Cisplatin-Induced Renal Fibrosis.* Kidney360, 2022. **3**(5): p. 818-833.
224. Stritt, M., A.K. Stalder, and E. Vezzali, *Orbit Image Analysis: An open-source whole slide image analysis tool.* PLOS Computational Biology, 2020. **16**(2): p. e1007313.
225. Seger, S., et al., *A fully automated image analysis method to quantify lung fibrosis in the bleomycin-induced rat model.* PLOS ONE, 2018. **13**(3): p. e0193057.
226. Orwick, A., et al., *Lung cancer-kidney cross talk induces kidney injury, interstitial fibrosis, and enhances cisplatin-induced nephrotoxicity.* Am J Physiol Renal Physiol, 2023. **324**(3): p. F287-F300.
227. Hanna, N. and L.H. Einhorn, *Testicular cancer: a reflection on 50 years of discovery.* J Clin Oncol, 2014. **32**(28): p. 3085-92.
228. Osanto, S., et al., *Long-term effects of chemotherapy in patients with testicular cancer.* J Clin Oncol, 1992. **10**(4): p. 574-9.
229. Husain-Syed, F., et al., *Cardio-Pulmonary-Renal Interactions: A Multidisciplinary Approach.* J Am Coll Cardiol, 2015. **65**(22): p. 2433-48.
230. Husain-Syed, F., A.S. Slutsky, and C. Ronco, *Lung-Kidney Cross-Talk in the Critically Ill Patient.* Am J Respir Crit Care Med, 2016. **194**(4): p. 402-14.
231. Khamissi, F.Z., et al., *Identification of kidney injury released circulating osteopontin as causal agent of respiratory failure.* Sci Adv, 2022. **8**(8): p. eabm5900.
232. Winslow, M.M., et al., *Suppression of lung adenocarcinoma progression by Nkx2-1.* Nature, 2011. **473**(7345): p. 101-104.
233. Shultz, L.D., et al., *Human lymphoid and myeloid cell development in NOD/LtSz-scid IL2R gamma null mice engrafted with mobilized human hemopoietic stem cells.* J Immunol, 2005. **174**(10): p. 6477-89.
234. Barve, A., et al., *Comparative utility of NRG and NRGS mice for the study of normal hematopoiesis, leukemogenesis, and therapeutic response.* Exp Hematol, 2018. **67**: p. 18-31.
235. Wunderlich, M., et al., *Improved chemotherapy modeling with RAG-based immune deficient mice.* PLoS One, 2019. **14**(11): p. e0225532.

236. Group, U.C.S.W., *United States cancer statistics: 1999–2010 incidence and mortality web-based report.* Atlanta: US Department of Health and Human Services, Centers for Disease Control and Prevention and National Cancer Institute, 2013. **201**.
237. Howlader, N., et al., *SEER cancer statistics review, 1975–2010.* National Cancer Institute, 2014.
238. White, M.C., et al., *Age and cancer risk: a potentially modifiable relationship.* Am J Prev Med, 2014. **46**(3 Suppl 1): p. S7-15.
239. Sears, S.M., et al., *Pharmacological inhibitors of autophagy have opposite effects in acute and chronic cisplatin-induced kidney injury.* Am J Physiol Renal Physiol, 2022. **323**(3): p. F288-F298.
240. Gallina, G., et al., *Tumors induce a subset of inflammatory monocytes with immunosuppressive activity on CD8+ T cells.* J Clin Invest, 2006. **116**(10): p. 2777-90.
241. Hayes, C., et al., *The oncogenic and clinical implications of lactate induced immunosuppression in the tumour microenvironment.* Cancer Lett, 2021. **500**: p. 75-86.
242. Noy, R. and J.W. Pollard, *Tumor-associated macrophages: from mechanisms to therapy.* Immunity, 2014. **41**(1): p. 49-61.
243. Lin, Y., J. Xu, and H. Lan, *Tumor-associated macrophages in tumor metastasis: biological roles and clinical therapeutic applications.* Journal of Hematology & Oncology, 2019. **12**(1): p. 76.
244. Jang, H.R. and H. Rabb, *Immune cells in experimental acute kidney injury.* Nat Rev Nephrol, 2015. **11**(2): p. 88-101.
245. Lee, S.A., et al., *Role of Immune Cells in Acute Kidney Injury and Repair.* Nephron, 2017. **137**(4): p. 282-286.
246. Bonavia, A. and K. Singbartl, *A review of the role of immune cells in acute kidney injury.* Pediatr Nephrol, 2018. **33**(10): p. 1629-1639.
247. Burne, M.J., et al., *Identification of the CD4(+) T cell as a major pathogenic factor in ischemic acute renal failure.* J Clin Invest, 2001. **108**(9): p. 1283-90.
248. Liu, M., et al., *A pathophysiologic role for T lymphocytes in murine acute cisplatin nephrotoxicity.* J Am Soc Nephrol, 2006. **17**(3): p. 765-74.
249. Masri, S., et al., *Lung Adenocarcinoma Distally Rewires Hepatic Circadian Homeostasis.* Cell, 2016. **165**(4): p. 896-909.
250. DuPage, M., A.L. Dooley, and T. Jacks, *Conditional mouse lung cancer models using adenoviral or lentiviral delivery of Cre recombinase.* Nat Protoc, 2009. **4**(7): p. 1064-72.
251. Hanahan, D. and R.A. Weinberg, *Hallmarks of cancer: the next generation.* Cell, 2011. **144**(5): p. 646-74.
252. Gonzalez, H., C. Hagerling, and Z. Werb, *Roles of the immune system in cancer: from tumor initiation to metastatic progression.* Genes Dev, 2018. **32**(19-20): p. 1267-1284.
253. Hiam-Galvez, K.J., B.M. Allen, and M.H. Spitzer, *Systemic immunity in cancer.* Nature Reviews Cancer, 2021. **21**(6): p. 345-359.
254. Jia, P., et al., *Chemokine CCL2 from proximal tubular epithelial cells contributes to sepsis-induced acute kidney injury.* Am J Physiol Renal Physiol, 2022. **323**(2): p. F107-F119.
255. Peng, X., et al., *CX3CL1-CX3CR1 Interaction Increases the Population of Ly6C(-)CX3CR1(hi) Macrophages Contributing to Unilateral Ureteral Obstruction-Induced Fibrosis.* J Immunol, 2015. **195**(6): p. 2797-805.
256. Yang, Q., et al., *Bone marrow-derived Ly6C(-) macrophages promote ischemia-induced chronic kidney disease.* Cell Death Dis, 2019. **10**(4): p. 291.
257. Egeblad, M., E.S. Nakasone, and Z. Werb, *Tumors as Organs: Complex Tissues that Interface with the Entire Organism.* Developmental Cell, 2010. **18**(6): p. 884-901.

258. Kartikasari, A.E.R., et al., *Tumor-Induced Inflammatory Cytokines and the Emerging Diagnostic Devices for Cancer Detection and Prognosis.* Frontiers in Oncology, 2021. **11**.
259. Pabla, N., et al., *Inhibition of PKCdelta reduces cisplatin-induced nephrotoxicity without blocking chemotherapeutic efficacy in mouse models of cancer.* J Clin Invest, 2011. **121**(7): p. 2709-22.
260. Solanki, M.H., et al., *Magnesium protects against cisplatin-induced acute kidney injury without compromising cisplatin-mediated killing of an ovarian tumor xenograft in mice.* Am J Physiol Renal Physiol, 2015. **309**(1): p. F35-47.
261. Kumar, G., et al., *Magnesium improves cisplatin-mediated tumor killing while protecting against cisplatin-induced nephrotoxicity.* Am J Physiol Renal Physiol, 2017. **313**(2): p. F339-F350.
262. Ravichandran, K., et al., *CD4 T cell knockout does not protect against kidney injury and worsens cancer.* Journal of Molecular Medicine, 2016. **94**(4): p. 443-455.
263. Dupre, T.V., et al., *The 5-hydroxytryptamine receptor 1F stimulates mitochondrial biogenesis and angiogenesis in endothelial cells.* Biochem Pharmacol, 2019. **169**: p. 113644.
264. Hanahan, D. and R.A. Weinberg, *The hallmarks of cancer.* Cell, 2000. **100**(1): p. 57-70.

CURRICULUM VITAE

Andrew Orwick, Pharm.D., M.S.
University of Louisville School of Medicine
Department of Pharmacology & Toxicology
505 South Hancock Street (CTRB 252 G)
Louisville, KY 40202
E-mail: andrew.orwick@louisville.edu

EDUCATION

M.S., Pharmacology and Toxicology 2021, University of Louisville School of Medicine
Doctor of Pharmacy 2012, Sullivan University College of Pharmacy
Biology Minor 2009, IUPUI

RESEARCH

Ph.D. Candidate/Graduate Fellowship — August 2019-Current
Department of Pharmacology & Toxicology
University of Louisville School of Medicine
Onconephrology

Clinical Research, Doctor of Pharmacy Candidate — May 2010-May 2012
Sullivan University College of Pharmacy
Post-Operative Pediatric GI Surgical patients' Outcomes

INDUSTRY POSITIONS HELD

Vice-President of Operations, Precision Compounding Pharmacy — July 2016-July 2019
Operations Manager, Precision Compounding Pharmacy — August 2014-July 2016
Compounding Pharmacist, Precision Compounding Pharmacy — June 2012-August 2014
Compounding Pharmacy Intern, Precision Compounding Pharmacy — May 2009-May 2012

AWARDS

NIH - Ruth L. Kirschstein Predoctoral Individual National Research Service Award (F31)
April 2022

TEACHING

Dental Hygienist Guest Lecture – Antineoplastic Drugs November 2021, 2022
Dental Hygienist Guest Lecture – Emergency Drugs November 2021, 2022
Dental Hygienist Guest Lecture – Antineoplastic Drugs October 2020

PUBLICATIONS

Orwick A, Sears SM, Sharp CN, Doll MA, Shah PP, Beverly LJ, Siskind LJ. Lung cancer-kidney cross talk induces kidney injury, interstitial fibrosis, and enhances cisplatin-induced nephrotoxicity. Am J Physiol Renal Physiol. 2023 Mar 1;324(3):F287-F300. doi: 10.1152/ajprenal.00317.2022. Epub 2023 Feb 2. PMID: 36727944; PMCID: PMC9988526.

Sears SM, **Orwick A**, Siskind LJ. Modeling Cisplatin-Induced Kidney Injury to Increase Translational Potential. Nephron. 2023;147(1):13-16. doi: 10.1159/000525491. Epub 2022 Jul 6. PMID: 35793615; PMCID: PMC9816344.

Sears SM, Feng JL, **Orwick A**, Vega AA, Krueger AM, Shah PP, Doll MA, Beverly LJ, Siskind LJ. Pharmacological inhibitors of autophagy have opposite effects in acute and chronic cisplatin-induced kidney injury. Am J Physiol Renal Physiol. 2022 Sep 1;323(3):F288-F298. doi: 10.1152/ajprenal.00097.2022. Epub 2022 Jul 7. PMID: 35796459; PMCID: PMC9394729.

SELECTED ORAL PRESENTATIONS

Lung cancer induces kidney fibrosis and primes the kidneys for cisplatin-induced nephrotoxicity June 2022
The role of PGC-1α in repeated low-dose cisplatin-induced kidney injury and the progression to chronic kidney disease May 2021

POSTERS

Orwick A, Sears SM, Sharp CN, Doll MA, Shah PP, Beverly LJ, Siskind LJ. (November 2022). Lung cancer induces kidney fibrosis and primes the kidney for cisplatin-induced nephrotoxicity. American Society of Nephrology Kidney Week. Orlando, Florida.

Orwick A, Sears SM, Doll MA, Shah PP, Beverly LJ, Siskind LJ. (September 2022). 5-hydroxytryptamine 1F Receptor Agonist Protects from Repeated Low Dose Cisplatin Induced Nephrotoxicity. Research! Louisville. Louisville, Kentucky.

EDUCATIONAL CONFERENCES

ASN: Kidney Week, Orlando, FL November 2022
Onco-Nephrology Symposium, Boston, MA, September 2022

APS/ASN CONFERENCE: CONTROL OF RENAL FUNCTION IN HEALTH AND DISEASE, Charlottesville, VA, June 2022
AAPS DRUG TRANSPORTERS IN ADME: From the Bench to the Bedside, April 2022
IACP Compounders on Capitol Hill, Washington, D.C., June 2018
PCCA International Seminar, Houston, TX, November 2014
PCCA International Seminar, Houston, TX, October 2013
PCCA Comprehensive Compounding Course, Houston, TX, September 2013
PCCA PK Software Advanced Users Course, Houston, TX, April 2013
PCCA Aseptic Technique Compounding Course, Houston, TX, January 2013

SKILLS

Leadership
Problem Solver
Time Management
Public Speaking
Teaching
Teamwork
Adaptability/Flexibility
Interpersonal Skills

TECHNICAL SKILLS

qRT-PCR, Western Blots, ELISA, Histology, Flow Cytometry, Animal modeling, transgenic animal modeling.

ORGANIZATIONS

American Society of Nephrology (ASN)
American Physiological Society (APS)

LICENSES AND CERTIFICATES

State of Indiana Pharmacist License

REFERENCES AVAILABLE UPON REQUEST